Technische Universität München
Fakultät für Medizin

T cell receptor-dependent protection, recruitment and phenotypes of OVA-specific $CD8^+$ T cells with different avidities in a murine MC38-OVA tumor model

Anna Purcarea

Vollständiger Abdruck der von der Fakultät für Medizin der Technischen Universität München zur Erlangung einer

Doktorin der Medizinischen Wissenschaft (Dr. med. sci.)

genehmigten Dissertation.

Vorsitz: Prof. Dr. Jürgen Ruland

Prüfer*innen der Dissertation:

1. Prof. Dr. Dirk H. Busch
2. Prof. Dr. Percy A. Knolle
3. TUM Junior Fellow Dr. Maike Buchner-Mayr

Die Dissertation wurde am 09.09.2022 bei der Technischen Universität München eingereicht und durch die Fakultät für Medizin am 19.04.2023 angenommen.

Parts of this thesis have been published:

Purcarea A, Jarosch S, Barton J, et al. Signatures of recent activation identify a circulating T cell compartment containing tumor-specific antigen receptors with high avidity. Sci Immunol. 2022;7(74). https://doi.org/10.1126/sciimmunol.abm2077

Table of contents

Table of figures

Abbreviations

ACT	adoptive cell transfer
ACT	ammonium chloride tris
ANOVA	analysis of variance
APC	allophycocyanin
APC	antigen presenting cell
APC-Cy7	allophycocyanin-cyanine 7
APL	altered peptide ligands
BHI	brain heart infusion
BSA	bovine serum albumin
CD	cluster of differentiation
CDU	collagen digestion units
CFU	colony forming unit
CRISPR	clustered regularly interspaced short palindromic repeats
CTL	cytotoxic T lymphocytes
d	dies (day)
dLN	draining lymph nodes
DMEM	Dulbecco's modified eagle medium
DMSO	dimethyl sulfoxide
DNA	deoxyribonucleic acid
DNAse	deoxyribonuclease
DPBS	Dulbecco's phosphate buffered saline
EC_{50}	half maximal effective concentration
EDTA	ethylenediaminetetraacetate
EMA	ethidium monoacid bromide
FACS	fluorescence-activated cell sorting
FCS	fetal calf serum
Fc-Block	fragment crystallizable block
FITC	fluorescein isothiocyanate
FBS	fetal bovine serum
FSC	forward scatter
g	gravitational acceleration or gram
Gy	gray
HCl	hydrogen chloride
hi	high
HPS	hematopoietic stem cells
i.p.	intraperitoneal
i.v.	intravenous
ICCS	intracellular cytokine staining
IFNγ	interferon-γ
IL-2	interleukin-2
K_d	dissociation constant
K_{off}	off-rate
K_{on}	on-rate
L.m.	listeria monocytogenes
LAG-3	lymphocyte-activation gene-3
LCMV	lymphocytic choriomeningitis virus
lo	low
LTα	lymphotoxin α
mCMV	murine cytomegaly virus

MHC	major histocompatibility complex
MIH	institute for medical microbiology, immunology and hygiene
ndLN	non-draining lymph nodes
OVA	ovalbumin
p-value	value for level of significance
PBMC	peripheral blood monocytic cells
PBS	phosphate buffered saline
PCR	polymerase chain reaction
PE	phycoerythrin
PD-1	programmed cell death protein-1
PD-L1	programmed cell death-1-ligand 1
PE-Cy7	phycoerythrin-cyanine 7
PB	pacific blue
PerCP-Cy5.5	peridinin chlorophyll protein-cyanine 5.5
PFA	paraformaldehyde
PI	propidium iodide
Plat-E	Platinum-E
PMA	phorbol myristate acetate
pMHC	peptide-MHC
rpm	revolutions per minute
s.c.	subcutaneous
$t_{1/2}$	half-life time
TBI	total body irradiation
TCR	T cell receptor
tg	transgenic
TIL	tumor infiltrating lymphocytes
TIM-3	T-cell immunoglobulin and mucin-domain containing-3
TME	tumor microenvironment
TNFα	tumor necrosis factor α
T_{reg}	regulatory T cells
TRIS	tris(hydroxymethyl)aminomethane
TXR	texas red
U	Unit
WT	wildtype

1 Introduction

T cells are main mediators of the cellular immune response and thus constitutive to tumor immunity. They are able to directly recognize and subsequently kill tumor cells via their specific T cell receptors (TCR). While the peptide major histocompatibility complex (pMHC)-TCR interaction is believed to be a key determinant of T cell efficacy (Busch & Pamer, 1999; L. J. McHeyzer-Williams et al., 1999), there are diverging data as to which factors enable a successful antitumoral response. On a cellular level, the term TCR avidity comprises the binding strength of several associated TCRs with their pMHC-molecules (Nauerth, Wing, et al., 2016). It is used to characterize the T cell- antigen interaction, thus allowing for conclusions regarding their ability to eliminate the tumor. This study uses k_{off}-rate and functional avidity measurements to identify and characterize antigen-specific TCRs in order to investigate their spatio-temporal distribution and protective capacities in tumors. For this purpose, a unique system of ovalbumin (OVA) specific retrogenic TCRs has been created for single-cell as well as simultaneous transfer experiments into an antigen-specific tumor system. In this setting, it can be shown that lowest numbers of transferred precursor cells suffice for a detectable progeny, identified via flow cytometry and observed tumor control depending on their TCR avidity. Also, certain phenotypes indicating differing levels of T cell activation and/or exhaustion could be distinguished, allowing for identification of highly functional TCRs. Up-regulation of the marker programmed cell death protein-1 (PD-1) outside the tumor could be shown to correlate with highly protective TCRs in our mouse model, thus allowing for identification and recovery of those T cells from peripheral blood.

Identifying T cells with optimal properties for therapeutic application could help development of cellular immune therapies, such as adoptive T cell transfer, which so far have encountered considerable success but also challenges in cancer therapy (June & Sadelain, 2018; Ribas & Wolchok, 2018).

1.1 Background

1.1.1 T Cells

1.1.1.1 Overview

The human immune system consists of an innate as well as an adaptive (acquired) immune response. Both systems include a multitude of cellular and soluble effectors, which together protect the host from infection, toxins and other threats. While lymphocytes can be seen as main mediators of the adaptive immune response, the subgroup of T lymphocytes are responsible for cell-mediated immunity (Murphy & Weaver, 2017c). Those so-called T cells originate from the bone marrow and mature in the thymus. Through positive and negative selection, it is ensured that T cells recognize endogenous structures as such, while limiting their attack to foreign antigens (Kumar et al., 2019). Taking functional aspects into account, there are two main groups of T cells, divided by their surface protein into cluster of differentiation 4 positive ($CD4^+$) or $CD8^+$ cells. Ultimately, these surface markers act as co-receptors, modulating the process of antigen-recognition by T cells and their subsequent activation. This is facilitated via interaction with MHC types I and II, either one being expressed by endogenous cells (Murphy & Weaver, 2017c; Reiser et al., 2000). Those MHC-molecules are used by cells to present self-proteins, as well as foreign products which can result from invasive viral replication or malign transformation. Hence, antigen recognition via T cells is dependent on cellular presentation (Murphy & Weaver, 2017c). As a result, the TCR mediates antigen-specific interaction via both peptide and MHC.

1.1.1.2 T cell receptor

The TCR is a heterodimeric molecule, containing both a glycoprotein alpha and beta chain, traversing the lipid cell membrane of the lymphocytes (Murphy & Weaver, 2017b). While the extracellular component of these chains is made up from a variable and constant region each, they are connected by a disulfide bridge (Al-Lazikani et al., 2000; Murphy & Weaver, 2017b).

During thymic maturation, the process of somatic recombination takes place in the region of genes coding for the TCR (Alanio et al., 2010; Nikolich-Žugich et al., 2004). This results in continuous rearrangement of the genetic material and facilitates the enormous diversity of receptors which distinguishes the human TCR repertoire (Davis & Bjorkman, 1988). It is estimated that this spectrum contains up to 2.5×10^7 different clones (Arstila et al., 1999; Casrouge et al., 2000) in one individual host at a given time point, contributing to a broad repertoire of

antigen specific receptors. Moreover, fine-tuning of T cell immunity is enabled by functional and structural diversity of this system (Nikolich-Žugich et al., 2004). In this context, functional diversity of antigen specific T cells is enabled via differentiation into distinguished cellular phenotypes upon activation (Belz et al., 2001; Echchakir et al., 2002). The structural component on the other hand is defined by somatic recombination of TCR-coding segments during maturation minus thymic selection (Davis & Bjorkman, 1988). Combined, they enable a versatile immune response that is highly coordinated.

1.1.1.3 T cell induced cytotoxicity

In contrast to the before mentioned vast diversity of the TCR repertoire, the number of clones specific for a given antigen before activation is minimal. Their range is estimated to contribute to less than one in 10^5 (Moon et al., 2007; Obar et al., 2008). Therefore, to ensure effective control of pathogenic antigens, those few clones must be mobilized and activated to undergo substantial expansion and proliferation.

It could be shown in infectious models that the recruitment of antigen-specific clones corresponds to a highly efficient process. It thereby seems that a successful immune response depends more on adequate clonal proliferation on antigen presenting level rather than the applied dose of the pathogen (Jeroen W. J. van Heijst et al., 2009).

Once antigen-specific $CD8^+$ T cells are successfully mobilized and activated, they transform into their cytotoxic effector type (CTL). They recognize pathogen-infected, somatic cells via surface peptide-MHC-class-I-molecules (Tscharke et al., 2015). Elimination of target cells is enforced by induced cell death, facilitated by a range of different mechanisms. Among those, the production of cytokines such as interferon-γ (IFNγ) and tumor-necrosis-factor-α (TNFα) plays an important role (Schietinger & Greenberg, 2014). IFNγ, for example enhances MHC-class-I expression while recruiting and activating macrophages. TNFα acts synergistically with IFNγ but is also able to directly induce cell death (Murphy & Weaver, 2017a). Altogether, activated $CD8^+$ T cells in form of CTL are highly potent mediators of the adaptive immune response.

1.1.2 T cell receptor avidity

1.1.2.1 Definition

Interaction of peptide-bound antigen and the TCR is a prerequisite for T cell activation and subsequent pathogen elimination. Besides antigen specifity, the affinity of TCR binding to its

ligand is generally believed to be a key determinant of the T cell response (Busch & Pamer, 1999; L. J. McHeyzer-Williams et al., 1999; Tscharke et al., 2015). For further characterization of this binding, the terms of avidity and affinity are often used synonymously. However, in this context, precise distinction is essential to adequately describe the complexity and consequences that the strength of TCR-pMHC-interaction entails. TCR affinity implies the physical strength to which each TCR binds to a pMHC molecule (Hebeisen, Allard, et al., 2015). TCR avidity on the other hand relates to the association of several TCRs with their pMHC-molecules on a cellular level and is dependent on TCR affinity as well as other factors such as TCR surface-density, co-receptors and T cell activation (Nauerth, Weißbrich, et al., 2013; Nauerth, Wing, et al., 2016). It is comprehensible that this complex synergy requires further differentiation.

Functional avidity is used to describe the antigen-specific TCR-pMHC-interaction in relation to functional properties of the T cell. Thus, *in vitro* characterization includes measurements of proliferation, cytokine production as well as cytotoxic activity (Hebeisen, Allard, et al., 2015; Nauerth, Stemberger, et al., 2016). Hence, functional avidity correlates most accurately to antigen-sensitivity and is a measure of response to an antigen, dependent on its concentration (Dudley et al., 1999; Dutoit et al., 2001). Structural avidity on the other hand is expressed by biophysical measurement of the binding strength of multiple TCRs and their pMHC-molecules (Hebeisen, Schmidt, et al., 2015; Nikolich-Žugich et al., 2004).

1.1.2.2 Measurement and appliance via k_{off}-rate assays

Correlations between high TCR avidity and improved effector function *in vitro* as well as *in vivo* have been shown in several studies (Derby et al., 2001; Dutoit et al., 2001; Zeh et al., 1999) For the purpose of identifying those TCRs, different methods can be applied. Functional assays, such as quantification of cytokine production or *in vitro* cell lysis, are broadly deployed for measuring T cell effector capacities. However, functional properties are not only result of TCR-pMHC-interaction but also influenced by other variables (Nauerth, Wing, et al., 2016).

For a more practicable approach, assays quantifying structural avidity have continuously been further developed and refined. They are mostly based on pMHC multimer staining, allowing conclusions on pMHC binding strength and dissociation kinetics (Busch & Pamer, 1999; Lyons et al., 1996). pMHC staining intensity alone however does not necessarily provide reliable assessment of binding avidity (Nauerth, Weißbrich, et al., 2013).

Potentially more reliable, investigation of TCR-pMHC dissociation kinetics has been shown to be a promising approach. The equilibrium constant K_D is used to describe this dynamic process,

which results from the half-life times values of association (k_{on}-rate) and dissociation (k_{off}-rate) in relation to each other (Nauerth, Wing, et al., 2016). In this context, a low ratio, or rather a long half-life (high k_{off}-rate) correlate with high avidity TCR-pMHC-interaction. Furthermore, those slow dissociation kinetics have been linked to increased T cell functionality as well (Hombrink et al., 2013; Nauerth, Weißbrich, et al., 2013).

However, common pMHC-multimer dissociation assays are susceptible to a range of technical and material associated limitations. Among those are the dependency on efficient multimerization, the fact that the k_{on}-rate is not measured as well as the unknown number of pMHC-molecules expressed on the surface of single T cells and the fraction of which is reached by the multimer (Wang & Altman, 2003).

In order to surpass those limitations, D. H. Busch and colleagues developed a method based on reversible multimers, so called *Streptamers* (Knabel et al., 2002), allowing for the tracking of TCR-pMHC dissociation on a monomeric level on living T cells (Figure 1) (Nauerth, Weißbrich, et al., 2013). In order to do so, antigen-specific $CD8^+$ T cells are multimerized with dichromatic *Streptamer*. A *Strep*-Tactin backbone conjugated with fluorochrome allophycocyanin (APC) is used to assemble multiple MHC-molecules, bound specifically by cellular TCRs, and thus to label the antigen-specific T cell. Addition of D-biotin leads to the displacement of *Strep*-Tactin, leaving only monomeric, bound pMHC-molecules on the cell surface. Their subsequent dissociation is measured by decline of fluorescence intensity of the Alexa Fluor 488 fluorochrome-labeled pMHC-molecules over time. By means of this assay, a correlation between k_{off}-rate and functionality or rather *in vivo* protectivity of T cells could be shown. Up to now, these findings were limited to chronic and acute infectious mouse models (Nauerth, Weißbrich, et al., 2013).

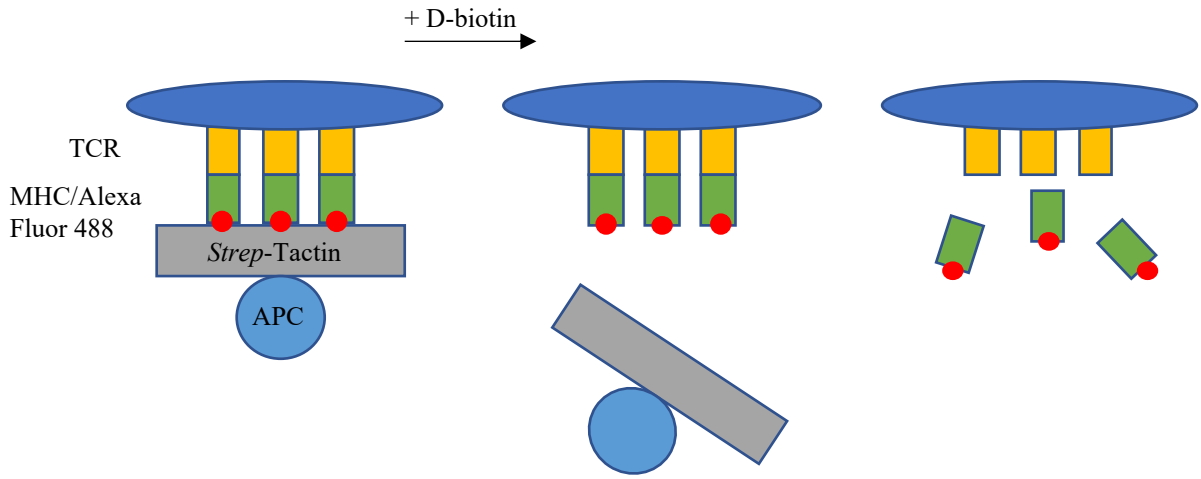

Figure 1 Schematics of k_{off}-rate assay
Surface-bound TCRs bind to dichromatic *Streptamer* consistent of Alexa Fluor 488 linked MHC-molecules bound to a *Strep*-Tactin-APC backbone. Upon addition of D-biotin, *Strep*-Tactin-APC dissolves leaving monomeric MHC-molecules behind. The dissociation of the latter is then registered over time as decay in fluorescence intensity. Adapted from (Nauerth, Weißbrich, et al., 2013).

1.1.3 Tumor immunology

1.1.3.1 Tumor pathogenesis

The term „tumor "derives from Latin and generally stands for swelling of any kind. Upon further discrimination, it is used to describe an abnormal neoplasm of tissue cells as a result of acquired or hereditary genetic dysregulation, leading to cellular proliferation and differentiation (Riede et al., 2017). In this context, a range of cancer hallmarks have been described on molecular as well as cellular level, as postulated in a landmark publication (Hanahan & Weinberg, 2000). These characteristics have found universal application to tumor entities since, and have been adjusted and extended according to new findings in the field (Hanahan & Weinberg, 2011). Among those hallmarks, abilities like angioneogenesis, tissue invasion and metastasis are included, as well as replicative immortality via continuous proliferation signals, insensibility to growth suppressors and induction of apoptosis. Almost ten years later, further hallmarks were added, with a new focus on tumor impacts on and interactions with the cellular immune response. While tumor-associated inflammation is seen as supportive factor for tumor pathogenesis, the ability to evade elimination by the immune system crystallizes as an important characteristic of cancer (Hanahan & Weinberg, 2011). These characteristics do not only serve descriptive purposes but also provide a range of therapeutical targets.

The before mentioned inflammation is being sustained by the so-called tumor microenvironment (TME), which not only includes cancer cells but also a diverse mix of inflammation mediators from the innate immune response: lymphocytes, fibroblasts, endothelial cells and soluble components of extracellular matrix (Hanahan & Coussens, 2012; Quail & Joyce, 2013). Interaction of these constituents within the TME can facilitate recruitment of CTL into the tumor and thus be immunogenic. However, these CTL are also often impaired in their function due to expression of inhibitory co-receptors of those very same TME components (Joyce & Fearon, 2015).

Thus, it becomes clear that the endogenous immune response plays an ambiguous role in cancer, working towards protection as well as potentially facilitating progression. This duality has been recognized by the concept of *immunoediting* (Schreiber et al., 2011).

1.1.3.2 The role of $CD8^+$ T cells – Immunosurveillance vs. Immunoediting

$CD8^+$ T cells are known to be main mediators of the cellular immune response to tumors. This is supported by the considerable clinical success of immunotherapies based on the enhancement of the T cell response in cancer patients (Hodi et al., 2010; Topalian et al., 2014). Furthermore, it has been shown in murine tumor models, that mice lacking a functional cellular immune response were more susceptible to spontaneous and chemically induced tumors (Kaplan et al., 1998). This leads to the conclusion, that T cells should be considered able to recognize tumor antigens presented via MHC-class-I molecules on the surface of tumor cells (Schumacher & Schreiber, 2015).

The perception of the adaptive immune response controlling tumor pathogenesis in immunocompetent individuals, has been postulated in the form of *immunosurveillance* (Burnet, 1957). In this context, an essential role has been contributed to so-called neoantigens (Schumacher et al., 2019). They result from genetic mutation during neoplastic transformation of the tumor cell and can be recognized and targeted by $CD8^+$ T cells analogous to foreign antigens. This is facilitated by the fact that the mechanisms of central tolerance, a state which is achieved via selection processes during thymic maturation, do not apply to neoantigen specific TCRs, since this would lead to the elimination of those highly avide autoreactive T cells (Schumacher et al., 2019). Accordingly, there seems to be a positive correlation between cytolytic activity and thus reactivity of those neoantigen specific T cells in tumor patients and the mutational burden, represented by the amount of neoantigens in the tumor (Rooney et al., 2015).

The fact that tumors are able to evade the host immune response via inhibition of endogenous cellular components finds recognition in the before described concept of *immunoediting* (Schreiber et al., 2011). Here, not solely the protective and thus quantitative contribution of the adaptive immune response to tumor immunity is taken into account, but also the qualitative properties of this interaction mediating tumor immunogenicity.

Furthermore, their understanding of *immunosurveillance* implies a dynamic process, which is characterized by three phases (Schreiber et al., 2011) and whose success depends on the quality of initial tumor control in regard to future development as elaborated in the following paragraph. Thus, if complete tumor elimination on a cellular level during the *elimination phase* cannot be achieved, it is possible that rare, resistant tumor cell clones are selected and persist in a so-called *equilibrium phase*, a sort of inactive stand-by mode. While the tumor cells rest, this state is sustained by continuous regulatory activity of the adaptive immune system, whose mediators apply further selection pressure on the a priori genetically instable tumor. Consequences include the potential development of further cell variants that present altered surface proteins facilitating immunosuppressive interactions with the TME. Overall, according to Schreiber, this could allow for the tumor to elude the adaptive immune response. This phenomenon is described as the *evasion phase*, where immunological control is no longer possible, and the disease progresses to its full extension.

1.1.3.3 T cell exhaustion and PD-1

Recognition of foreign antigens by T cells is normally followed by activation, proliferation and finally differentiation into effector cells, whose cytolytic activity leads to pathogen control and elimination. Simplified, an initial phase of expansion is followed by a drastic contraction of cell numbers, usually caused by programmed cell death of the majority of effector cells (Schietinger & Greenberg, 2014). The residual T cells form the resting memory pool, a population of antigen-specific cells which can undergo massive proliferation upon renewed antigen contact and thus contributes to long-term immunity (Kaech et al., 2002; Obar & Lefranois, 2010).

However, T cell differentiation amounts to a highly complex process and is dependent on the context and nature of antigen-contact. Thus, instead of initializing expansion and attack, activation can also lead to immediate functional impairment or even death of the antigen-specific T cell (Schietinger & Greenberg, 2014).

The term T cell dysfunction is used to describe the inability of antigen-specific T cells to control their target, without enabling conclusions as to the cause or their appearance (Schietinger et al.,

2012; Schietinger & Greenberg, 2014). Central tolerance, as the most original concept of lacking functional responsiveness, implies the necessary tolerance towards self-antigens (Hogquist et al., 2005). T cells should acquire this ability during their central thymic maturation via negative selection (Kumar et al., 2019). In reality, this process is incomplete, leading to a residual number of autoreactive cells to circulate systemically (Schietinger et al., 2012). Thus, it is necessary to prevent those T cells from proliferating and attacking their targets, which would be endogenous structures. This is facilitated by distinctive mechanisms, among which the immunosuppressive properties of so called regulative T cells (T_{reg}), but also the induction of cell intrinsic programs for functional impairment play a role (Schietinger et al., 2012).

Furthermore, loss of function can present as T cell exhaustion, which had foremost been described for chronic lymphocytic choriomeningitis virus (LCMV) infections (Barber et al., 2006; Wherry et al., 2007; Zajac et al., 1998). While acute infection usually results in immediate pathogen control, persisting antigen stimulation in a chronic setting is followed by exhaustion of antigen specific CTL (Freedman et al., 1993). This prolonged antigen exposure ultimately results in the up-regulation of inhibitory receptors, thus introducing the dysfunctional state of the T cell (Thommen & Schumacher, 2018). Characterized as a progressive and long-term process, it usually takes place after initial proliferation and at least partial development of effector capacities (Schietinger & Greenberg, 2014). Hereby, the loss of functional properties occurs hierarchically over the time, resulting in initial decline of the ability to proliferate and the autocrine signaling cascades revolving around IL-2 production, until eventually other essential cytokines such as IFNγ and TNFα are no longer produced (Wherry, 2011; Wherry et al., 2003).

It has been shown that loss of function for T cells in chronic infections is accompanied by the expression of inhibitory co-receptors such as PD-1, lymphocyte-activation gene-3 (LAG-3) and T-cell immunoglobulin and mucin-domain containing-3 (TIM-3) (Blackburn et al., 2009). Here, simultaneous expression of these markers positively correlates with functional exhaustion of antigen-specific T cells and is ultimately linked to prolonged infection (Virgin et al., 2009; Wherry, 2011). Blockage of these receptors on the other hand improves the efficacy of the T cell response and facilitates pathogen elimination *in vivo* (Blackburn et al., 2009), highlighting their pivotal role in T cell dysfunction.

The PD-1 receptor and its ligand programmed cell death-1-ligand 1 (PD-L1) play a central role in T cell exhaustion. This is supported by the possibility of reinvigorating those dysfunctional cells via antibodies blocking the PD-1/PD-L1 axis (so called checkpoint inhibition). Thus, in a clinical setting both antiviral (Day et al., 2006; Petrovas et al., 2006) as well as antitumoral

(Brahmer et al., 2012; Topalian et al., 2014) immune responses could be improved. However, the extent of PD-1 contribution and whether it is essential to exhaustion or not, remains unknown. On the contrary, studies show that in a chronic LCMV infection model T cell exhaustion can occur in the absence of PD-1 (Odorizzi et al., 2015).

PD-1 expression is temporarily upregulated on activated T cells as a physiological process to circumvent immunopathology (Ishida et al., 1992). On the contrary, exhausted T cells that are no longer able to control the infection maintain high levels of PD-1 expression throughout (Barber et al., 2006). On a molecular level, PD-1 is activated after binding its ligand derived from the PD-L family and subsequently inhibits signaling cascades that usually maintain T cell activation (Pardoll, 2012). Additionally, PD-1 displays TCR modulating functions and thus exerts influence on the duration of contact between receptor and target (Fife et al., 2009; Pardoll, 2012). Therefore, upregulation of this receptor could not only associate T cells with a dysfunctional state, but also be an indicator of previous, specific TCR-antigen-interaction.

Since PD-1 expression does not necessarily entail T cell exhaustion, its role is not solely limited to rendering T cells dysfunctional. More accurately, the inhibitory axis of PD-1/PD-L considerably contributes to the reduction of cellular hyperreactivity and autoimmunity, thus preventing cell mediated tissue damage associated with an overwhelming immune reaction. (Odorizzi et al., 2015; Schietinger & Greenberg, 2014)

1.1.3.4 Tumor-induced T cell dysfunction and tumor microenvironment

Similar to chronic infections, T cells among tumor infiltrating lymphocytes (TIL) are exposed to a high, persistent antigen load. Moreover, phenotypical as well as functional analogies to exhausted $CD8^+$ T cells from the chronic infection setting have been described (Fourcade et al., 2010; Zippelius et al., 2004). Among those, upregulation of inhibitory co-receptors such as PD-1, but also the before mentioned gradual loss of effector functions can be found.

A range of immunosuppressive factors are particular to the tumor setting. Tumor cells themselves can mediate T cell dysfunction but often require interaction with the TME. Thus, the different cellular and stromal components of the tumor play an important role concerning local immunosuppression (Fang & DeClerck, 2013; Quail & Joyce, 2013; Rodriguez-Garcia et al., 2021). As already mentioned, the TME consists of a variety of immune cells, such as leukocytes and other tissue resident cells, but also non-cellular, soluble components derived from extracellular matrix. Hanahan and colleagues even postulated that the majority of immunosuppressive and immunoevasive abilities that tumors own are derived from and

maintained by the different classes and subsets of surrounding fibroblasts (Hanahan & Coussens, 2012), cells not traditionally considered partial to the immune response.

Nevertheless, the underlying mechanisms and factors which constitute to this functional impairment of T cells, remain not fully understood. Among those, time point and nature of antigen recognition are believed to be of importance, but also the immunosuppressive properties of the TME, antigen specifity, TCR avidity as well as differential states of the T cell, to name a few (Schietinger & Greenberg, 2014). In conclusion, tumor induced T cell dysfunction seems to encompass a heterogenous spectrum of functional states, influenced by intrinsic as well as extrinsic factors (Thommen & Schumacher, 2018).

1.1.4 Adoptive T cell transfer

Since their clinical introduction, immunotherapeutical approaches have led to notable breakthroughs in cancer therapy. Especially checkpoint-inhibitors as well as chimeric antigen receptor (CAR) T cells have shown considerable success applied to clinical settings and benefitted numerous cancer patients (June & Sadelain, 2018; Ribas & Wolchok, 2018). Those strategies are ultimately based on the ability of T cells to identify and eliminate tumor cells, as described above.

Among those immunotherapeutical, cell-based approaches, adoptive T cell transfer (ACT) and its administration to patients have been of growing interest after promising results in clinical trials. ACT has classically been a personalized therapeutical strategy, since T cells from the patients themselves are being identified and extracted, followed by *in vitro* expansion and subsequent reinfusion in order to combat tumors (Guedan et al., 2019). In 1986, Steven Rosenberg and colleagues were the first to use autologous tumor antigen-specific TILs derived from melanoma patients and observed first successful responses (Rosenberg et al., 1986). Further breakthroughs were achieved by the same group in 2006, when transgenic re-expression of antigen-specific TCRs was used to treat melanoma patients with these genetically modified cell products (Morgan et al., 2006). Nowadays, biotechnological approaches such as the clustered regularly interspaced short palindromic repeats (CRISPR)-Cas9 system allow for extremely precise construction of tumor antigen-specific TCRs *in vitro* and thus open the doors to entirely new possibilities for personalized tumor therapy (Roth et al., 2018; Schober et al., 2019).

The recent FDA (*US Food and Drug Administration*) approval of two distinct CAR-T cell therapies for monoclonal B cell neoplasms in children as well as in adults can be seen as major

landmarks in the field of immunotherapy. Therapies based on TCR-transgenic cell products also seem promising. NY-ESO-1 specific TCRs have shown objective clinical response in different tumor entities and are expected to be approved by the FDA soon (Rapoport et al., 2015; Robbins et al., 2015). In conclusion, immunotherapeutic strategies yield great hope regarding the treatment of cancer patients. Despite considerable clinical success, there remains a number of patients, whose tumors do not respond to ACT. Moreover, and unfortunately so, complete long-term remissions remain rare. Therefore, it is of great interest to investigate the underlying cellular mechanisms, in hope for a better grasp of what defines optimal cell products and the most suitable therapy for each individual patient.

1.2 Scientific issue and models

1.2.1 Scientific issue

TCR affinity for a given antigen is generally known to be an important parameter for the efficacy of the cellular immune response. While improved tumor infiltration has been mostly attributed to high-affinity TCRs (Black et al., 2014; Bos et al., 2012; Janicki et al., 2008; Martínez-Usatorre et al., 2018; Weiss et al., 2012), those T cells specific for tumor antigens seem also to be more prone to exhaustion (Martínez-Usatorre et al., 2018). However, contrary evidence for low-affinity TCRs to preferentially undergo exhaustion in tumors exists (Bos et al., 2012). Interestingly enough, both low- (Caserta et al., 2010) and high-affinity (Allard et al., 2017; Zhong et al., 2013) TCRs have been shown to mediate superior tumor control. Therefore, the influence of TCR binding properties on T cell mediated tumor protection remains subject to further investigation (Hebeisen, Allard, et al., 2015).

High TCR avidity is commonly associated with enhanced effector functions of the T cell, thus, it could be assumed that high TCR avidity generally benefits anti-tumor immunity. Changes in TCR repertoire regarding prevailing affinities have been investigated by K. Schober, F. Voit and colleagues for antigen-specific T cells with different TCR avidities during chronic antigen exposure after murine cytomegaly virus (mCMV) infection (Schober et al., 2020). In this study, TCRs of high avidities were preferentially recruited and expanded upon antigen encounter during early phases of acute infection. However, it could be shown that throughout the course of chronic infection, there seemed to be a shift towards the domination of clones with lower TCR avidity. This late clonal expansion was precedented by the loss of function of high avidity TCR T cells, albeit without signs of classical exhaustion, but rather through a terminally differentiated,

senescent state induced by excessive proliferation. TCRs of lower avidity were less subject to such antigen-driven proliferation, reflected by their functional state and dominance towards the later phases of chronic infection. Since tumors and chronic infections share similarities concerning the evoked cellular immune response especially regarding persisting antigen exposure and T cell dysfunction, an important question is whether similar findings apply to the cancer setting.

Correlations between structural avidity, as quantified by the k_{off}-rate assay, and TCR functionality have been shown for murine models of chronic and acute infection (Nauerth, Weißbrich, et al., 2013). The present study aims to investigate the spatio-temporal fate and protective capacity of T cells with different TCR-MHC-k_{off}-rates and functional avidities in tumors. For this purpose, a murine MC38-OVA tumor model was established and combined with the pre-emptive transfer of ovalbumin peptide-specific transgenic or retrogenic $CD8^+$ T-cells with different TCR avidities. Via transfer of single TCRs, or several thereof in combination, the fate of TCRs with distinct avidities concerning their spatio-temporal distribution during tumor disease could be analyzed. Furthermore, it was aimed to gain insights into the functional states of these antigen specific TCRs both in the tumor and in the periphery. Finally, the ability to control tumors upon MC38-OVA challenge was to be determined depending on structural and functional properties of the transferred TCRs.

1.2.2 Tumor-mouse model and adoptive cell transfer

1.2.2.1 OVA-specific TCRs with different avidities

Ovalbumin (OVA), a well-known and extensively characterized model peptide, is able to induce humoral as well as cellular immune reactions (Beck & Spiegelberg, 1989; Ke et al., 1995). Among the first epitopes to be identified, octapeptide $OVA_{257-264}$ containing the amino acid sequence SIINFEKL, is directly recognized by T cells (Rötzschke et al., 1991). OT-1 transgenic mouse lines produce MHC-class-I-restricted, ovalbumin-specific, $CD8^+$ T cells. These so called OT-1 cells recognize the SIINFEKL peptide presented on H-$2K^b$ with high affinity (Hogquist et al., 1994).

While the TCR-pMHC-interaction of OT-1 cells has been previously characterized, for the present study analyses were combined with a unique system of retrogenic, ovalbumin-specific $CD8^+$ TCRs with different structural and functional avidities towards the OVA epitope H-$2k^b$/SIINFEKL peptide (Figure 2) (Schober et al., 2020). By this means, it was envisioned to

depict the natural, polyfunctional antigen specific TCR repertoire in a more accurate way, thus enabling the investigation and characterization of those TCRs during tumor disease.

In order to generate this panel of TCRs, ovalbumin specific $CD8^+$ T cells were isolated during acute and chronic mCMV infection, which yielded more than 20 different TCRs. It should be noted that biotechnological structure-based approaches allow for synthetic construction of TCRs with different binding strengths towards the same antigen, even achieving supramaximal binding strength and providing a fine-tuned, detailed affinity spectrum (Malecek et al., 2014; Zoete et al., 2013). However, our presented approach has its own, unique benefits, since its depiction of the endogenous, antigen specific TCR repertoire is arguably more physiological.

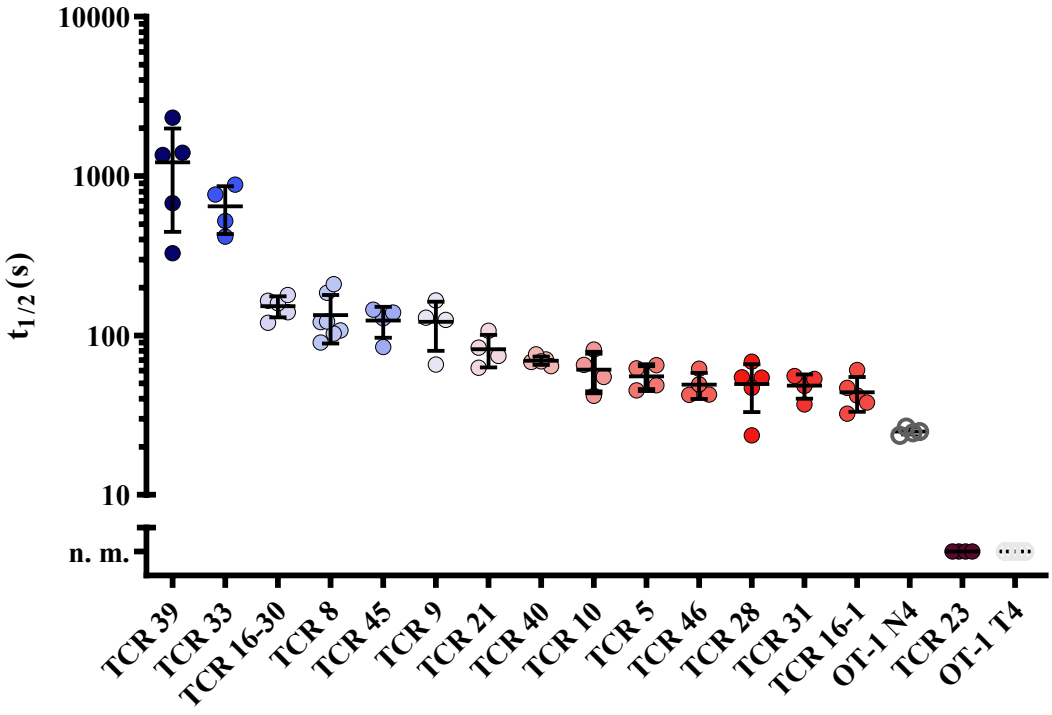

Figure 2 Library of structural avidity of retrogenic TCRs
Spectrum of retrogenic TCRs identified by Kilian Schober and colleagues, displaying different k_{off}-rates quantified by half-life time ($t_{1/2}$) of dissociation. Mean of 2-3 technical replicates depicted for each retrogenic (transgenic for OT-1) donor. n=4-5, representative of at least two individual donor mice in at least two independent experiments. Adapted from (Schober et al., 2020).

For the purpose of *in vivo* TCR re-expression, hematopoietic stem cells were retrovirally transduced to express a distinct TCR and transferred into lymphodepleted recipients, which thus became so-called retrogenic mice (for further details see methods section). After a couple of weeks, retrogenic TCRs could be identified in peripheral blood and submitted to further

characterization. TCR-pMHC-dissociation kinetics were measured using the previously described k_{off}-rate assay, which allowed for a classification of those retrogenic TCRs according to structural avidity. Retrogenic TCRs were also deeply characterized with regard to their functional avidity, as reflected through peptide sensitivity.

1.2.2.2 The MC38-OVA tumor model

MC38-OVA, a well characterized syngeneic murine colon adenocarcinoma cell line (Perez-Ruiz et al., 2019; Singer et al., 2016; Yadav et al., 2014), expresses the ovalbumin SIINFEKL peptide which is subsequently recognized by $CD8^+$ T cells. For the purpose of better quantification of tumor growth, a heterotopic approach was adopted: tumor cells were injected subcutaneously (s.c.) in the right flank of receiving mice, allowing for non-invasive, continuous measurements via a caliper.

The MC38 wildtype tumor is known to be highly immunogenic due to a high mutational burden, thus yielding multiple targets for the endogenous cellular immune response (Hos et al., 2020). However, it has been described for both tumor cells and cellular components of the micro environment to usually express PD-L1, thus facilitating evasion from the endogenous immunological control (Juneja et al., 2017).

Based on the described properties, combined with the expression of ovalbumin as a defined neoantigen and target for T cells, the MC38-OVA tumor setting is an attractive model that allows to investigate the fate of antigen specific T cells and the role of TCR avidity.

1.2.2.3 Adoptive T cell transfer

The physiological frequency of T cells specific for a given antigen in the human repertoire is low, thus challenging the investigation and characterization of those populations during immune responses (M. G. McHeyzer-Williams & Davis, 1995). In order to imitate physiological conditions, the focus of the present study lies on the pre-emptive transfer of lowest cell numbers. Early investigations regarding re-infusion of autologous TILs in melanoma patients show that sustained persistence of transferred cells was only achieved when patients underwent lymphodepletion beforehand (Dudley et al., 2002). Assumably, this process creates better conditions for T cell proliferation and functionality, which in return optimizes the engraftment of the transferred cells (Gattinoni, Finkelstein, et al., 2005; Klebanoff et al., 2005). As another factor for successful engraftment, the differential state displayed by the transferred cells seems to be of importance. While highly differentiated T cells are able to effectively eliminate tumor

cells *in vitro*, they were less suitable for *in vivo* tumor treatment than T cells derived from earlier stages of development (Gattinoni, Klebanoff, et al., 2005). The latter include larger proportions of naïve cells as well as memory cells, which show improved proliferation capacities in the host. Arguably, less differentiated cells are more likely to persist long-term and provide sustainable replenishment of antigen specific CTL, which ultimately mediate tumor control (Guedan et al., 2019).

For this thesis, $CD8^+$, $CD44^{low\ (lo)}$ cells were transferred into recipients following total body irradiation (TBI) with 5 Gy. CD44, a transmembrane glycoprotein commonly associated with T cell activation, is upregulated after antigen specific stimulation and continuously expressed by memory T cells (Budd et al., 1987). Therefore, naïve T cells were distinguishable by low levels of CD44 expression. Myeloablative, non-lethal TBI with 5 Gy was applied for the purpose of lymphodepletion (Gattinoni, Finkelstein, et al., 2005) and conditioning mice for T cell transfer. The next day, tumor inoculation for 10^6 MC38-OVA cells was performed s.c. into the right flank (Figure 3). Tumor growth was monitored over time with measurements by a caliper every two to three days. Mice were sacrificed for organ analyses on different time points.

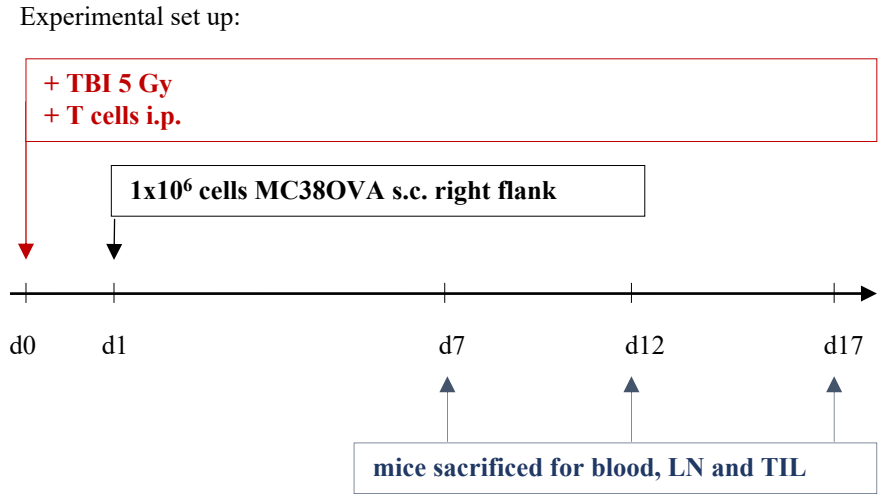

Figure 3 Set up for MC38-OVA tumor experiments and pre-emptive ACT
Mice were irradiated with 5 Gy TBI and treated with T cells intraperitoneal i.p.; followed by injection of 10^6 cells MC38-OVA s.c. (right flank) the next day. Mice were sacrificed for blood, draining lymph nodes (dLN), non-draining lymph nodes (ndLN) and TILs on days (d) 7, 12 and 17. For protection experiments, mice were monitored until termination criteria were reached. Adapted from (Purcarea et al., 2022).

In the present study, two different approaches of ACT were utilized to enable the investigation of the retrogenic TCRs: a single-transfer strategy and a polyclonal transfer setting. The individual

transfer of a single TCR population allowed for the characterization of the respective TCR clone regarding their antitumor protection. In this setting, it was possible to identify the most potent TCRs regarding tumor control. However, in order to identify possible synergistic or complementary effects among TCRs of different avidity, and to provide more physiological conditions, simultaneous transfers of multiple TCRs into the same host were administered. The latter approach also provided more standardized conditions to compare different TCRs with regards to their spatiotemporal distribution side-by-side, as a bias from interhost variability was excluded. Identification of separate TCRs in this setting was possible via distinct congenic marker background according to the congenic matrix previously published by Veit Buchholz and colleagues (Figure 4) (Buchholz et al., 2013). Therefore, retrogenic TCRs were labeled with a unique combination of congenic markers CD45.1/.2 and CD90.1/.2.

A CD90.1/.1 CD45.1/.1	**D** CD90.1/.2 CD45.1/.1	**G** CD90.2/.2 CD45.1/.1
B CD90.1/.1 CD45.1/.2	**E** CD90.1/.2 CD45.1/.2	**H** CD90.2/.2 CD45.1/.2
C CD90.1/.1 CD45.2/.2	**F** CD90.1/.2 CD45.2/.2	**recipient** CD90.2/.2 CD45.2/.2

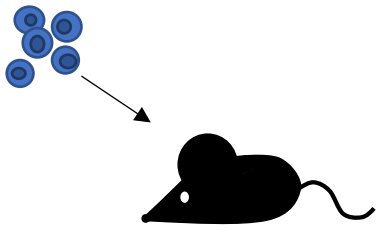

Figure 4 Scheme for the congenic matrix
Identification of transgenic cells via the combination of four different alleles of CD45 and CD90, resulting in nine unique combinations. Table representing possible genotypes of OT-1 donor mice (A-H) and C57Bl/6 WT. Adapted from (Buchholz et al., 2013).

1.3 Translational relevance

Antigen-specific T cells are essential mediators of the antitumoral immunity, recognizing tumor cells via their TCR. Understanding the role of the TCR amid T cells interacting with neoplastic cells is vital for further development of immunotherapeutic strategies. This notion is supported by the clinical success shown by therapeutic transfer of genetically modified T cells (Rapoport et al., 2015; Robbins et al., 2015) which is further supported by emerging technical advances for construction of customized TCRs (Malecek et al., 2014; Zoete et al., 2013) to combat cancer. Further insights should improve predictability of the engraftment and fate of those transferred cell products and thus allow for a better prognosis of patient responses. Furthermore, *de novo* identification of TCRs with optimal properties regarding tumor protectivity needs to be facilitated.

TCR affinity constitutes an important parameter of the pMHC-TCR-interaction, considerably influencing T cell activation, expansion and finally functionality (Aleksic et al., 2010; King et al., 2012). It is well known that TCR avidity is an important determinant of successful ACT. Applicational aspects are not limited to the identification of highly avide TCRs. In fact, the complex interaction of a multitude of antigen-specific T cells of different TCR avidities has to be investigated, always taking into consideration the constantly changing and merging functional states of T cells, as well as immunosuppressive properties of the surrounding TME.

The idea of investigating the fate of a panel of antigen-specific T cells with different TCR avidities in tumors is not necessarily new and has already been attempted. One study for example made use of a system consisting of seven TCRs specific for melanoma antigen gp100(209-217) with different affinities, in order to establish a connection between TCR affinity and tumor control (Zhong et al., 2013). Other studies included humanized mouse models for self-antigens (Black et al., 2014; Weiss et al., 2012) or the transfer of monoclonal cells for analysis of T cell fate (Allard et al., 2017; Zhong et al., 2013).

The novelty of the present study lies in the combination of a syngeneic (biologically meaningful) mouse model, the use of a comprehensive neo-epitope (ovalbumin) targeting TCR library and by the already mentioned simultaneous transfer of different avidities into the same host. These circumstances allow for a more authentic recreation of the natural polyclonal TCR repertoire (Shao et al., 2014; Sherwood, 2017; Sims et al., 2016), depicting its range of specific TCR avidities for a given antigen. Moreover, this approach facilitates a more profound analysis of tumor-specific T cells on a cellular level, by correlating properties of individual TCRs with their

phenotypic and spatiotemporal distribution as part of a polyclonal population. Finally, a compelling strength of this study is the transfer of extremely low T cell numbers, thereby still allowing for investigation of tumor protectivity and immunomonitoring. While other studies involved transfers of several millions of cells (Gattinoni, Klebanoff, et al., 2005; Sussman et al., 2004; Zhong et al., 2013), here it was aimed to titrate cell numbers to a minimum. Thus, the naturally low frequencies of antigen specific cells in the immune repertoire (Buchholz et al., 2013; Obar et al., 2008; Stemberger et al., 2014) could be imitated allowing for a more physiological and representative setting.

Overall, those optimized conditions could allow for further insights on synergistic interactions of the various mediators involved in antigen-specific T cell responses and thus facilitate a more profound understanding of the complex cellular relationships contributing to antitumoral immunity.

2. Material and methods

2.1 Material

2.1.1 Reagents and resources

Chemicals, Peptides and Enzymes	Supplier
Alexa Fluor 488 maleimide	Molecular Probes, Leiden, The Netherlands
Ammonium chloride (NH_4Cl)	Sigma-Aldrich, Taufkirchen, Germany
Bovine serum albumin (BSA)	Sigma-Aldrich, Taufkirchen, Germany
Collagenase from Clostridium histolyticum	Sigma-ALdrich, Taufkirchen, Germany
Cytofix/Cytoterm	BD Biosciences, Heidelberg, Germany
D-biotin	Sigma-Aldrich, Taufkirchen, Germany
Deoxyribonuclease I from bovine pancreas	Sigma-Aldrich, Taufkirchen, Germany
Dimethyl sulfoxide (DMSO)	Sigma-Aldrich, Taufkirchen, Germany
Ethanol	Klinikum rechts der Isar, Munich, Germany
Ethidium Monoacid Bromide (EMA)	Life Technologies, Carlsbad, USA
Fetal calf serum (FCS)	Biochrom, Berlin, Germany
Gentamycin	GibcoBRL, Karlsruhe, Germany
Gibco Dulbecco's modified eagle medium (DMEM)	Fisher scientific, Waltham, USA
Gibco Trypsin-EDTA (0.25%)	Fisher scientific, Waltham, USA
Golgi-Plug	BD Biosciences, Heidelberg, Germany
Hydrogen chloride (HCl)	Roth, Karlsruhe, Germany
Heparin-Natrium 25 000 I.E/5ml	Ratiopharm, Ulm, Germany
HEPES	GibcoBRL, Karlsruhe, Germany
Ionomycin (IONO)	Sigma-Aldrich, Taufkirchen, Germany
L-Glutamine	GibcoBRL, Karlsruhe, Germany
Natrium hydroxide (NaOH)	Roth, Karlsruhe, Germany
Penicillin	Roth, Karlsruhe, Germany
Percoll	GE Healthcare, Chicago, USA
Perm Wash	BD Biosciences, Heidelberg, Germany
Phorbol 12-myristate 13-acetate (PMA)	Sigma-Aldrich, Taufkirchen, Germany
Propidium Iodide (PI)	Life Technologies, Carlsbad, USA
Recombinant murine IL-6 Recombinant	PeproTech, Shenzhen, China
Recombinant murine SCF Recombinant	PeproTech, Shenzhen, China
RetroNectin	Takara Bio Europe, Göteborg, Sweden
RPMI 1640	GibcoBRL, Karlsruhe, Germany
Sodium ethylenediaminetetraacetic acid (Na-EDTA)	Sigma-Aldrich, Taufkirchen, Germany
Strep-Tactin-Allophycocyanin (APC)	IBA, Göttingen, Germany
*Strep*tavidin-Phycoerythrin (PE)	IBA, Göttingen, Germany
Streptomycin	Sigma-Aldrich, Taufkirchen, Germany
Tris-hydrochloride (Tris-HCl)	Roth, Karlsruhe, Germany
Trypan Blue solution	Sigma-Aldrich, Taufkirchen, Germany

Antibody	Clone	Supplier
aCD19 PE-CF594	6D5	BioLegend, San Diego, USA
aCD27 PE	LG7.F9	Life Technologies, Carlsbad, USA
aCD44 FITC	IM7	BioLegend, San Diego, USA
aCD45.1 FITC	A20	BioLegend, San Diego, USA
aCD45.1 PE	A20	BioLegend, San Diego, USA
aCD45.1 PerCP-Cy5.5	A20	BioLegend, San Diego, USA
aCD45.2 Pacific Blue	104	BioLegend, San Diego, USA
aCD45.2 PerCP-Cy5.5	104	BioLegend, San Diego, USA
aCD62L APC	MEL-14	BioLegend, San Diego, USA
aCD62L PE-Cy7	MEL-14	BioLegend, San Diego, USA
aCD8a Pacific Blue	53-6.7	BioLegend, San Diego, USA
aCD8a Pacific Orange	5H10	LifeTechnologies, Carlsbad, USA
aCD8a PE-Cy7	53-6.7	BioLegend, San Diego, USA
aCD90.1 APC	HIS51	Life Technologies, Carlsbad, USA
aCD90.1 FITC	HIS51	Life Technologies, Carlsbad, USA
aCD90.1 PE	HIS51	Life Technologies, Carlsbad, USA
aCD90.2 APC-eF780	53-2.1	Invitrogen, Carlsbad, USA
aIFNγ APC	XMG1.2	Life Technologies, Carlsbad, USA
aIL2 PE	JEs6-5H4	Life Technologies, Carlsbad, USA
aLAG-3 APC	eBioC9B7W	Life Technologies, Carlsbad, USA
aPD-1 FITC	J43	Life Technologies, Carlsbad, USA
aSca1 PE-Cy7	D7	Life Technologies, Carlsbad, USA
aTIM-3 PE-Cy7	B8.2C12	BioLegend, San Diego, USA
aTNFa PE-Cy7	Mp6-XT22	BD Biosciences, Heidelberg, Germany

Bacterial strains	Source
Listeria monocytogenes-OVA	MIH Munich, Germany

Cell lines	Source
MC38-OVA	Kind gift of Wolfgang Uckert
PancOVA	Kind gift of Max Schnurr
Platinum E cells	Cell Biolabs, San Diego, USA

MHC Multimer
H2-Kb Strep-tagIII/mβ2m cys67 Alexa488/ OVA 257−264-Strep-Tactin-APC
H2-Kb/mβ2m/Ova 257-264 Streptavidin-PE/APC

2.1.2 Non-reusable material

Plastic	Supplier
6-, 24-, 48- and 96-well plates (U-, flat bottom)	Corning, Corning, USA
70 µm Nylon Cell Strainer	Corning, Corning, USA
96-well plates FACS (V-bottom, non-sterile)	Josef Peske GmbH & Co. KG, Aindfing-Arnhofen, Germany
Eppendorf tubes (1,5 ml, 2 ml)	Eppendorf, Hamburg, Germany
FACS tubes 1,2 ml	Starlab, Hamburg, Germany

Plastic	Supplier
FACS tubes 5 ml	Corning, Corning, USA
Falcon Tube CELLSTARR (15 ml, 50 ml)	Greiner bio-one, Kremsmunster, Austria
Filter tips (10 µl, 20 µl, 200 µl, 1000 µl)	Starlab, Hamburg, Germany
Minisart Syringe Filters (0,45 µm)	Sartorius, Gottingen, Germany
Petri-dish 60 mm	Corning, Corning, USA
Serological pipettes (2 mL, 5 mL, 10 mL, 25 mL)	Greiner Bio-one, Frickenhausen, Germany
Sterican Cannulae (Gr. 18, 20)	Braun, Melsungen, Germany
Syringe 1 mL Sub-Q	BD, Franklin Lakes, USA
Syringes (1 ml, 5 ml, 10 ml, 20 ml)	Braun, Melsungen, Germany

2.1.3 Buffers and solutions

Buffers and solutions	Content
Ammonium chloride Tris (ACT)	0,17 M NH4Cl 0,3 M Tris-HCl, pH 7,5
cDMEM	1x DMEM 10% (v/v) FCS 5% (v/v) SC+
D-biotin 10 M stock solution	244.31 g D-biotin ad 100 ml H2O, pH was brought to pH 11 to facilitate solution of D-biotin, then back to pH 7
FACS buffer	1x PBS 0.5% (w/v) BSA 1.65% (v/v) NaN3 pH 7,45
$RP10^{+}$ cell culture medium	1x RPMI 1640 10% (v/v) FCS 5% (v/v) SC
Supplement complete (SC+) in 1L DMEM	1ml β-Mercaptoethanol 20 ml Gentamicin 23.83 g HEPES 4 g L-Glutamine 200 ml Penicillin/Streptomycin

2.1.4 Equipment

Equipment	Model	Manufacturer
Flow cytometer	CyAn ADP	Beckman Coulter, Fullerton, USA
	MoFlo Legacy Cell Sorter	Beckman Coulter, Fullerton, USA
	FACSAria III	BD Bioscience, Heidelberg, Germany
Microscope	Axiovert S100	Carl Zeiss, Jena, Germany
	Leica SP 5	Leica, Bensheim, Germany

Equipment	Model	Manufacturer
Centrifuges	Biofuge fresco	Heraeus, Hanau, Germany
	Multifuge 3 S-R	Heraeus, Hanau, Germany
	Sorvall® RC 26 Plus	Heraeus, Hanau, Germany
	Varifuge 3.0RS	Heraeus, Hanau, Germany
	Biofuge stratos	Heraeus, Hanau, Germany
Incubators	Cytoperm 2	Heraeus, Hanau, Germany
	Minitron	Infors, Bottmingen, Switzerland
	BE 500	Memmert, Schwabach, Germany
In vitro tumor killing device	xCELLigence®	Roche/ACEA Biosciences
Flow cytometry-based koff-rate cooling device		Qutools, Munich, Germany
Laminar flow hood	HERA safe,	Heraeus, Hanau, Germany
Hemocytometer	Neubauer chamber	Schubert, Munich, Germany
Photometer	BioPhotometer	Eppendorf, Hamburg, Germany
Bench pH/mV meter	MultiCal® pH 526	WTW, Weilheim, Germany
Precision weighting balance	CP 124 S	Sartorius, Göttingen, Germany

2.1.5 Mice

Mice used for *in vivo* tumor experiments were female C57BL/6JOlaHsd mice, usually aged six to eight weeks, purchased from ENVIGO. SIINFEKL peptide-specific TCR transgenic, OT-1 (C57Bl/6-(transgenic)Tg(TcraTcrb)1100Mjb/J) mice, also females aged 6-24 weeks, were originally acquired from The Jackson Laboratory and were bred under specific, pathogen free conditions in the animal facility of the Technical University of Munich. Different combinations of congenic background markers CD45.1/.2 and CD90.1/.2 were created in own breeding (Buchholz et al., 2013). Animal trials were approved by the district government of upper Bavaria (Department V – Environment, Health and Consumer Protection).

Organisms/ strains	Supplier
C57Bl/6JOlaHsd	Envigo, Rossdorf, Germany

2.1.6 Software and algorithms

Software and algorithms	Supplier
FlowJo V10	Treestar, Ashland, USA
Microsoft Excel	Microsoft, Redmond, USA
Prism 8	GraphPad Software, La Jolla, USA
RTCA Software 2.0	ACEA Bioscience, San Diego, USA

2.2 *In vivo* Tumor experiments

2.2.1 Cell lines and cell culture

MC38-OVA, a murine colon adenocarcinoma cell line expressing surface ovalbumin peptide derived from C57BL/6 mice, was used for in vivo tumor experiments. Cells were cultured in T25 cell culture flasks at 37 °C in cell culture medium (if not otherwise specified, always cDMEM). For optimal growth conditions, cells were regularly splitted in a ratio of 1:10, resuspended in fresh medium and transferred to new containers. This process involved removal of consumed medium while remaining adherent cells were incubated with 1 ml trypsin for five minutes at 37°C. Incubation was stopped with 9 ml fresh medium. The cell suspension created was then returned into cell culture or further processed for in vivo tumor experiments. Cell counting was performed for 10 µl cell suspension in 80 µl phosphate buffered saline (PBS) and 10 µl trypan blue resulting in a ratio of 1:10 and counted under an optical microscope. Cell viability was determined by exclusion of the trypan dye, while dead cells with compromised membranes were stained blue (Chan et al., 2020).

2.2.2 Tumor inoculation

Recipient mice were injected with 10^6 MC38-OVA cells s.c. in the right flank. For this purpose, cultured cells were splitted two to three days in advance, optimally reaching 70% adherence on the day of injection. Processing of cells was performed as described above. MC38-OVA cells were resuspended in sterile PBS in a concentration of $5x10^6$/ml and transferred to polystyrene round-bottom tubes. The smooth surface of these tubes prevented adherent cells from sticking to the wall of their containers and thus minimized cell loss. Mice were labeled by holes punched in their ears following a distinct identification system. Then, they were injected with 200 µl of the prepared cell suspension, amounting to 10^6 MC38-OVA cells per mouse. Injections were performed in the right flank, successful s.c. application was indicated by a visible fluctuating tumor beneath the skin.

2.2.3 Tumor growth

Tumor growth was measured at least two times per week, normally every two to three days by caliper. Animals were monitored and scored according to their well-being and behavior. Physical aspects such as significant weight loss or visibly fluid gathering of the intraperitoneal cavity in the sense of ascites were also included. Tumor size was calculated via product of two orthogonal

diameters. Immediate termination criteria were reached by tumor size more than 15 mm x 15 mm or superficial ulceration of the tumor.

2.2.4 Organ processing and analysis

Organ analyses were performed at determined time points. Usually, mice were bled before they were sacrificed by neck fracture and then dissected.

2.2.4.1 Peripheral blood and red blood cell lysis

Bleeding was performed by buccal puncture of the facial vein by lancet and collecting the sample in Eppendorf containers pretreated with 20 µl heparin in order to prevent blood from clotting. Red blood cell lysis was performed in two steps, always at room temperature, including a first incubation in 10 ml ACT for 10 min followed by centrifugation at 1500 revolutions per minute (rpm) for 8 min at 20°C. After the supernatant was removed, cells were resuspended in 5 ml ACT for 5 min. Lysis was then stopped with 5 ml cDMEM and cells were washed in fluorescence-activated cell sorting (FACS) buffer. Further processing was performed at 4° C on ice.

2.2.4.2 Spleens

Spleens were removed after euthanasia of the donor mice, by subcostal marginal incision with a scalpel and then carefully extracted by forceps. Splenocytes and mashed through 70-µm cell strainers and then washed in PBS. Erythrocyte lysis was performed in 5 ml ACT for 5 min at room temperature, then stopped with 5 ml of medium. Cell numbers were then counted by optical microscopy, usually in a ratio of 1:20, thus 10 µl cell suspension added to 180 µl PBS and 10 µl trypan blue. Volumes with required cell numbers were then resuspended with FACS buffer and stored on ice for further processing.

2.2.4.3 Lymph nodes

Axillary and inguinal lymph node packets were identified via anatomical landmarks and removed for both tumor draining and non-draining site. Lymph nodes were recovered by forceps and laid free from soft tissue. The next step involved mashing the lymph nodes through 40-µm cell strainers, followed by resuspension in FACS buffer and storage on ice awaiting further steps.

2.2.4.4 Tumor

The tumor was identified macroscopically s.c on the right flank and carefully removed by forceps (Figure 5). Large tumors presented the challenge of identifying inguinal draining lymph nodes, which had to be separated.

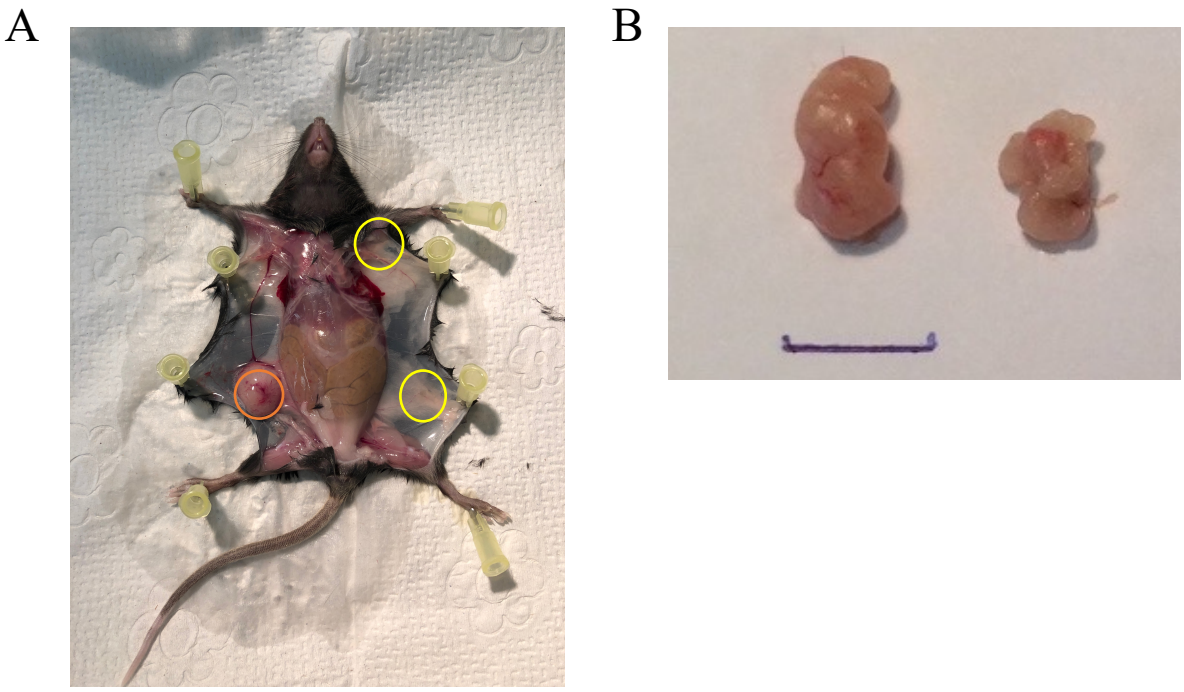

Figure 5 Tumor preparation
A.) Murine site with tumor s.c. on right flank (encircled orange). Mice were dissected by initial median skin incision and separating skin from peritoneum thus exposing the tumor. Lymph nodes were collected both axillary and inguinal (encircled yellow) B.) Tumor macroscopy (scale 1 cm).

Tumors were initially scaled, then mechanically disaggregated by scalpel and enzymatically digested with collagenase type VIII (125 collagen digestion units (CDU)/mg) and deoxyribonuclease (DNAse) I (2000 U/mg) for 60 min at 37°C. Final concentrations for the enzyme mix were 1 mg/ml collagenase and 100 ug/ml DNAse, which could be premixed and remain stable stored at 4° C for one to two weeks.

Tumor cell suspensions were passed through a 70 µm cell strainer and then washed in PBS. Lymphocytes were enriched by a Percoll density gradient (40% vs. 80%). For this purpose, Percoll was mixed with PBS for the required concentration. Tumor samples were resuspended in 4 ml of 40% Percoll and 4 ml of 80% Percoll were slowly pipetted via Pasteur pipettes on the bottom of the falcons. Thus, the lower density Tumor suspension was pushed above the higher density mix and two phases were created. The samples were then centrifuged at 3600 g for 20

min at 20°C, which lead to the enrichment of lymphocytes in an intermediate phase. Importantly, centrifugation was performed at reduced acceleration speed and without abrupt break in order to avoid mixing of the phases. A volume of 1 ml was carefully removed from this intermediate phase and washed in 9 ml of PBS. Finally, cells were washed in FACS buffer for subsequent surface staining.

2.2.5 Antibody surface staining

Staining of surface proteins was performed by incubation with fluorescent antibodies. First, created single cell suspensions for the different organs were transferred into a 96-well V-bottom plate and washed 1.5 times in FACS buffer. The desired antibody mix was prepared in volumes of 50 µl FACS buffer for every $5x10^6$ cells following antibody dilutions suggested by the manufacturer. Samples were resuspended with the antibody mix and incubated for 30 min on ice in the dark. Propidium iodide (PI) was added for living/dead staining for the last 5 min of incubation in a ratio of 1:100. Thus, unspecific antibody binding by dead cells could be excluded from analysis. After incubation, samples were washed 2.5 times in FACS buffer to remove superfluous antibodies. All following steps now had to occur at 4°C under exclusion of light in order to preserve fluorescent potential.

2.2.6 Flow cytometry

Preceding FACS analysis, samples were filtered through nylon meshes to avoid clogging of the flow cytometers. The CyAn ADP 9 color device required transfer into FACS tubes for read in, while analysis with the Cytoflex S flow cytometer allowed for plate read in. Calibration of lasers was performed by recording unstained and single-color samples. Finally, the FlowJo software was used for analysis.

2.2.7 *In vivo* T cell transfer

T cells for adoptive transfer were either extracted from peripheral blood or spleens of the donor mice, the latter yielding higher cell numbers if required. Since retrogenic mice showed a variable engraftment of retrogenic cells depending on factors such as transduction efficacy, major experiments often required for euthanasia and harvesting of the spleen. Furthermore, if not otherwise specified, adoptive transfer experiments included preparation of a wildtype (WT)

female C57BL/6 mouse for feeder splenocytes. All steps were performed in sterile conditions under a laminar flow hood.

Peripheral blood and spleens were processed as described above, by red blood cell lysis and creation of single cell suspensions, followed by regular surface staining. Samples were then washed 1.5x times in FACS buffer and finally filtered into fresh 15-ml-falcons for cell sort. Sorting of $CD19^-$, $CD8^+$, $CD44^{lo}$ cells was performed by the MoFlo legacy device in volumes of 200 µl fetal calf serum (FCS) into 96-well V-bottom plates. Those plates were pre-treated with $4x10^5$ murine splenocytes per well, serving as feeder cells for the nourishment and optimal engrafting of T cells. Immediately after sorting, T cells were injected i.p. into recipients.

2.3 Generation of retrogenic OVA-specific TCRs

2.3.1 Identification of OVA-specific TCRs

Retrogenic $CD8^+$ T cells with SIINFEKL-specific TCRs of different avidities were used for cell transfer experiments. Those TCRs were originally identified during an IE2 $OVA_{257-264}$ mCMV infection by Kilian Schober. Antigen-specific TCRs were then isolated via single cell sort, the material amplified by polymerase chain reaction (PCR) and finally sequenced. Thus, a library of more than 20 distinctive OVA-specific αβ -TCRs could be created.

2.3.2 Generation of retrogenic mice

The generation of retrogenic mice with distinctive congenic marker background (Buchholz et al., 2013) was performed according to existing protocols (Holst et al., 2006) with minor variations, in co-operation with Simon Grassmann, Ludwig Pachmayr, Justin Leube, Joel Eggert and Sophie Flommersfeld (Figure 6). All steps were performed under sterile conditions.

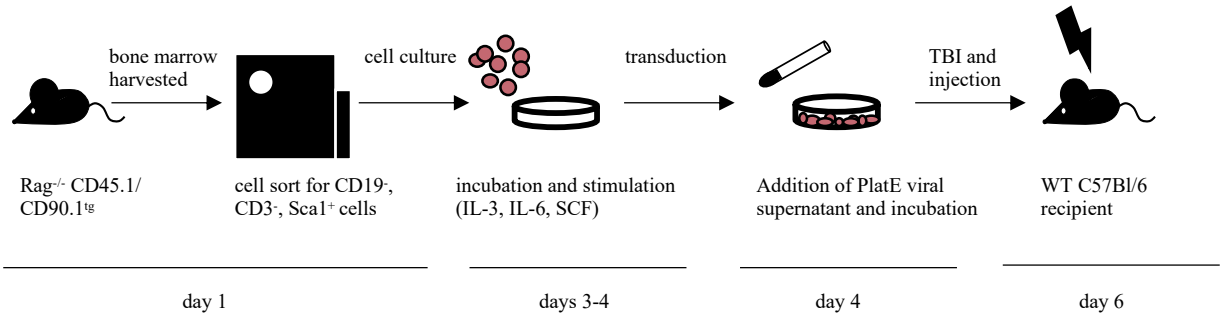

Figure 6 Generation of retrogenic mice
Bone marrow from Rag$^{-/-}$ CD45/CD90^{tg} donor mice was harvested and HPS isolated via purity sort. Subsequently, HPS were incubated and expanded in stimulative medium over several days. Retroviral transduction was performed with supernatants from virus producing, stable PlatE cells. Injection of transduced TCR-expressing HPS into recipients was preceded by two rounds of TBI with 4.5 Gy.

2.3.2.1 Virus production

Stable, virus producing cell lines for retroviral transduction were kindly provided by Simon Graßmann. Those adherent Platinum-E (PlatE) cells were cultured in cDMEM at 37 °C and regularly splitted in a ratio of 1:5 for optimal growth conditions. Originally, they had been transfected with retroviral vectors (mp71, kindly provided by Wolfgang Uckert) via calcium phosphate precipitation, that coded for a respective SIINFEKL-specific TCR. The produced virus then contained both alpha and beta chain of the desired TCR and could be extracted from supernatants 48 h and 72 h post transfection.

For this purpose, PlatE cells were cultured in cell culture medium until a dense cell layer had formed. Supernatants were carefully removed and collected in 15 ml vials. Samples were then centrifuged at 1500 rpm for 7 min at 20 °C to remove solid cell particles. Supernatants were again removed and held in storage for maximal four weeks at 4 °C.

2.3.2.2 Bone marrow preparation

To avoid distortion by endogenous TCRs and to guarantee expression of a single TCR, T cell deficient Rag$^{-/-}$ mice served as bone marrow donors (Kong et al., 2019). Moreover, mice were CD90.1/CD45.1 transgenic, allowing for labeling cells with a unique combination of those congenic markers (Buchholz et al., 2013).

In order to harvest bone marrow, donor mice aged 8-20 weeks were sacrificed and bones of the lower extremities were exposed. Bone cavities were opened, and bone marrow flushed with cell culture medium. Red blood cell lysis was performed with 3 ml ACT and stopped with medium

after three minutes. For subsequent surface staining, single cell suspensions were washed in FACS buffer.

2.3.2.3 Cell sorting and incubation

Hematopoietic stem cells (HPS) were sorted via surface protein *aLy6A/E* (*Sca1)*, while removing more differentiated $CD19^+$ and $CD3^+$ cells, thus purifying the cell suspension. Dead cells were removed by PI living/dead staining (1:100) right before cell sorting, increasing the number of expandable HPS for transduction. After cell sort, HPS were treated with stimulation medium for three to four days in concentrations of approximately $3x10^5$ per well in a tissue treated 48-well plate at 37° C.

Stimulation was performed by adding a combination of cytokines to cell culture medium, namely Interleukin-3 (1:5000) and both Interleukin-6 and Stem-cell-factor (SCF) in a ratio of 1:200. Preparing for transduction, HPS were splitted according to the density of cell layer formed after expansion, to ensure optimal growth conditions. Furthermore, wells were covered with RetroNectin according to producer's instructions in order to enhance virus-stem-cell interaction while reducing unspecific background protein-protein reactions.

2.3.2.4 Transduction

Supernatants containing the produced virus were removed as described above and transferred in volumes of 400 µl to mentioned wells pre-treated with RetroNectin. Then, for the purpose of spinoculation, the plate was centrifuged for 2 h at 3000 g at 32° C. In the meantime, HPS were washed in PBS and resuspended once again in stimulation medium. After centrifugation, a volume of 200 µl supernatant was carefully removed in order to leave the settled virus in the wells. HPS were added in a volume that resulted into the 1:1 ratio of cell suspension and virus supernatant. The next step included further centrifugation, this time for 90 min at 800 g at 32° C. Finally, the plate was incubated for 48 h at 37° C.

In order to verify transduction efficiency, remaining virus supernatants were used for mock transduction of 58 αβ-cells. Those cells lack both TCR alpha and beta chains, therefore indicating successful transduction after staining for respective structures followed by flow cytometric identification.

2.3.2.5 Transfer of transduced hematopoietic stem cells

Following incubation, each well was thoroughly flushed with PBS in order to avoid wasteful residues and minimize loss of HPS. The cells were washed in PBS and resuspended in filtered FCS, then immediately injected into recipients. In order to condition recipients for transfer, mice were irradiated with 4.5 Gy TBI twice, the second dose being applied approximately 6 h later. Recipients received HPS i.v. in a volume of 200 µl, applied to the tail vein. Depending on requirement, both C57BL/6 wildtype and $Rag^{-/-}$ mice were used. While T cell deficient $Rag^{-/-}$ mice ensured the expression of a single, desired TCR, wild type mice proved to be more robust and were more easily obtained.

Mice were regularly monitored and scored for their well-being. After approximately one month, mice were bled and analyzed for the engraftment of the desired cell population. A successful transduction was indicated by the identification cells by antibody surface staining and flow cytometry.

2.4 Characterization of retrogenic TCRs

2.4.1 Peptide-MHC (pMHC) multimer staining

pMHC-molecules for the generation of reversible multimers (*Streptamers*) were backfolded and multimerized as previously described (Nauerth, Weißbrich, et al., 2013). Biotinylated pMHC-molecules were used for the creation of non-reversible multimers (Busch et al., 1998). The creation of both pMHC-molecules mostly followed mentioned protocols and was performed by a cooperation of Anna Hochholzer, Bianca Weißbrich, Manuel Effenberger and Florian Voit.

Non-reversible multimer staining included preparing a mix of 5 µg Streptavidin-PE or Streptavidin-APC in 50 µl FACS Puffer for $5x10^6$ cells respectively, followed by incubation and thus multimerization for at least 30 min on ice in the dark. The multimerized mix was then added to the samples and incubated for another 30 min on ice. After 10 min, antibodies for the regular surface staining were added for the remaining 20 min. Living/dead staining was performed with PI (1:100) for the last 5 min.

Reversible *Streptamer* staining was based on a multimer mix, created from 1 µg Alexa-Fluor-488-conjugated pMHC I molecules (Strep-tagIII/mβ2m cys67) and 0.75 µg *Strep*-Tactin-APC in 50 µl FACS buffer for $5x10^6$ cells respectively. Again, multimerization required an incubation for 30 min minimum on ice. The multimer mix was then added to the samples and incubated for

another 45 min on ice. Antibodies for surface staining were added 25 min into incubation and living/dead staining was performed as described above.

Flow cytometric TCR-pMHC k_{off}-rate measurements (see below) involved a double staining of the unsorted single cell suspensions with both reversible and non-reversible multimer. *Streptamer* staining was performed as described above, while incubation with non-reversible multimer was reduced to 10 min. Thus, the identification of the target population was guaranteed.

2.4.2 k_{off}-rate measurements

Structural characterization of the isolated retrogenic TCRs was performed by a co-operation of Kilian Schober, Joel Eggert and Sebastian Jarosch via k_{off}-rate measurements.

Flow cytometric analysis of k_{off}-rates from TCR ligands was achieved as previously described (Nauerth, Stemberger, et al., 2016). To summarize, samples were transferred into pre-cooled FACS tubes, containing FACS buffer in a volume of 1 ml, which again were placed in a Peltier cooling device (qutools GmbH) at exactly 5.5 °C. After flow cytometric recording for 30 s, 1 ml of a cooled 2 mM D-biotin solution was added while measurements continued, resulting in overall 15 min of recorded dissociation kinetics. In order to analyze the k_{off}-rate data, decaying fluorescence intensity of dissociating MHC-multimer$^+$ T cells was exported from FlowJo to GraphPad Prism. Dissociation half-live times were quantified via monophasic exponential curves of decay.

2.4.3 Functional analysis

2.4.3.1 *Listeria monocytogenes*-OVA infections

Recombinant *listeria monocytogenes* expressing the surface peptide ovalbumin SIINFEKL (*L.m.*OVA) were stored in bacterial aliquots at -80 °C. Prior to infections, aliquots were defrosted for 15 min and the bacterial suspension in a volume of 15 µl was incubated in 4 ml brain heart infusion (BHI) medium for approximately 4-5 h at 37 °C. Titration of bacteria numbers was based on photometric concentration measurements.

For photometric calibration, pure BHI medium was used, followed by measurement of 1 ml of bacterial suspension. In order to reliably calculate concentrations, OD_{600} values between 0.05-0.1 were targeted. If necessary, incubation was continued, and measurements repeated until those

extinction values were reached. Bacterial concentration was then calculated via following formula:

$CFU/ml = 12 \times 10^8 \times (OD_{600})$

Target concentration of 5000 colony forming units (CFU)/ 200 µl was then obtained via dilution with sterile PBS. Successful titration was controlled by plating BHI plates with 100 µl of 0.25 CFU/ µl and counting colonies after one to two days.

First infections in naïve mice were performed with 5000 CFU *L.m.*OVA i.v., applied into the tail vein (Pope et al., 2001). Secondary or so-called recall infections of chronically infected mice were performed with $2x10^5$ CFU *L.m.*OVA.

2.4.3.2 *In vivo L.m.*OVA recruitment

Mice were treated with either naïve retrogenic or transgenic SIINFEKL-specific T cells before *L.m.*OVA infection. $CD8^+$, $CD19^-$, $CD45.1^+/CD90.1^+$, $CD44^{lo}$ cells were sorted into volumes of 200 µl FCS which contained $4x10^5$ murine feeder splenocytes. Injections were performed i.p. immediately after. Later the same day, mice were infected with 5000 CFU *L.m.*OVA by tail vein injections.

Mice were sacrificed and spleens harvested on day eight post infection. For the creation of single cell suspension, spleens were mashed through 70-µm cell strainers, resuspended in 10 ml $RP10^+$ and washed for 6 min at 1500 rpm at 20 °C. Thus, bacteria were eliminated by the antibiotic components of the complete medium. Then, red blood cell lysis was performed with 5 ml ACT and stopped with medium after 5 min. Cell numbers were counted as previously described. $15x10^6$ splenocytes per sample were then transferred into a 96-well V-bottom-plate and washed 2.5 times in FACS buffer.

Surface staining was performed in volumes of 150 µl and incubated for 30 min on ice in the dark. After 25 min, PI (1:100) for living/dead staining was added. Flow cytometric analysis then followed as described above.

For measurements of *in vivo* recruitment upon antigen encounter, frequency of the target population was quantified for the determined number of splenocytes and then calculated for the entire spleen according to previously counted splenocytes.

2.4.3.3 Intracellular cytokine staining

Mice were treated with 2000 retrogenic $CD8^+$, $CD19^-$, $CD45.1^+/CD90.1^+$ cells and subsequently infected i.v. with 5000 CFU *L.m.*OVA. On day 12, spleens were harvested and processed into single cell suspension as described above. *In vitro* antigen stimulation was performed for $3x10^6$ cells per well by incubating those with different concentrations (10^{-12} M, 10^{-11} M, 10^{-10} M, 10^{-9} M, 10^{-8} M, 10^{-6} M) of peptide $OVA^{257-264}$. For this purpose, lyophilized SIINFEKL peptide was dissolved in dimethyl sulfoxide (DMSO) creating a 10^{-2} Molar stock solution and then serially diluted in $RP10^+$. Negative control received pure $RP10^+$ medium without peptide while positive control was non-specifically stimulated with a mix of phorbol myristate acetate (PMA) (1:4000) and Ionomycin (1:25).

For homogenous peptide-splenocyte interaction, 96-well flat-bottom plates were used during stimulation. Samples were then incubated for overall 5 h at 37° C. In order to enrich cytokines in the cytosolic Golgi apparat, 2 µl/well Golgi-Plug were added after 1 h of incubation for the remaining 4 h. Importantly, this occurred without re-suspension as not to stir the cells and hamper with the stimulation. Before further processing of the cells, samples were transferred into 96-well V-bottom plates in order to minimize cell loss during the washing steps to come.

All following steps were performed at 4° C on ice. Next, cells were washed in FACS buffer and ethidium monoacid bromide (EMA)/ fragment crystallizable (Fc)-block staining (EMA 1:1000 and Fc-block 1:400). EMA is a reagent for living/dead discrimination distinguished by its stability face to permeabilization and fixation processes. Fc-Block on the other hand is necessary for reducing unspecific antibody binding by blocking Fc-receptors found on B lymphocytes. Since EMA requires UV-light exposure for covalently binding deoxyribonucleic acid (DNA) (Perfetto et al., 2006), incubation was performed for 15 min under light. Samples were then washed in FACS buffer 2.5x times. The next step included regular surface antibody staining for identification of the $CD8^+$, $CD19^-$, $CD45.1^+/CD90.1^+$ target population. Finally, cells were again washed 2.5x times in FACS buffer.

In order to permeabilize the cells for the following intracellular staining, samples were incubated with BD Cytofix/Cytoterm for 20 min. All the following washing steps and staining were then performed with Perm/Wash buffer (1:10 Perm/Wash and ddH_20). Next, intracellular staining of the produced cytokines IL-2, TNF-α and IFN-γ was performed for 30 min in the dark. Samples were then washed: twice in Perm/Wash buffer and once in FACS buffer before resuspension in 1% paraformaldehyde (PFA) (1:100 in PBS) for fixation. Analyses were performed by flow

cytometry. For quantification, maximal proportions of IFNγ$^+$ CD8$^+$cells were normalized to 100% and submitted to a nonlinear regression model.

2.4.3.4 *In vitro* tumor killing

Experiments were performed using the xCELLigence device, providing incubation conditions at 37 °C with 5% CO_2. For *in vitro* tumor killing assays, PancOVA, a syngeneic murine pancreatic adenocarcinoma cell line expressing the ovalbumin peptide was used. Cell culture conditions were analogous to those of MC38-OVA cells previously described.

In order to measure cytotoxic responses, 10^4 PancOVA cells were seeded in volumes of 200 µl cDMEM on 96-well E-Plates (E-Plate® 96) plated with gold micro-electrodes. Killing of those adherent tumor cells resulted in changes of impedance and was monitored in 15-minute intervals for up to 120 h (Figure 7).

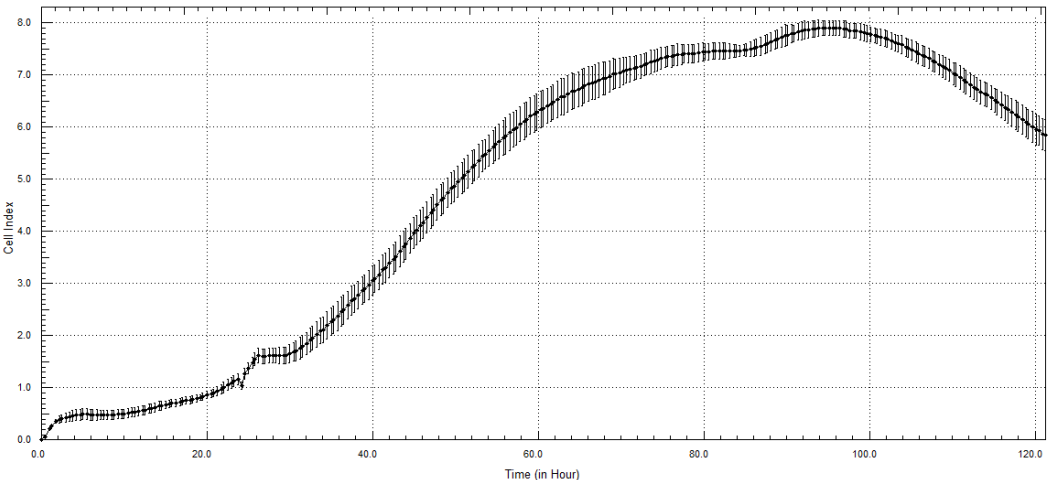

Figure 7 Cell index over time for 10^4 PancOVA cells
10^4 PancOVA cells were seeded in volumes of 200 µl cDMEM into the E-plates and incubated for 120 h at 37° C in the xCELLigence device. After 24 h, 100 µl supernatant was removed and replenished with cDMEM. Shown is primary data of three replicates with SD.

T cells for *in vitro* tumor killing were harvested from spleens of *L.m.*OVA infected mice in correspondence to *in vitro* peptide stimulation assays. Infections were performed with 5000 CFU *L.m.*OVA followed by the transfer of retrogenic TCR$^+$ cells. On day eight, mice were sacrificed, spleens processed as described before and single cell suspensions submitted to cell sorting for CD8$^+$, CD45.1$^+$/CD90.1$^+$ cells. Plated PancOVA cells were left to settle for 24 h, then supernatant in a volume of 100 µl was carefully removed in order to not disturb adherence of tumor cells. Next, sorted T cells of determined numbers were added in volumes of 100 µl cDMEM to the

culture and left to incubate. Negative controls received no T cells, supernatant was removed as described and replaced with fresh medium.

Cell index values were analyzed by the RTCA Software 2.0 and normalized to time point of T cell addition (Figure 7).

2.5 Statistical analysis

Statistical analyses were performed with the GraphPad prism software as indicated in graphs. If not otherwise specified, error bars correspond to standard deviation.

3. Results

The following results section is divided into three parts. First, results from the MC38-OVA tumor model in combination with transfer of OT-1 cells are presented, focusing on protection and recovery of lowest numbers of transferred cells. Here, phenotypical analyses are carried out for transferred populations among $CD8^+$ TIL compared to endogenous lymphocyte populations. Secondly, phenotypical and functional properties of the retrogenic TCRs are explored and put into relation with their structural avidity. Thirdly, retrogenic TCRs are investigated for their *in vivo* functionality by transferring them into the MC38-OVA model, allowing for analysis of tumor protection and their spatio-temporal distribution during tumor disease. In this context, TCR dependent PD-1 expression of tumor-specific CTL is investigated.

3.1 Transfer of OT-1 cells in the MC38-OVA tumor model

3.1.1 Establishing the tumor MC38-OVA model

Both for the protective and the descriptive approach of transfer experiments, OT-1 cells were transferred pre-emptively into the MC38-OVA model, recognizing surface ovalbumin peptide as a tumor neoantigen in this setting. Thus, OT-1 cells were already residing in the host organism when the tumor was induced, analogous to an endogenous antigen-specific population. In combination with total body irradiation (TBI) immediately before T cell treatment and followed by tumor inoculation the next day, optimal conditions for tumor growth and engraftment of the transferred cells were provided.

For early tumor experiments different approaches for the growth of subcutaneous MC38-OVA tumor model and time points of adoptive T cell transfer were investigated. Without TBI tumor growth proved to be more varied with no tumor engraftment at all or early tumor rejection. As a consequence, therapeutic transfer approaches applying TBI and cell transfer on later time points proved difficult. TBI of 5 Gy the day before tumor inoculation on the other hand allowed for a more distinctive and evenly distributed growth among the experimental groups. Future experiments were therefore focused on preemptive TBI and cell transfer, as depicted for 5000 naïve OT-1 (Figure 8 A).

Further analyses aimed to determine optimal harvest conditions for tumor cells prior to inoculation. Here, no major impact on tumor engraftment could be discerned, depicted for

chemical lysis of adherent tumor cells via trypsin digestion or mechanical removal using a cell scraper (Figure 8 B). For future experiments lysis via trypsin was continued.

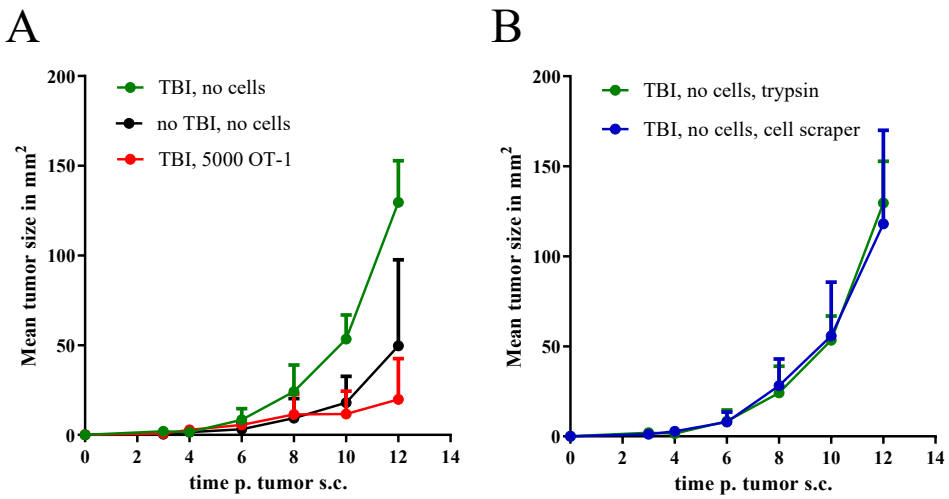

Figure 8 Establishing the MC38-OVA tumor model
Mice were either irradiated with 5 Gy TBI and treated with A.) 5000 $CD44^{lo}$, $CD8^{+}$, $CD45.1^{+}$ OT-1 cells i.p., received only TBI or no treatment at all, followed by injection of 10^{6} cells MC38-OVA s.c. the next day. B.) Adherent tumor cells were either processed via trypsin lysis or mechanically using a cell scraper. Shown is mean tumor growth with SD (n=5).

3.1.2 Spatio-temporal distribution of OT-1 cells

In order to investigate the distribution of transferred OT-1 cells among different organs depending on time points and titration, experimental groups received 5000 naïve $CD8^{+}$, $CD45.1^{+}$ OT-1 cells and were sacrificed on days 7, 12 and 17 allowing for organ analysis. On day 12, two more groups treated with 128 and 800 OT-1 cells, respectively, were analyzed. For this purpose, peripheral blood was drawn and both draining (dLN) and non-draining lymph nodes (ndLN) as well as the tumor were removed. For processing of organs see the methods section. Analysis was performed via surface protein staining of extracted leucocytes and subsequent flow cytometry.

Transferred OT-1 cells could be identified at all time points for each organ among the T cell population via staining of congenic marker CD45.1 and flow cytometry, thus allowing for detection in the different organs analyzed. Shown are primary data in form of FACS plots with exemplary gating for each organ. Visibly, among the $CD8^{+}$ population a $CD45.1^{+}$ subset for every organ could be distinguished, corresponding to the transferred OT-1 cells (Figure 9).

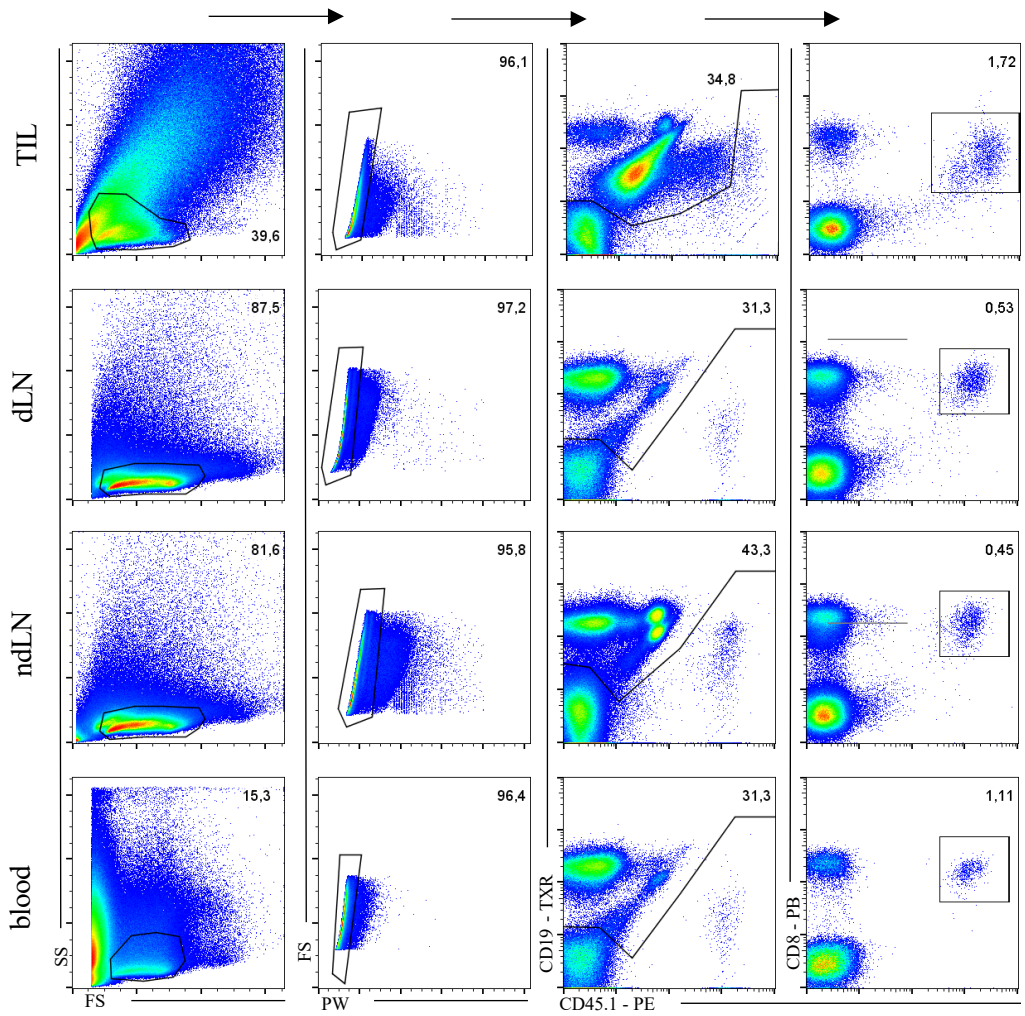

Figure 9 Primary data for OT-1 enrichment in different organs
Mice were irradiated with 5 Gy TBI and treated with 5000 $CD44^{lo}$, $CD8^+$, $CD45.1^+$ OT-1 cells i.p.; followed by injection of 10^6 cells MC38-OVA s.c. the next day. Mice were sacrificed for blood, dLN, ndLN and TIL on days 7, 12 and 17. Gating strategies with frequencies of recovered $CD8^+$, $CD45.1^+$ OT-1 T cells for each organ on day 12. Adapted from (Purcarea et al., 2022).

Quantification of the data showed that enrichment of OT-1 was accentuated among TILs. The intermediate time point on day 12 generally showed the highest percentage of transferred cells among $CD8^+$ populations, constituting around 70% of TILs (Figure 10 A). Peripheral blood also showed enhanced enrichment of OT-1 cells on day 12, but with overall lower frequencies (around 30% of $CD8^+$ cells). Here a significant contraction of the OT-1 population towards day 17 could be observed. The same trend could be shown for lymph nodes, albeit more discretely. Also, overall frequencies and cell numbers were rather low. Nevertheless, transferred cells amounted up to 10% of the $CD8^+$ populations within lymph nodes on their peak of expansion.

Regarding absolute cell numbers (Figure 10 B), most OT-1 cells could already be found on day 7 in draining lymph nodes, while non-draining lymph nodes show comparable cell numbers only

later, on days 12 and 17. In the tumor, observed cell numbers yielded no significant differences depending on time point of recovery. Absolute cell numbers among peripheral blood monocytic cells (PBMC) were not suitable for comparison of different experiments, since taken blood volume was not consistently documented or standardized.

Frequencies of antigen-specific T cells among the natural TCR repertoire are generally low and therefore challenging in terms of characterization (M. G. McHeyzer-Williams & Davis, 1995). Interestingly, OT-1 cell progeny numbers pointed towards no differential expansion depending on transferred cell titration, as observed at day 12 (Figure 10 D). Visibly, transfer of lowest numbers of 128 cells yielded detectable progeny in all organs at any time point. Neither percentages of $CD8^+$ cells nor absolute cell numbers recovered increased with higher transferred cell numbers for lymph nodes and blood (Figure 10 C, D). However, a significant increase among TIL progeny could be observed between 128 and 800 transferred OT-1 cells. A further 6.25-fold rise to 5000 transferred cells however did not lead to further enrichment, implying that low precursor numbers already yield maximal expansion (Figure 10 C).

In conclusion, engraftment of OT-1 cells proved to be time point dependent, with day 12 presenting as peak of enrichment. Even lowest numbers of transferred cells led to detectable progeny at any time point of analysis for each organ, allowing for a more physiological experimental ACT setting. Moreover, transfer of higher of cell numbers did not significantly enhance the frequencies or recovery of transgenic cells.

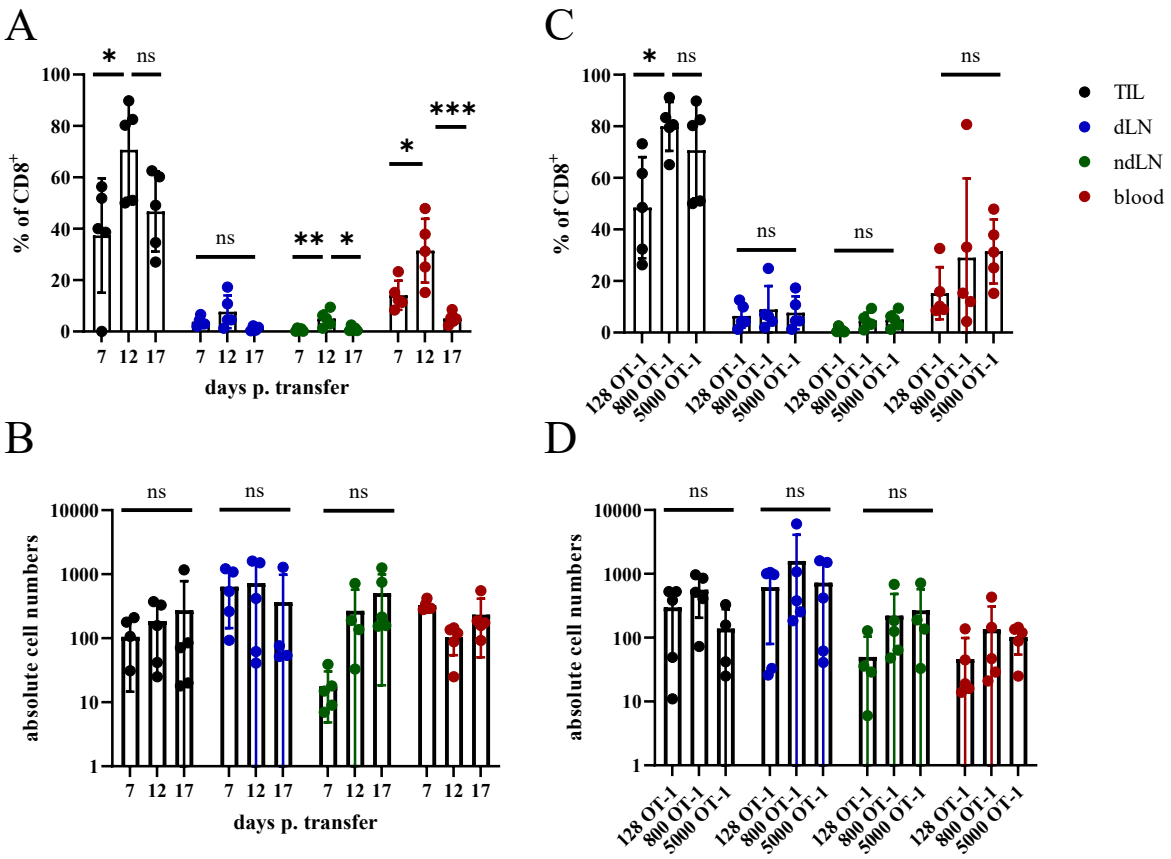

Figure 10 Enrichment of OT-1 cells depending on time point and titration

Mice were irradiated with 5 Gy (TBI) and treated with OT-1 cells i.p., followed by injection of 10^6 cells MC38-OVA s.c. the next day. A.-B.) Mice were sacrificed for blood, dLN, ndLN and TIL on days 7, 12 and 17. A.) Enrichment in percentage of $CD8^+$ cells and B.) recovery of 5000 transferred OT-1 cells on different time points color coded for organs of origin. C-D) Mice were treated with either 128, 800 or 5000 OT-1 cells and sacrificed for TIL, dLN and ndLN and blood on day 12. C.) Enrichment in percentage of $CD8^+$ cells and D.) recovery of transferred cells also color coded. Absolute cell numbers for blood are shown for consistency. Statistical testing by ordinary one-way analysis of variance (ANOVA) (* for TILs, ** for ndLN and *** for blood) followed by Tukey's multiple comparisons test with n=5 (results of which are indicated in graph). ns, not significant. * p value < 0.05, ** p value < 0.01, *** p value < 0.001. Adapted from (Purcarea et al., 2022).

3.1.3 Phenotypic characterization of TIL

Early experiments investigated the activation signature of transferred cells by analyzing surface CD44 expression. Commonly associated with T cell activation, CD44 can be upregulated in an antigen unspecific manner (Budd et al., 1987). Following TBI with 5 Gy and transfer of 5000 OT-1 cells, MC38-OVA was subcutaneously implanted as described above.

Shown are histograms comparing differential CD44 expression of transferred and endogenous cells for different organs on day 7 respectively (Figure 11 A). As quantified in Figure 11 B, transferred cells demonstrated a significant higher mean fluorescence intensity (MFI) for CD44 compared to endogenous $CD8^+$ cells in blood and lymph nodes. Among TILs however, endogenous cells displayed a similar MFI as transferred cells, with the transferred population showing a significantly weaker signal compared to $CD44^+$ cells in the peripheral blood. This could indicate for an antigen dependent activation in the periphery whereas TILs recruited into the tumor could show an activation signature independent of their antigen specifity. Also, in the tumor, antigen specific activation in general could be curbed by inhibitory factors of the TME.

This trend was also mirrored by percentages of $CD44^+$ cells (Figure 11 C). Independently of organ and time point more than 80% of $CD45.1^+$ cells were positive for surface CD44. Endogenous cells however showed much lower frequencies of $CD44^+$ cells in blood and lymph nodes. Nevertheless, early on day 7, CD44 expression amounted up to 95% among TILs and still around 70% among PBMC. Interestingly, towards the later time point, frequencies seemed reduced for both populations. Since this trend did not apply to the transferred cells, this could possibly indicate a shift towards antigen specific activation dominating the tumor response towards later time points.

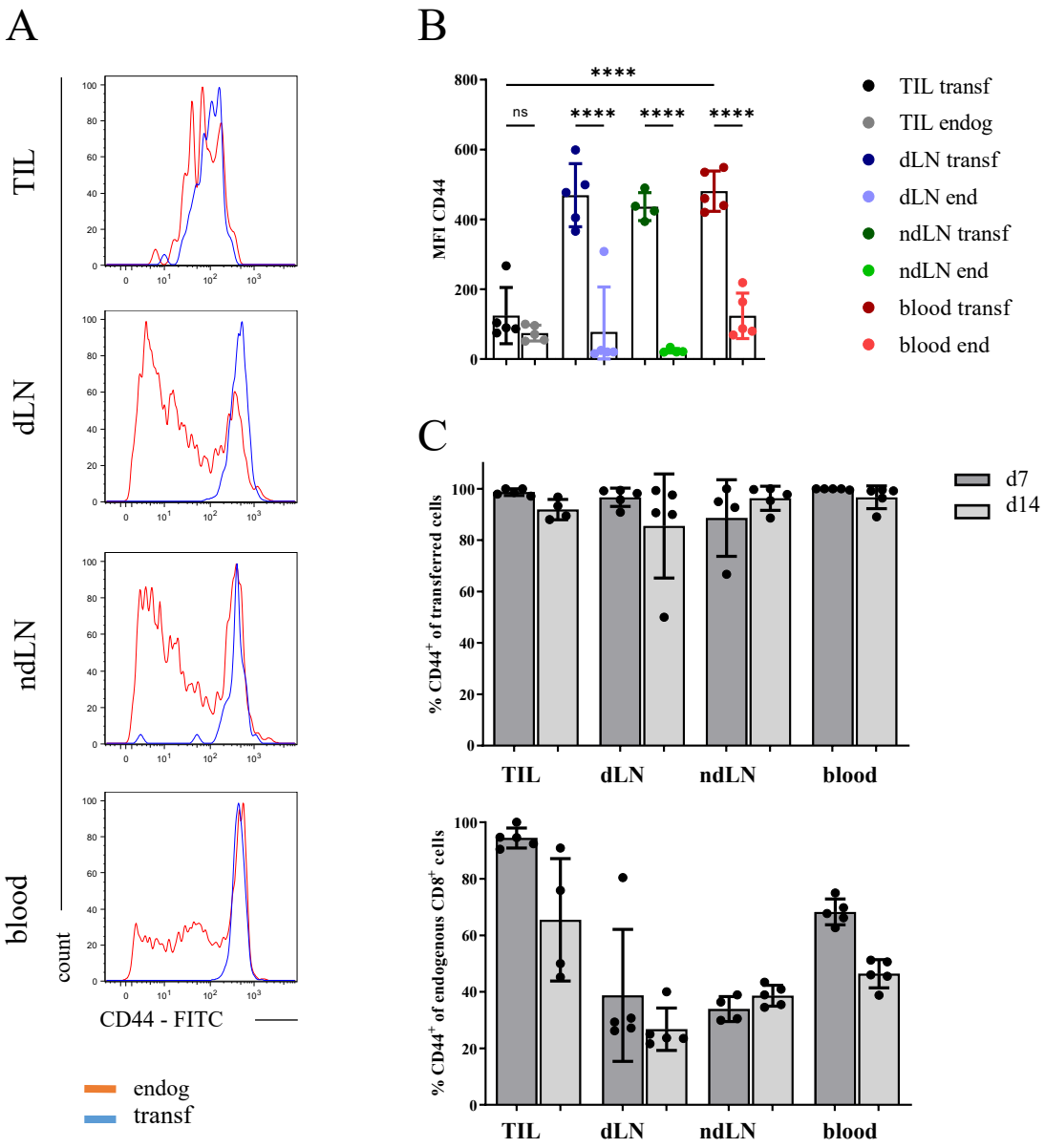

Figure 11 CD44 Expression of transferred cells
Mice were irradiated with 5 Gy TBI and treated with 5000 OT-1 cells i.p.; followed by injection of 10^6 cells MC38-OVA s.c. the next day. Mice were sacrificed for TIL, dLN, ndLN and blood on days 7 and 14. A.) Shown is representative primary data for CD44 expression for each organ. Transferred ("transf") and endogenous ("endog") cells are color coded as indicated. B.) Quantification of CD44 expression via MFI on day 7 for all organs. Statistical testing by one-way ANOVA (****) followed by Tukey's multiple comparison test (results of which are indicated in graph). ns, not significant. **** p value < 0.0001. C.) Quantification of $CD44^+$ cells for all organs and timepoints for transferred (above) and endogenous (below) cells for n=5.

For a more differential insight on the phenotypical changes upon T cell transfer, analyses regarding exhaustion markers of T cell progeny were performed. This was realized by first transferring either 128, 800 or 5000 OT-1 cells immediately after TBI, then inoculation of the MC38-OVA tumor the next day. Day 12 was chosen for analyzing peripheral blood, draining

and non-draining lymph nodes as well as the tumor itself. Transferred cells were identified via congenic marker CD45.1. and expression of PD-1, TIM-3 and LAG-3 was investigated to allow for conclusions regarding antigen-specific activation and/or exhaustion of T cells.

For the purpose of quantifying the data, both MFI and the percentage of PD-1$^+$, TIM-3$^+$ and LAG-3$^+$ cells among the CD8$^+$ population were taken into account. The gating strategy for identifying the cut-off of those positive populations is depicted in Figure 12. Shown by the histograms is the adaptation to endogenous CD8$^+$ populations for reference. Through this, it is immediately apparent that the transferred populations tend to yield higher percentages of positive cells regarding all analyzed inhibitory co-receptors compared to the endogenous control.

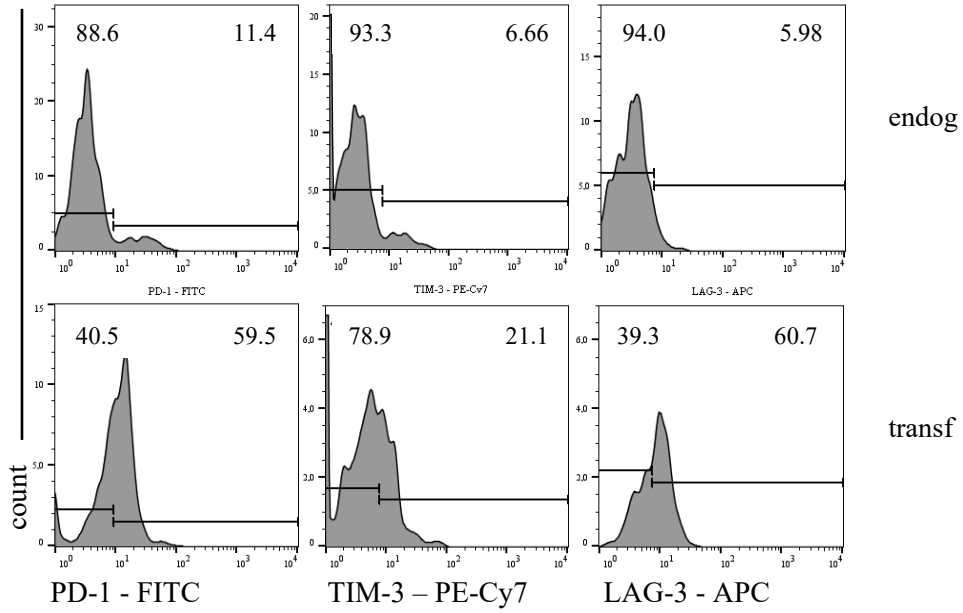

Figure 12 Histograms for expression of PD-1, TIM-3 and LAG-3
Mice were irradiated with 5 Gy TBI and treated with 800 OT-1 cells i.p.; followed by injection of 10^6 cells MC38-OVA s.c. the next day. Mice were sacrificed for TIL, dLN, ndLN and blood. Shown is the gating strategy for the identification of PD-1$^+$, TIM-3$^+$ and LAG-3$^+$ cells in peripheral blood on day 12 for both endogenous ("endog") and transferred ("transf") CD8$^+$ cells.

Upon further quantification, the data show that transferred OT-1 cells were associated with higher expression levels of inhibitory co-receptors regardless of the organ of recovery. This was mirrored by both MFI and percentage of positive cells from CD8$^+$ populations compared to the corresponding endogenous population (Figure 13 A, B).

MFI of inhibitory co-receptors was generally higher on transferred OT-1 cells than on the equivalent endogenous population (Figure 13 A). Moreover, among transferred cells, TILs

displayed significantly higher MFI of all three inhibitory co-receptors compared to peripheral blood. PD-1 MFI among endogenous cells also indicated an increase for TILs, however on a much smaller level. MFI of TIM-3 and LAG-3 were generally lower compared to PD-1 on transferred OT-1 cells yet still significantly increased for TILs compared to peripheral blood. Among endogenous cells, differential MFI of TIM-3 and LAG-3 for the individual organs could not be detected.

PD-1$^+$ cells constituted the majority of recovered OT-1 cells, reaching frequencies of more than 90% among TILs as well as draining lymph nodes and still around 60% in the peripheral blood (Figure 13 B). This trend applied to frequencies of TIM-3$^+$ and LAG-3$^+$ cells too, albeit more discretely. Here, positive cells amounted up to 70% of transferred cells in the tumor. Among endogenous CD8$^+$ TILs, PD-1$^+$ cells seemed slightly enriched; however, this did not become apparent for neither TIM-3$^+$ nor LAG-3$^+$ cells. Interestingly, PD-1 expression both in terms of frequencies and MFI seemed to follow an organ-dependent gradient, TILs exhibiting highest values, followed by draining and non-draining lymph nodes and lastly peripheral blood.

The simultaneous expression of multiple co-inhibitory markers is thought to be a reliable indicator of functional T cell exhaustion (Wherry, 2011). For quantification of general up-regulation of inhibitory co-receptors, populations positive for all three markers PD-1, TIM-3 and LAG-3 were identified for all organs. Such triple positive cells were enriched among transferred cells, shown here for day 12 after transfer of 128 OT-1 cells (Figure 13 C).

Moreover, triple positive cells followed a similar organ dependent gradient as PD-1 expression, highest frequencies being observable in the tumor, followed by lymph nodes and finally peripheral blood. In the tumor, those cells constituted to around 60% among transferred TILs compared to 15% in peripheral blood (Figure 13 C). Correlation of percentage of simultaneous expression of PD-1, TIM-3 and LAG-3 with PD-1 MFI proved to be linear (Figure 13 D). Also, triple marker expression correlated with frequencies of PD-1$^+$ cells depending on the organ (Figure 13 E), indicating that PD-1 MFI could serve as a marker of functional exhaustion.

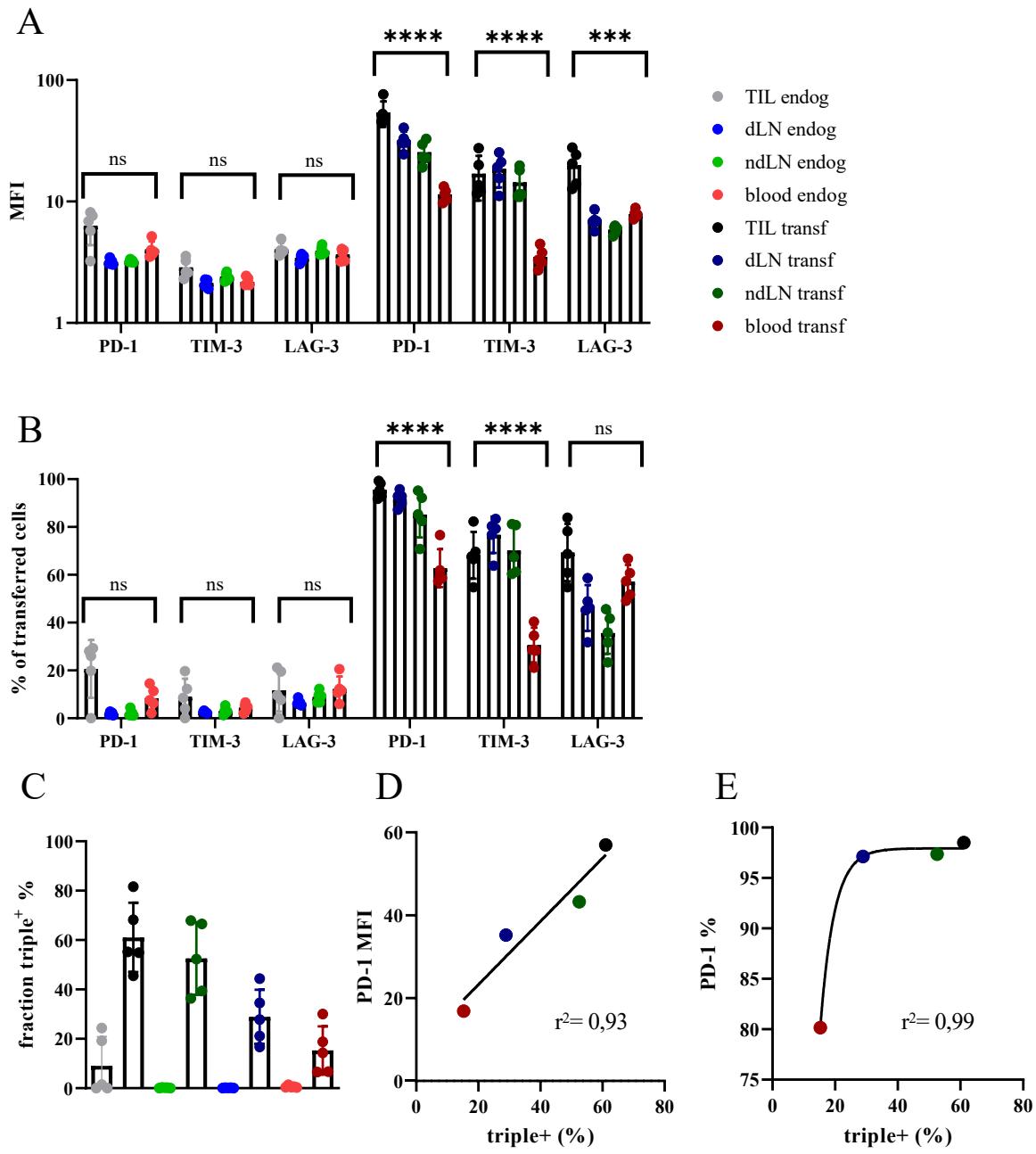

Figure 13 Up-regulation of inhibitory co-receptors PD-1, TIM-3 and LAG-3
Mice were irradiated with 5 Gy (TBI) and treated with OT-1 cells i.p., followed by injection of 10^6 cells MC38-OVA s.c. the next day. Mice were sacrificed for TIL, dLN, ndLN and blood on day 12. A.) PD-1 MFI shown as geometric mean for n=5. B.) Percentage of PD-1^+, TIM-3^+ and LAG-3^+ cells of $CD8^+$, color coded respective of population and organ following transfer of 800 OT-1 cells, for transferred ("transf") and endogenous ("endog") cells, also n=5. Statistical testing by two-way ANOVA (****) followed by Tukey's multiple comparison test. (results of which are indicated in graph). ns, not significant. *** p value < 0.001, **** p value < 0.0001. C.) Percentage of triple$^+$ cells among $CD8^+$populations for 128 transferred cells, color coded for population and organ. D.) Correlation of triple$^+$ frequencies and PD-1 MFI, fitted with a linear regression (*) with n=5. E.) Correlation of triple$^+$ frequencies and percentage of PD-1^+, fitted with a non-linear regression, also n=5. Adapted from (Purcarea et al., 2022).

3.1.4 OT-1 mediated tumor protectivity

In order to investigate OT-1 mediated protection against the MC38-OVA tumor, transfer experiments with different cell titrations were performed. This aimed at identifying the threshold of T cells mediating tumor control while minimizing numbers of transferred cells to best reflect physiological precursor frequencies. Since earlier findings had shown that lowest cell numbers transferred allowed for detectable progeny, it was of interest to see whether these populations managed to mediate tumor protection as well.

Naïve ($CD44^{lo}$) $CD8^{+}$ $CD45.1^{+}$ OT-1 cells were sorted with high purity and adoptively transferred as already described, with either 128, 320, 800, 2000 or 5000 cells transferred. Thus, every titration step included a 2.5-fold increase of transferred OT-1 cells. As a negative control, one group of mice received 5000 P14 cells specific for the irrelevant LCMV antigen gp33. Two independent experiments were performed. Tumor growth was measured by a caliper every two to three days, while tumor size was calculated from the product of two vertical and horizontal diameters. As displayed in tumor growth curves over time (Figure 14 A), nearly all the mice that received either 5000 or 2000 OT-1 cells managed to reject the MC38-OVA tumor after initial growth, without apparent relapse over the time of observation (approximately 60 days). For these groups, individual mice developed tumors after initial tumor control, potentially reflecting immune escape. With decreasing numbers of transferred OT-1, tumor elimination was less likely achieved. The control group that received P14 cells showed an aggressive, uncontrollable tumor growth.

The described trend could be visualized by comparing mean tumor growth at an early time point such as day 16 (Figure 14 B), when termination criteria were not yet reached by the majority of individuals. Mice receiving 128 OT-1 cells displayed only a weak reduction in tumor growth compared to the control group. However, already a further 2.5-fold increase to 320 OT-1 cells resulted in a statistically significantly reduced mean tumor size. Groups with both 2000 and 5000 OT-1 cells consistently showed a distinctively reduced tumor size despite initial tumor development (Figure A).

These findings were reflected in the survival data, quantified by Kaplan-Meier-survival analysis (Figure 14 C). While lowest cell numbers of 128 OT-1 only managed a discrete increase in survival, a much more distinctive trend could be observed by a further 2.5-fold increase of OT-1 cells transferred. Here, median survival for as few as 320 cells was more than doubled compared to 128 cells (48 days vs. 23 days) and even tripled compared to control (48 days vs. 16

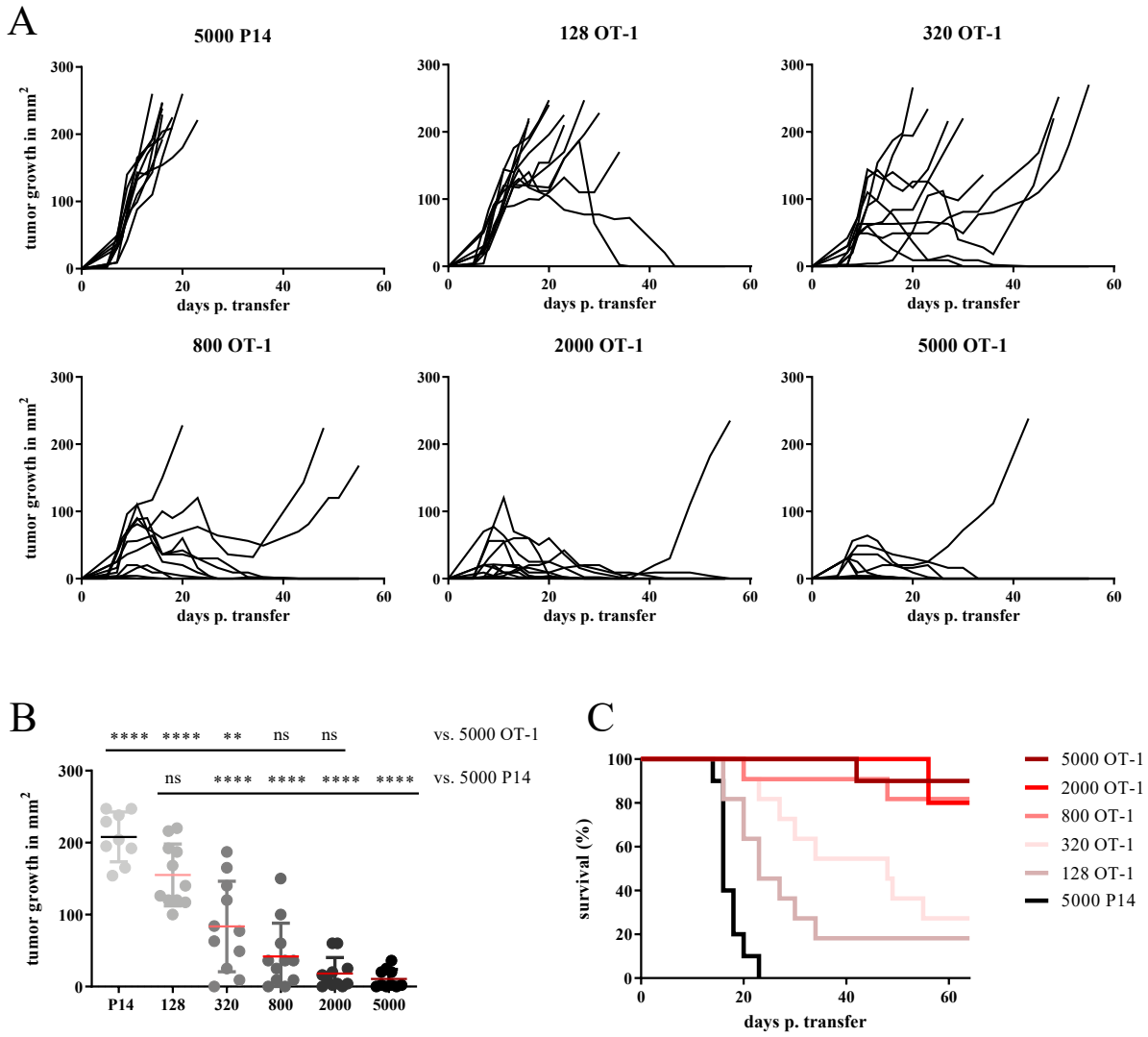

Figure 14 OT-1 mediated tumor protectivity
Mice were irradiated with 5 Gy (TBI) and treated with OT-1 cells i.p., followed by injection of 10^6 MC38-OVA cells s.c. the next day. Administration of either 128, 320, 800, 2000 or 5000 OT-1 cells, negative control was performed with 5000 P14 cells. A.) Tumor growth curves shown for each replicate (n=11). B.) Mean tumor growth on day 16 post transfer for n=11, statistical testing by ordinary one-way ANOVA (****) followed by Tukey's multiple comparisons test (results of which are indicated in graph). C.) Survival curves (n=11). Statistical testing by log-rank (Mantel-cox) test (****) for trend. Data are representative of two independent experiments with n=5-6 mice. ns, not significant. ** p value < 0.01, **** p value < 0.0001. Adapted from (Purcarea et al., 2022).

days). Departing from 800 cells and more, survival rates of 80% and more could be achieved. In conclusion, very low numbers of transferred OT-1 cells were able to inhibit tumor growth. Tumor control was achieved with increasing cell numbers, resulting in tumor elimination and near complete survival with as few as 800 T cells.

3.2 Repertoire of OVA-specific TCRs with different avidities

Structural and functional characterization of the retrogenic TCRs was performed in collaboration with Kilian Schober, Simon Graßmann, Joel Eggert and Sebastian Jarosch.

3.2.1 Phenotypical characterization of the retrogenic TCRs

Retrogenic TCRs could be identified and recovered from peripheral blood of retrogenic mice departing from three to four weeks after their generation. Since the TCRs had distinctive structural properties, it was of interest to investigate whether those were related to their phenotypes. Therefore, mice were bled and TCR^+ cells identified via congenic markers and multimer staining for OVA-specifity.

TCR^+ cells could be identified by their congenic background via CD45.1 and/or CD90.1 for each individual replicate (Figure 15 A). While there was no significant difference to be found between TCRs regarding CD8 expression (Figure 15 C), TCR16-30 showed significantly higher fluorescence intensity for the MHC multimer staining. This trend was visualized by both quantification and histograms of primary data (Figure 15 B, D). Here, high avidity TCR16-30 showed significantly elevated levels of MFI compared to lower avidity TCRs 9, 28 and 39. The other surface markers investigated, namely CD62L, CD27, CD44 and CD45.1/CD90.1 showed no significant difference regarding their expression level on the different TCR^+ cells (Figure 15 E).

Overall, no significant differential phenotypes among naïve retrogenic TCR^+ cells could be observed. However, TCRs showed avidity dependent differences concerning MHC multimer staining.

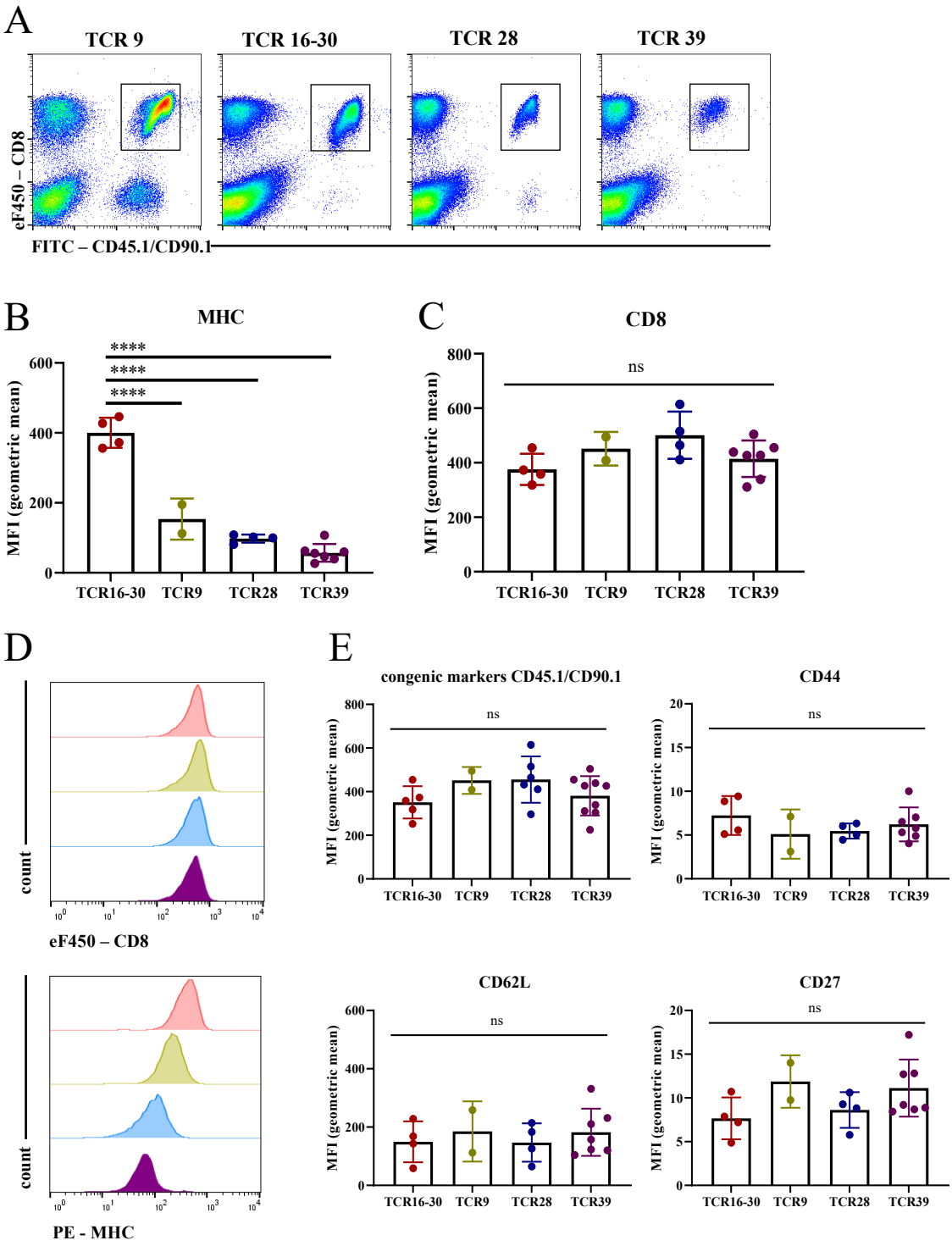

Figure 15 Phenotypical analysis of retrogenic TCRs

Retrogenic TCRs were identified and recovered from peripheral blood of retrogenic mice for surface staining and FACS analysis. A.) Primary data for TCRs 9, 16-30, 28 and 39, shown as $CD8^+$, $CD45.1^+/CD90.1^+$ population. Graphs showing B.) CD8 and C.) MHC expression. D.) Histograms for CD8 and MHC MFI color coded for TCRs. E.) Graphs showing expression of CD62L, CD27, CD44 and congenic markers CD45.1/CD90.1. Statistical testing by ordinary one-way ANOVA (**** for MHC) followed by Tukey's multiple comparison test (results of which are indicated in graph) with n=2-9 mice. ns, not significant. **** p value < 0.0001. Adapted from (Purcarea et al., 2022).

3.2.2 Functional analysis

In order to investigate the functionality of retrogenic TCRs, different approaches were used, such as *in vitro* cytokine production and tumor cell killing as well as *in vivo* recruitment capacities upon antigen stimulation. Hereby, a more substantial assessment of affinity dependent functional properties was aimed for.

Upon antigen stimulation, T cells produce cytokines such as IFNγ$^+$, a feature which is widely used in order to quantify the effectiveness of their immune response (Irving et al., 2012). ICCS was performed for TCRs 8, 9, 21, 28 and 39, corresponding to the repertoire used for early tumor experiments at the beginning of this thesis; some of these TCRs were replaced during the working process with more suitable specimens for representation of a larger range of avidities. Following transfer of naïve retrogenic TCRs and i.v. infection with 5000 CFU *L.m.*OVA, splenocytes were harvested on day 12 and treated by *in vitro* ovalbumin SIINFEKL peptide stimulation.

Transferred retrogenic CD45.1$^+$ cells could be identified for each TCR and antigen stimulation led to detectable cytokine production (Figure 16 A). The measured production of IFNγ, TNFα and IL-2 by antigen-specific cells was quantified according to peptide concentration (Figure 16 B) and half-maximal effective concentration (EC_{50}) for the respective cytokines were calculated. Every TCR yielded IFNγ$^+$, TNFα$^+$ and IL-2$^+$ cells, including double and triple positive populations. Cut-offs for IL-2, IFNγ and TNFα were determined in reference to negative control. Among the analyzed cytokines, IFNγ seemed to be produced most differentially according to transferred TCRs. While TCRs 8, 9, 21 and 28 generally performed rather alike in terms of IFNγ production, TCR 39 showed significantly lower EC_{50} values of IFNγ$^+$ cells compared to all other TCRs (Figure 16 C).

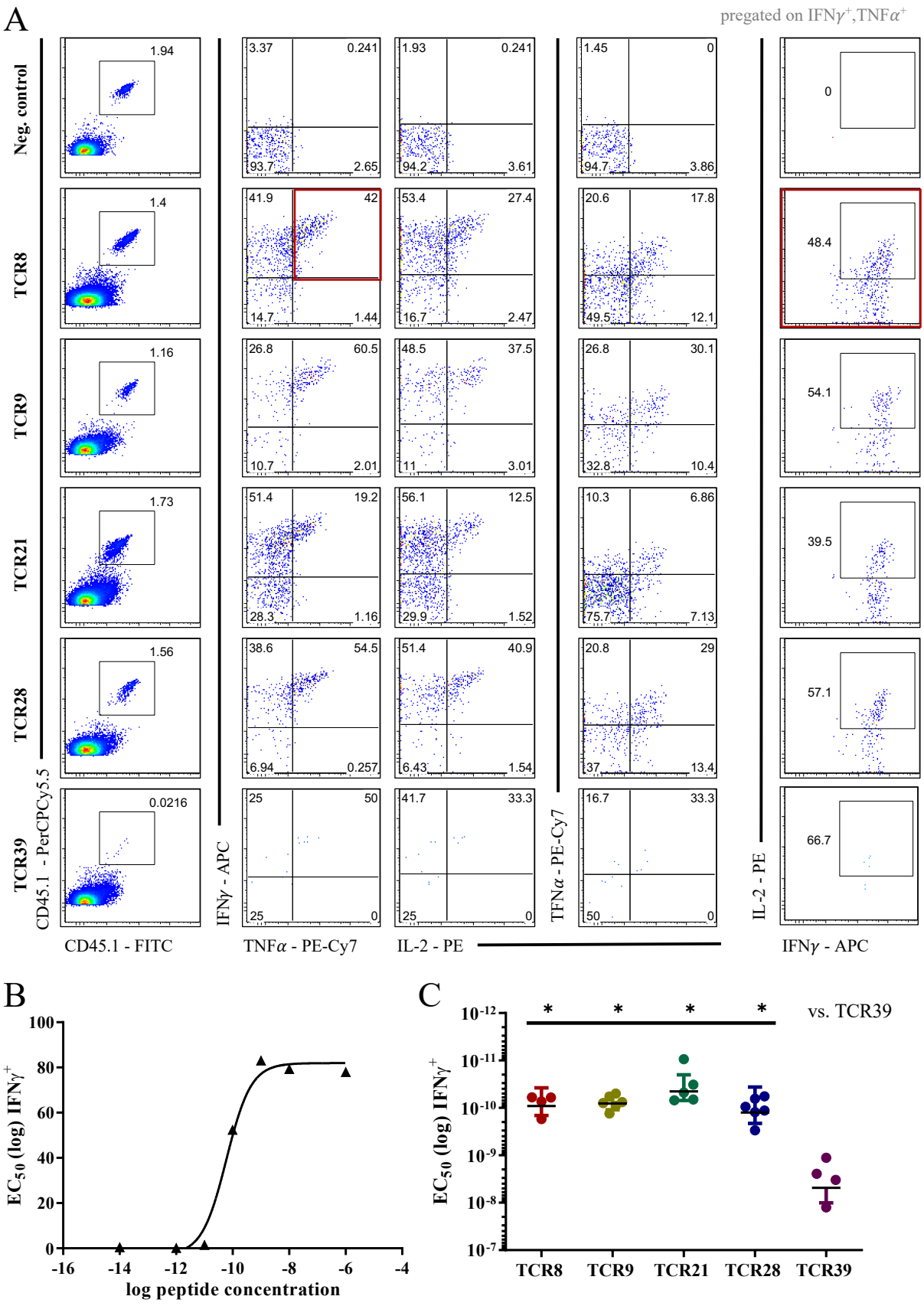

Figure 16 Cytokine production of retrogenic TCRs upon *in vitro* antigen stimulation
Functional analysis by peptide stimulation and subsequent intracellular cytokine staining. Mice were injected with retrogenic TCRs and infected with 5000 CFU *L.m.*OVA and sacrificed on day 12, splenocytes were stimulated with SIINFEKL peptide, no peptide or PMA/Ionomycin. A.) Primary data

showing double positive staining for CD45.1$^+$ cells and cytokine production with double and triple positive populations for TCRs 8, 9, 21, 28 and 39 and negative control. Triple positive population pregated on IFNγ^+, TNFα^+ cells as indicated for TCR8. B.) Peptide concentration for the half maximal effector concentration (EC_{50}) was calculated by fitting a non-linear regression curve, here shown for IFNγ for a replicate of TCR28 C.) Comparison of EC_{50} values for IFNγ production for a panel of retrogenic TCRs. Each dot represents a biological replicate ±SD. Data representative of two independent experiments with n=3. Statistical testing by ordinary one-way ANOVA (*) followed by Tukey's multiple comparison test. * p value < 0.05.

Besides cytokine production, clonal expansion of T cells is generally known to be another effector mechanism upon antigen stimulation (Buchholz et al., 2013). In order to measure *in vivo* recruitment upon antigen encounter, *L.m.*OVA recruitment assays for TCRs 9, 16-30, 28 and 39 were performed. These TCRs were chosen since their EC_{50} values of IFNγ$^+$ cells in other experiments (data not shown) indicated that they would more comprehensively reflect the full avidity spectrum. Mice received 100 TCR$^+$ cells i.p. followed by i.v. infection with 5000 CFU *L.m.*OVA. Expansion of the transferred cells was measured in spleens on day 8 post infection. Supporting previous work of Kilian Schober, Simon Graßmann, Joel Eggert and Sebastian Jarosch (data not shown), TCR39 displayed lower expansion capacities (Figure 17). This was expressed by more variable and altogether lower recovered cell numbers (10^4 for TCR39 vs. 10^5 for TCR16-30).

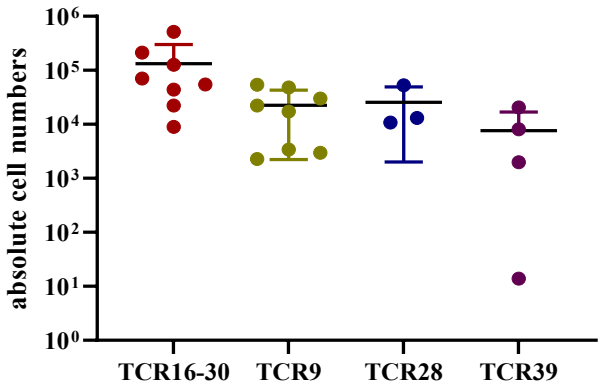

Figure 17 ***In vivo*** **recruitment of retrogenic TCRs**
Mice were injected with 100 retrogenic T cells for each TCR, then infected with 5000 CFU *L.m.*OVA i.v.. On day 8 post infection, spleens were harvested and analyzed. Shown are absolute cell numbers calculated from a sample of defined size for the whole spleen for TCRs 9, 16-30, 28 and 39, n=3-8.

Further functional analysis was performed by investigating the *in vitro* killing capacities of the retrogenic TCRs in preparation for later *in vivo* tumor experiments. For detailed information on the xCELLigence assay see the methods section. Since the elimination of adherent PancOVA

tumor cells was represented by a decreasing cell index over time, this readout was used as measure for antigen-specific killing by the deployed TCRs.

However, establishing a reliable negative control proved challenging. For earlier experiments OVA-MHC$^-$ CD8$^+$ cells were used for negative control. As depicted in Figure 18 A, adding 1000 OT-1 cells lead to reduced tumor growth compared to the same number of MHC$^-$ cells, indicating for antigen specific killing. However, inoculation with highest numbers starting from 5000 MHC$^-$ cells (Figure 18 B) resulted in a comparable decrease of the cell index relative to the experimental groups. This questioned the avidity-dependence of tumor killing and possibly indicated for unspecific killing by other factors such as sheer cell numbers or competitive media consumption.

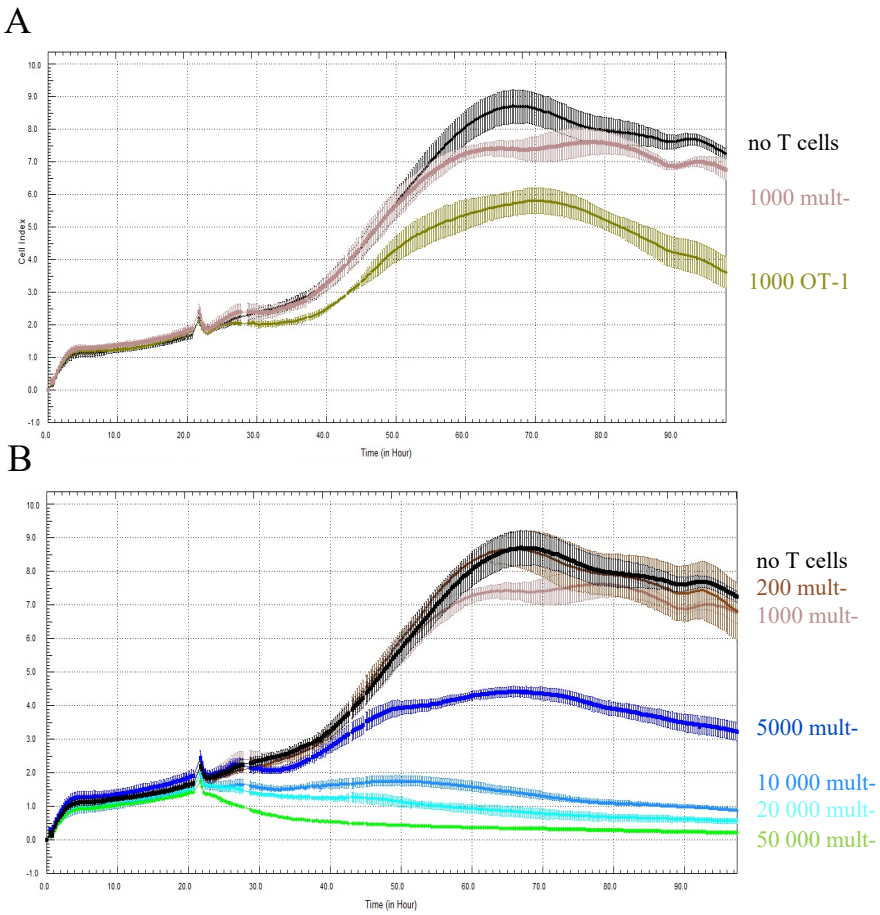

Figure 18 Establishing a negative control for the xCELLigence
10^4 PancOVA cells were seeded in volumes of 200 µl cDMEM into the E-plates and incubated for 120 h at 37° C. After 24 h, CD8$^+$, CD45.1$^+$, CD62L$^-$ either A.) 1000 CD45.1$^+$ and 1000 OVA-MHC$^-$ (mult$^-$) cells or B.) only OVA-MHC$^-$ cells were added according to titration. Shown is primary data from the xCELLigence assay for three replicates with SD.

Therefore, shown results are limited to lowest cell numbers in order to circumvent the described effect of large cell numbers. Supporting the validity of this approach, differences in killing could be shown between different TCRs (Figure 19).

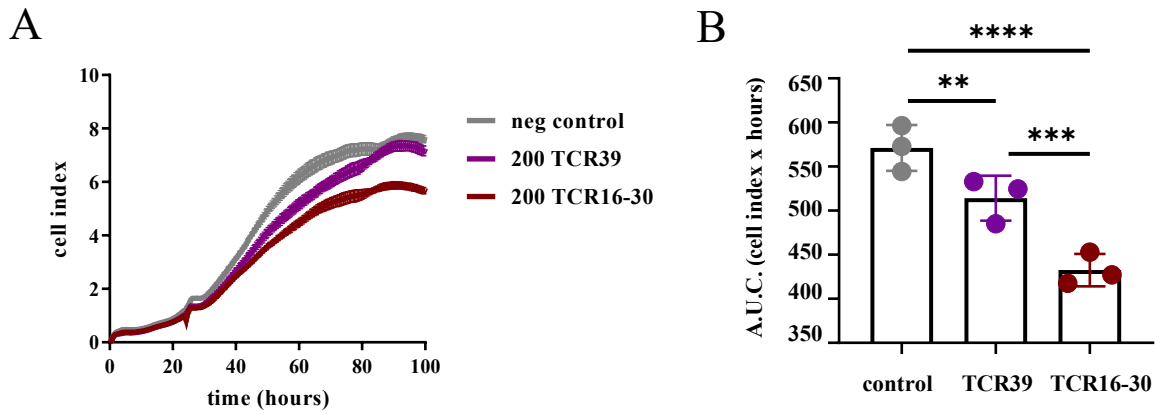

Figure 19 ***In vitro*** **killing capacities of retrogenic TCRs**
In vitro killing capacity of retrogenic TCRs tested via xCELLigence killing assay. Mice were injected with retrogenic TCRs or OT-1 cells and infected with 5000 CFU *L.m.*OVA. Mice were sacrificed on day 8 post infection and their spleens harvested. $CD8^+$, TCR^+ cells were then incubated with PancOVA cells. Killing was quantified via A.) cell index over time and B.) area under the curve (AUC) for no cells and 200, either TCR39 or TCR16-30 cells. Statistical testing by ordinary one-way ANOVA (**) followed by Tukey's multiple comparisons test (results of which are indicated in graph) with n=3 technical replicates. ** p value < 0.01, *** p value < 0,001, **** p value < 0.0001. Adapted from (Purcarea et al., 2022).

For further experiments, negative control consisted of tumor cells without addition of T cells. As shown above, maximal cell indices were reached by day 4, after around 100 h. Afterwards, cell indices began to decrease, assumedly due to cell death after consumption of nutritive cell culture medium. The addition of 200 TCR16-30 (highest affinity) or TCR39 (lowest affinity) cells showed a reduced increase of cell indices (Figure 19 A). Area-under-the-curve (AUC)-analyses showed that 96 h after plating of the tumor cells, thus until the peak of cell index values for the negative control, a significant difference regarding the killing through TCRs 16-30 and 39 could be found (Figure 19 B).

Overall, the described analyses showed that TCR functionality differences in terms of *in vitro* cytokine production and tumor killing as well as *in vivo* proliferation proved subtle between higher avidity TCRs, but all high-avidity TCRs performed markedly better than lowest avidity TCR39.

3.3 Transfer of retrogenic TCRs in the MC38-OVA tumor model

After having established the MC38-OVA model with OT-1 cells and having determined optimal time points of analysis and cell numbers for recovery and observable tumor protection, it was of interest to investigate the described retrogenic TCRs specific for ovalbumin peptide with different structural and functional properties with regards to their in vivo functionality. In this context, retrogenic TCRs were transferred – analogous to OT-1 cells – pre-emptively in combination with TBI, followed by MC38-OVA tumor inoculation the next day. The data presented is limited to a few chosen TCRs, which were examined in-depth *in vitro* and *in vivo*. The aim was to investigate avidity-dependent spatio-temporal T cell fate over the course of tumor disease and to what extent those TCRs would offer tumor protection. Analysis after transfer of single TCRs was thereby performed in parallel to simultaneous transfer of multiple TCRs, thus recreating a spectrum of avidities in reference to a natural, polyclonal TCR repertoire. The TCR repertoire used for the following experiments consisted of four TCRs, representing a spectrum of avidity. TCR16-30 proved to be of highest functionality as supported by the previously shown data. On the other end of the spectrum, TCR39 performed worst in terms of functionality. Meanwhile, TCRs 9 and 28 proved to be of intermediate avidity.

3.3.1 TCR mediated tumor protectivity

In order to investigate the impact of TCR avidity on tumor protectivity depending on transferred cell numbers, titration experiments were performed. For this purpose, either 128, 320, 800, 2000 or 5000 of either TCR16-30 or TCR39 cells were transferred to recipients.

TCR16-30 achieved near-complete tumor protection, departing from low numbers such as 320 cells (Figure 20 A). Upon transfer of 128 TCR^+ cells, protective capacities were surpassed, and tumor growth could no longer be controlled. This was indicated in regard to mean tumor growth early on day 11 as well, where a considerable leap between these titrations could be observed (Figure 20 C). Here, departing from 320 cells a statistically significantly reduced mean tumor growth compared to negative control could be observed. Moreover, further 2.5-fold increase to 800 transferred cells and more resulted in complete tumor control after initially detectable growth.

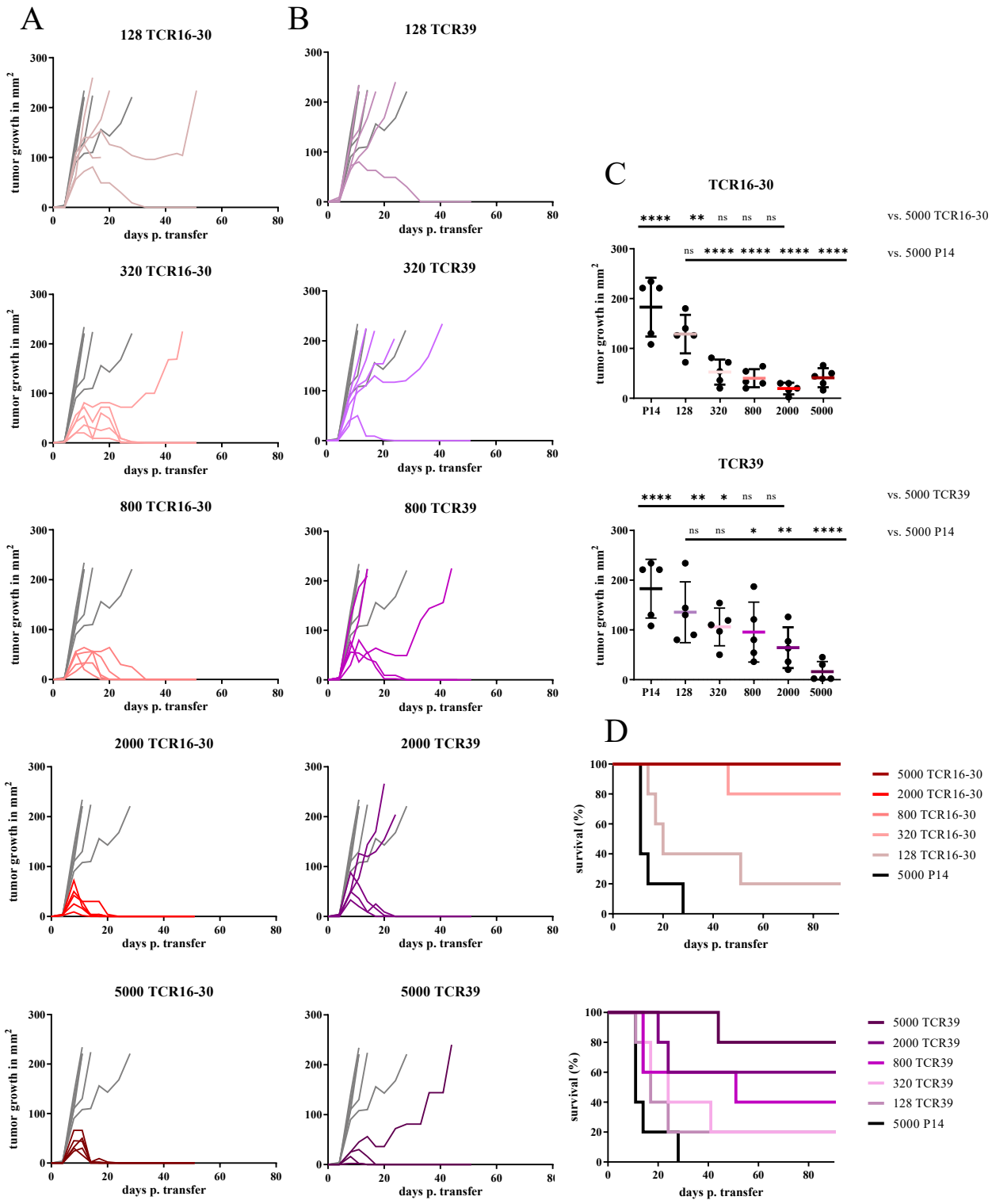

Figure 20 Tumor protectivity mediated by TCRs 16-30 and 39 depending on titration
Mice were irradiated with 5 Gy TBI and treated with TCR$^+$ cells i.p.; followed by injection of 10^6 cells MC38-OVA s.c. the next day. Administration of A.) 128, 320, 800, 2000 or 5000 either TCR16-30 or TCR39 cells (in colors), negative control with 5000 P14 cells in grey. B) Mean tumor growth for day 11 for n=5. Statistical testing by ordinary one-way ANOVA (**** for TCR16-30 and *** for TCR39) followed by Tukey's multiple comparison test. ns, not significant. * p value < 0.05, ** p value < 0.01, *** p value < 0.001, **** p value < 0.0001. D.) Survival. Statistical testing by log rank (Mantel-cox) for trend (**** for TCR16-30, ** for TCR 39) with n=5. Adapted from (Purcarea et al., 2022).

TCR39 as well displayed differential protection according to cell numbers transferred. Contrary to TCR16-30, near-complete tumor rejection was only achieved by the highest titration of 5000 TCR39 cells (Figure 20 B), with far less tumor control among lower cell numbers. Concerning mean tumor growth, statistically significantly reduced tumor size compared to control was only achieved by 800 transferred cells and more (Figure 20 C). Lowest numbers of TCR39 did not perform well, barely distinguishing themselves from controls.

The described trends were mirrored among survival rates, where high avidity TCR16-30 performed better than low avidity TCR39 (Figure 20 D). Strikingly, departing from 800 transferred TCR16-30 cells, all recipients survived the MC38-OVA tumor challenge and even lower numbers were still able to increase median survival (20 days vs. 11 days median survival for 128 TCR16-30 cells against controls). TCR39 performed worse overall, with only 80% survival rates for the highest titration. Lower cell numbers were still able to improve survival, albeit at a much lower level than same cell numbers of TCR16-30 (17 days median survival for 128 TCR39 cells).

In conclusion, lowest numbers of high avidity TCR16-30 – departing from 320 cells – achieved nearly perfect tumor control as displayed by tumor growth and survival. TCR39 on the other hand, which is of low avidity, managed comparable tumor control only among the highest titration of 5000 cells, while lower cell numbers beginning with 800 cells were able to significantly reduce tumor growth compared to control, a trend also mirrored by overall survival.

Since differential protective capacities seemed to be most detectable between titrations of either 320 or 800 cells, another experiment was performed which aimed to compare TCRs 9, 16-30, 28 and 39 in the same setting. Thus, each experimental group received either 320 or 800 cells of those retrogenic TCRs respectively. All groups displayed initial tumor growth, while controls with P14 cells resulted in aggressive, not controllable tumors which reached termination criteria within 20 days (Figure 21 A, B). Tumor control was achieved in varying degrees among experimental groups, in which differential tumor growth could be observed depending on the transferred TCR. Strikingly, for most TCRs already as few as 320 cells managed to slow tumor development. Moreover, in accordance with earlier findings, groups receiving high avidity TCR16-30 regardless of titration were able to entirely reject the tumor over time. While TCR9, which is also of high avidity, was able to mediate some tumor protection, low to intermediate avidity TCRs 28 and 39 allowed for tumor growth comparable to negative control.

For the purpose of quantification, survival was depicted by Kaplan-Meier-analysis and compared between TCRs and cell numbers transferred (Figure 21 C, D). Regarding protection mediated by

either 320 or 800 TCR16-30 cells, all recipients survived the tumor challenge thus supporting previous findings. While survival rates among TCRs 28 and 39 were lower and compared to control, TCR9 seemed to offer intermediate tumor protection, especially distinguishable among low cell numbers of TCRs transferred.

Overall, tumor control could be mediated by lowest cell numbers of high-affinity TCRs while results pointed towards differential control among lower affinity TCRs. Notably, a 2.5-fold increase of cell numbers thereby did not necessarily improve the outcome.

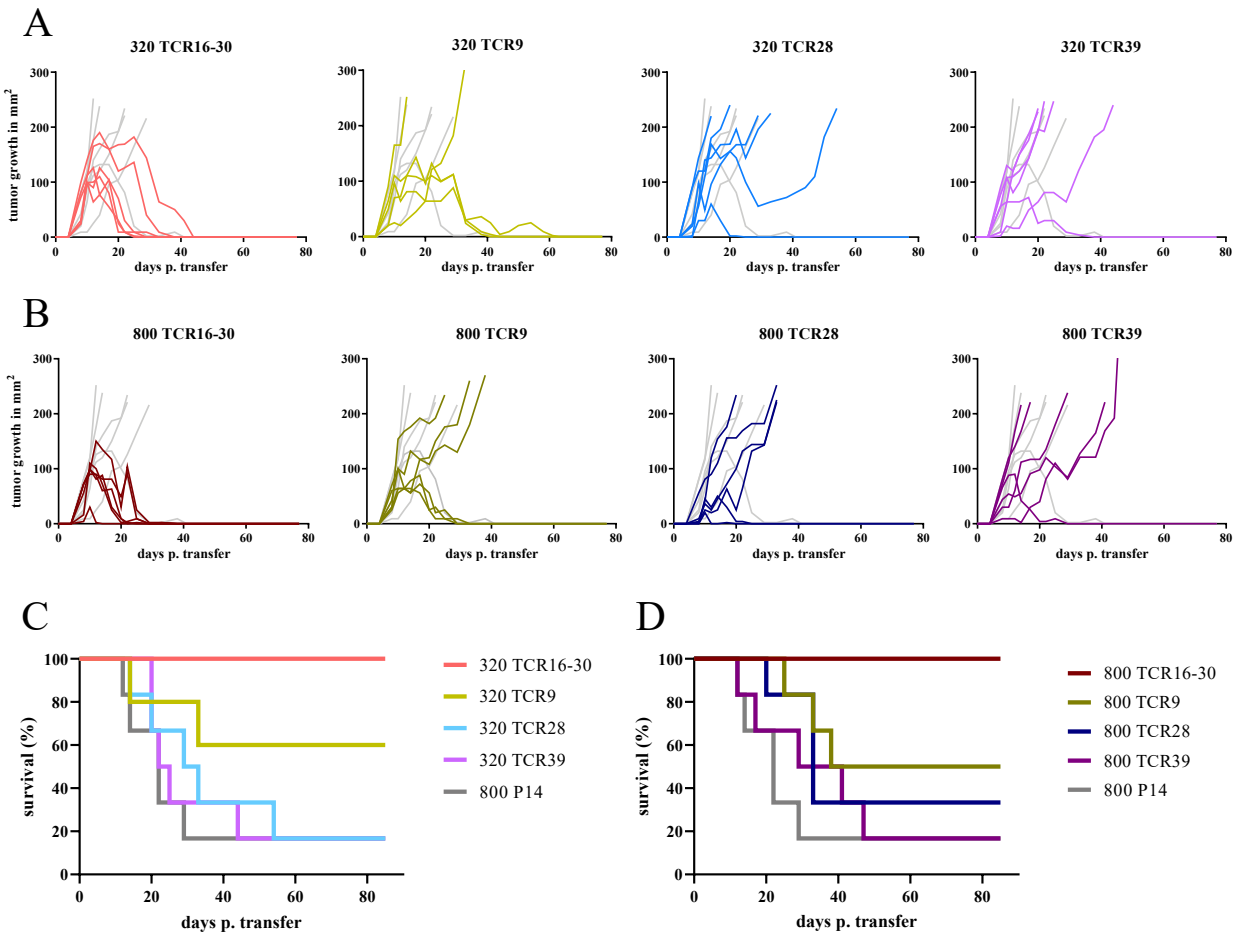

Figure 21 Tumor protectivity mediated by either 320 or 800 retrogenic TCRs
Mice were irradiated with 5 Gy TBI and treated with TCR^+ cells i.p.; followed by injection of 10^6 cells MC38OVA s.c. the next day. Administration of 320 or 800 cells of either TCR16-30, TCR9, TCR28 or TCR39, 800 P14 cells for negative control. Shown are tumor growth compared to control for A.) 320 TCRs and B.) 800 TCRs. Survival for C.) 320 TCRs and D.) 800 TCRs. Statistical testing by log rank (Mantel-cox) for trend (*) with n=5. * p value < 0.05. Adapted from (Purcarea et al., 2022).

3.3.2 Spatio-temporal distribution of recovered retrogenic TCRs

In order to minimize host-to-host variability while also allowing for the investigation of synergic interactions among retrogenic TCRs, polyclonal transfer experiments were performed. Therefore, combinations of different TCRs with distinct avidities were transferred into the same host. This was made possible by labeling those cells according to the congenic matrix as previously described (Buchholz et al., 2013). For this purpose, a unique congenic marker background of CD45.1/.2 and CD90.1/.2 alleles was used for each TCR, facilitating their identification during flow cytometric analyses. Thus, respective populations could be recognized via isotypic-specific antibodies and subsequently characterized.

Overall, recipients were treated with 2000 naïve retrogenic TCRs, comprising 500 cells of TCRs 16-30, 9, 28 and 39 respectively. Hereby, their determined range of avidities could be deployed to mirror a physiological TCR repertoire. Time points of analysis were days 7 or 8, 12 and 17 to allow for observations of the role of TCR avidity at earlier and later moments during tumor disease. Those low cell numbers were aimed at representing physiological precursor frequencies, but still allowed for recovery of retrogenic populations from peripheral blood, both draining and non-draining lymph nodes as well as the tumor (Figure 22). Within the respective gates, transferred TCRs could be identified via their unique expression of CD45.1/.2 and CD90.1/.2 as shown by the exemplary gating.

The enrichment of retrogenic TCR T cells was quantified expressed by percentage of $CD8^+$ cells for blood and all other sites, and recovery was quantified by absolute cell numbers for solid organs (tumor and lymph nodes) (Figure 23). The early time points of analysis displayed varying, rather low numbers of retrogenic cells with no distinctive pattern regarding TCR preference. Even though it may seem that TCR28 dominates among TILs concerning absolute cell numbers (Figure 23 A), this impression is given by the extremely low numbers overall, mostly less than 10 TCR^+ cells. Still, this could reflect an interesting finding of early tumor recruitment of T cells with a low-to-intermediate affinity TCR.

Concerning TCR recovery and enrichment among lymph nodes, again no distinctive affinity dependent trend could be observed. Low frequencies of retrogenic TCRs on the early time point did not really allow for general conclusions. Interestingly, later time point day 17 proved to be more revealing for TCR recovery from solid organs.

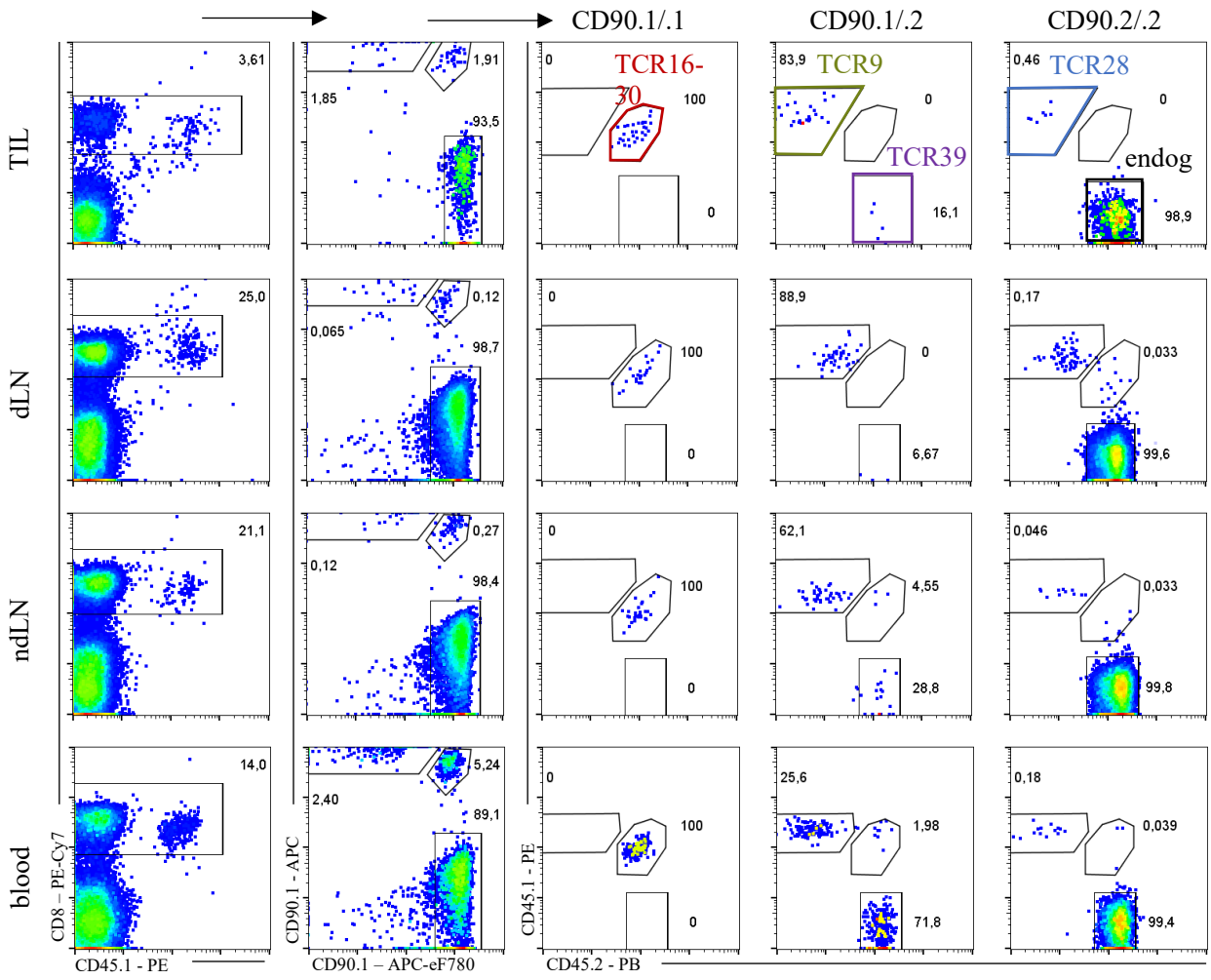

Figure 22 Primary data for recovery and identification of retrogenic TCRs
Mice were irradiated with 5 Gy TBI and treated with 500 TCR16-30 (CD45.1.2/CD90.1.1), TCR9 (CD45.1.1/CD90.1.2), TCR28 (CD45.1.1/CD90.2.2) and TCR39 (CD45.2.2/CD90.1.2) respectively resulting in 2000 cells overall i.p.; followed by injection of 10^6 cells MC38-OVA s.c. the next day. Mice were sacrificed for blood, dLN, ndLN and TIL on days 7 (day 8 for blood), 12 and 17. Primary data with exemplary gating for identification of transferred cells via congenic markers for each organ. Adapted from (Purcarea et al., 2022).

Here, both draining and non-draining lymph nodes showed larger proportions of high-to-intermediate affinity TCRs as opposed to TCR39; even statistically significantly so for non-draining lymph nodes regarding both enrichment and recovery (Figure 23 C). This could point towards TCRs exceeding a threshold avidity being preferably selected and recruited into the tumor and the lymphoid tissue over time.

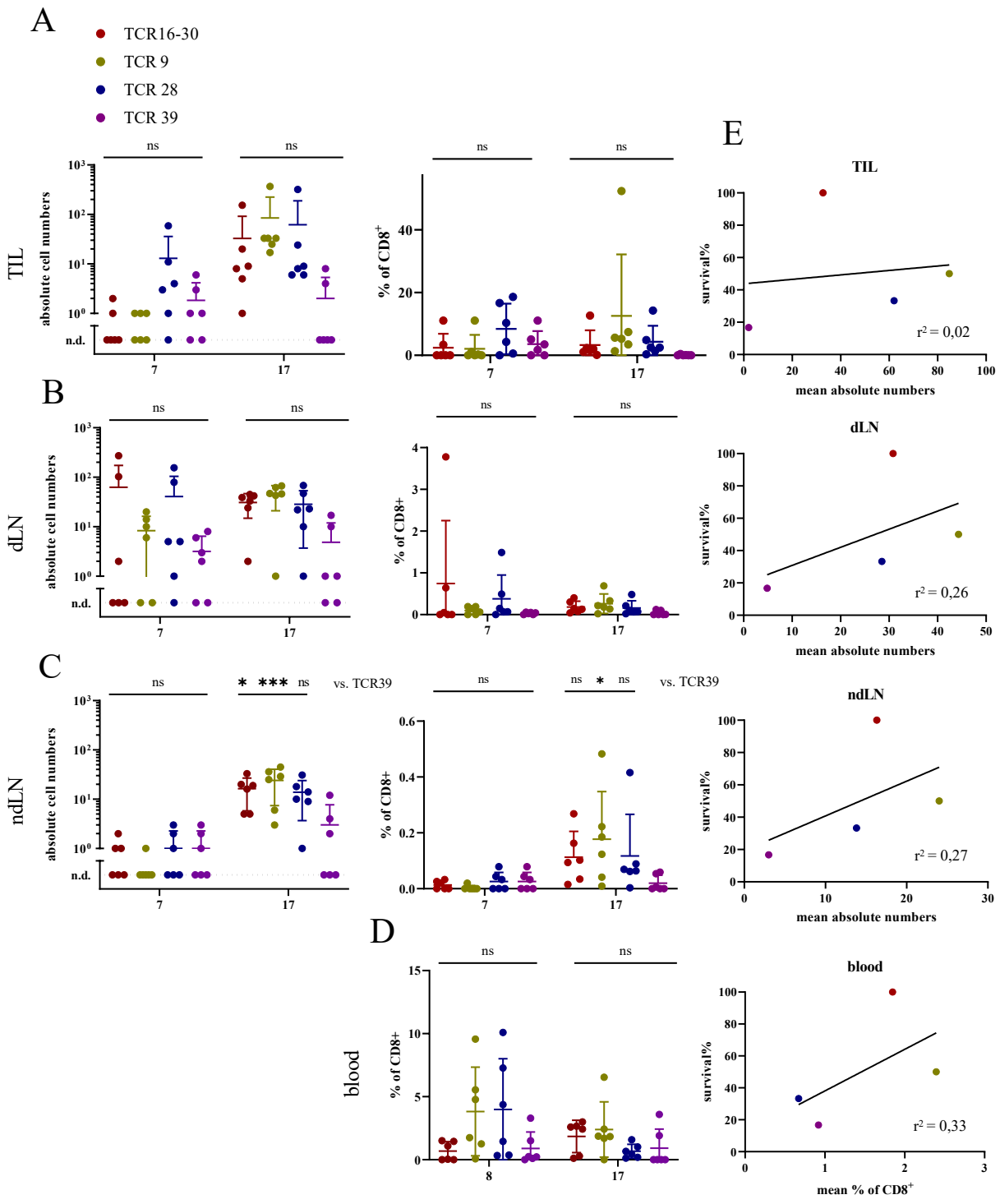

Figure 23 Organ and time dependent recovery of retrogenic TCRs
Mice were irradiated with 5 Gy TBI and treated with 500 TCRs 16-30, 9, 28 and 39 i.p. respectively resulting in 2000 cells overall; followed by injection of 10^6 cells MC38-OVA s.c. the next day. Mice were sacrificed for blood, dLN, ndLN and TIL on days 7 (day 8 for blood), 12 and 17, color coded for organs see legend below. Absolute cell numbers and percentage of $CD8^+$ cells for A.) TIL, B.) dLN and C.) ndLN. D.) Percentage of $CD8^+$ cells for blood. Statistical testing by two-way ANOVA (* for ndLN) followed by Tukey's multiple comparison test. E.) Correlation of survival and absolute cell numbers of transferred cells (percentage of $CD8^+$ for blood) for day 17 depending on organ. Fitted with linear fit with n=6. ns, not significant. * p value < 0.05, *** p value < 0.001. Adapted from (Purcarea et al., 2022).

In peripheral blood, enrichment of the retrogenic TCRs did not follow any clear-cut trend either (Figure 23 D). However, day 8 discretely points towards differential TCR enrichment among PBMCs. Here, both TCRs 9 and 28 seem to make up larger proportions of the $CD8^+$ population compared to the other TCRs. Again, this could point to a differential role of intermediate avidity TCRs, similar to findings among TIL. This trend as well as any other cannot be reproduced on day 17, where this distinction is lost.

Regarding protective capacities earlier demonstrated of the retrogenic TCRs, no pattern of preferential enrichment or recruitment could be shown (Figure 23 E). In this context, no correlation for any organ analyzed could be found. Overall, the subtle trends described above may prove to reflect real biology if further investigated. In the investigated settings, the affinity of TCRs did not lead to major and consistent differences in abundance of T cells at the indicated time points and organs.

3.3.3 PD-1 expression of retrogenic TCRs

The polyclonal transfer setting also allowed for examining the expression of inhibitory co-receptors of retrogenic TCRs depending not only on organ and time point of recovery, but also on TCR avidity. Since PD-1 expression levels had proven to correlate with global upregulation of co-inhibitory markers for transferred OT-1 cells (Figure 13 E, F), studies with retrogenic TCRs focused on this marker.

For the purpose of quantifying PD-1 expression, both by mean fluorescence intensity and percentage, $PD\text{-}1^+$ cells were compared for different organs and time points depending on transferred TCRs. As expected, transferred TCRs expressed higher levels of PD-1 compared to the endogenous $CD8^+$ population of reference, indicating for antigen-specific recognition and target interaction (Figure 24 A-C).

Taking into account the overall higher levels of PD-1 expression in the tumor, differential cut offs regarding PD-1 positivity among TIL and peripheral organs were investigated rather than a dichotomous approach. In reference to the endogenous populations, this allowed for identification of a $PD\text{-}1^{high\ (hi)}$ population found only among TILs rendering peripheral $PD\text{-}1^+$ populations intermediate level (Figure 24 A, B). As described before for OT-1 cells, high PD-1 expression levels could be the result of T cell exhaustion upon persistent antigen stimulation in the tumor, resulting in loss of function and impairment of the anti-tumor response. On the other hand, intermediate PD-1 expression, as described via PD-1 positivity in lymph nodes and blood

could be seen as sign of antigen-specific activation, not necessarily implicating the described dysfunctional state.

Upon further quantification, more than 80% of TCR^+ TILs were also $PD\text{-}1^+$, opposed to only 20% among the endogenous $CD8^+$ population (Figure 24 C). Outside the tumor, frequencies were more varied and overall lower. Here, in both draining and non-draining lymph nodes and especially peripheral blood, intermediate levels allowed for the identification of distinctive TCR dependent PD-1 expression (Figure 24 B). About 80% of TCR16-30 cells were $PD\text{-}1^+$ in the lymph nodes (about 65% among PBMCs), followed by around 50-60% for TCR9 (about 40% among PBMC). Interestingly, harboring about 50% $PD\text{-}1^+$ cells, low-to-intermediate avidity TCR28 cells took second place in peripheral blood, corresponding to earlier findings concerning enrichment of these cells. This pattern was also mirrored by mean fluorescence intensity (Figure 24 B), where high avidity TCR16-30 showed highest levels of PD-1 expression, followed by TCR9 in lymph nodes and TCR28 in blood, respectively. Independent of organ, low avidity TCR39 showed lowest levels of PD-1 expression, both in MFI and percentage. However, due to minimal enrichment of this TCR and lowest numbers recovered it often failed to surpass a chosen threshold of 5 cells for phenotypic analysis, limiting interpretability.

Intriguingly, regarding *in vivo* functionality of the retrogenic TCRs upon monoclonal transfer, a strong positive correlation with their PD-1 expression could be shown for the periphery (Figure 24 D). In this context, TCR16-30 which had previously mediated tumor control even at lowest numbers, expressed the highest levels of PD-1 in the lymph nodes as well as in blood. Interestingly, this was explicitly not the case in the tumor. Here, PD-1 expression followed no avidity dependent pattern whatsoever. Overall, these data point toward differential PD-1 expression levels on T cells outside the tumor, which seem to follow a gradient depending on TCR avidity.

For the purpose of further investigation, both endogenous and transferred CD8+ populations from different organs were divided into multiple fractions regarding their expression levels of PD-1. This allowed for a stratified analysis of TCR enrichment among these established sub-populations in relation to their PD-1 up-regulation (Figure 24 E). Therefore, the top PD-1 expressing fraction for each individual replicate was defined instead of setting a general MFI threshold. In peripheral blood, but not in the tumor, high avidity TCR16-30 was significantly enriched among the top 4% or top 10% PD-1 fraction.

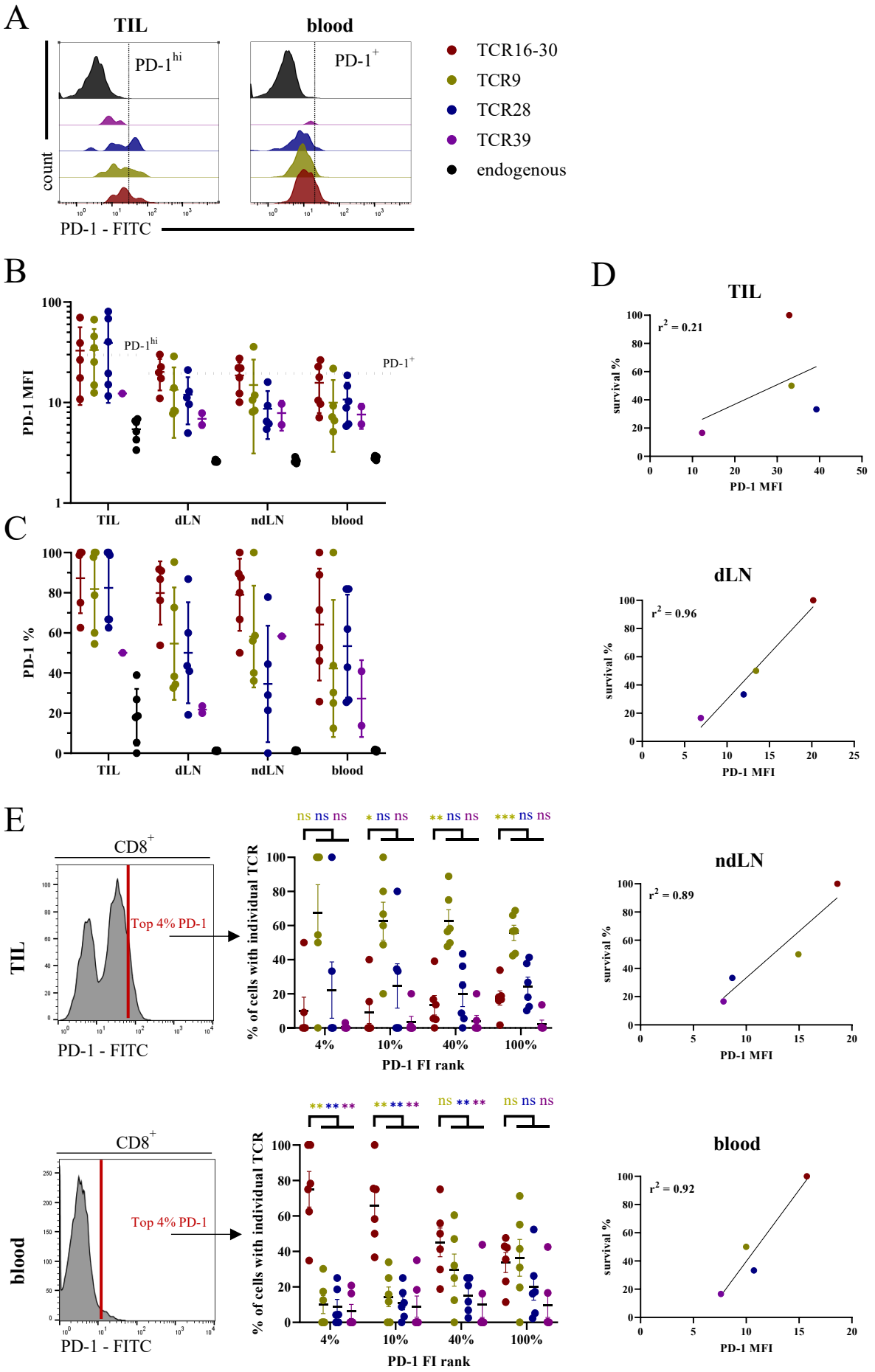
A
TIL
blood
PD-1hi
PD-1+
count
PD-1 - FITC
TCR16-30
TCR9
TCR28
TCR39
endogenous
B
PD-1 MFI
TIL
dLN
ndLN
blood
C
PD-1 %
D
TIL
r2 = 0.21
survival %
PD-1 MFI
dLN
r2 = 0.96
ndLN
r2 = 0.89
blood
r2 = 0.92
E
CD8+
Top 4% PD-1
% of cells with individual TCR
PD-1 FI rank
4%
10%
40%
100%

Figure 24 PD-1 expression of retrogenic TCRs depending on time and organ
Mice were irradiated with 5 Gy TBI and treated with 500 TCRs 9, 16-30, 28 and 39 respectively resulting in 2000 cells overall i.p.; followed by injection of 10^6 cells MC38-OVA s.c. the next day. Mice were sacrificed for blood, dLN, ndLN and TIL on days 7, (day 8 for blood) 12 and 17. A.) Histograms representing PD-1 expression of $CD8^+$ cells for TIL and blood. Exemplary gating for PD-1^{hi} and PD-1^+ populations. B.), C.) percentage of PD-1^+ cells and MFI in different organs compared to the endogenous population. For a more accurate representation, a cut-off at 5 cells was established. Each dot represents one biological replicate, data shown for d17, color coded for TCRs. D.) Correlation of survival and PD-1 MFI for the different retrogenic TCRs per organ via nonlinear regression with n=5. E.) Gating strategy and identification of retrogenic TCRs in TIL and blood, identifying top 4% of PD-1^+ cells, pregated on $CD8^+$ cells. B.) Percentage of PD-1 rank of transferred cells versus percentage of individual population and $CD8^+$ cells for TIL and blood. Dot plots for PD-1 FI ranks at 4%, 10%. 40% and 100%. Statistical testing by two-way ANOVA (*) followed by Tukey's multiple comparison test for n=5. ns, not significant. * p value < 0.05, ** p value < 0.01, *** p value < 0.001. Adapted from (Purcarea et al., 2022).

For the top 40% fraction, low avidity TCR28 and TCR39 still were significantly less represented than higher avidity TCRs. On the other hand, this pattern was not mirrored in the tumor, where TCR16-30 failed to enrich in any PD-1 fraction. Strikingly, starting from the top 10% PD-1 fraction, TCR9 proved to be significantly enriched among transferred cells, albeit being less protective than TCR16-30. Since previously it had been shown that the latter failed to enrich among TIL, this could be a sign for the differential role of intermediate TCR avidity in the tumor.

In conclusion, these findings point towards high PD-1 expression levels identifying highly protective tumor-specific TCRs, but only outside the tumor.

4. Discussion

4.1 Tracking of physiological low cell numbers

This study aimed to create most physiological conditions in order to allow for the investigation of the dynamics as well as the protectivity of tumor-specific T cells, using the MC38-OVA tumor model. The transfer of lowest possible cell numbers was intended to recreate the natural repertoire of antigen-specific T cells. Considerable protective capacities of minimal T cell numbers have recently been demonstrated for infection models (Buchholz et al., 2016; Graef et al., 2014). Therefore, titration experiments were performed to identify minimal numbers of transferred cells, still allowing for tumor protectivity and tracking in the host organism.

Identification of transferred T cells was facilitated by their congenic background labeling which could thus be discriminated against the endogenous $CD8^+$ population. While absolute cell numbers recovered gave a good impression on the extent of *in vivo* recruitment, they were not suited to compare the recovery between solid organs and blood. Because of this, the enrichment of the transferred cells in peripheral blood was indicated by percentage of the total $CD8^+$ population, thus allowing for the comparison of different organs and also in between experiments. As a limitation, it has to be mentioned that *in vivo* proliferation or cell death were not measured directly. However, cellular abundance is widely recognized as a solid indicator of *in vivo* recruitment.

Overall, it could be observed that upon transfer of 5000 OT-1 cells, expansion in the peripheral blood, lymph nodes and the tumor itself could be detected by flow cytometric analysis on each time point. Furthermore, preferential enrichment of transferred cells took place in the tumor, independent from titration and time point of analysis. In some recipients, the transferred OT-1 cells temporarily constituted more than 90% among TILs (see Figure 10), thus markedly dominating the intratumoral immune response. However, there seemed to be a dependency on the time point of analysis regarding maximal enrichment, with the intermediate time point on day 12 identified as peak of expansion. Both peripheral blood and TILs showed significant differences in enrichment of OT-1 between days 7 and 12, with a significant decline of frequencies towards day 17 limited to PBMCs. This could suggest for a plateau of OT-1 enrichment reached as early as day 12 mediating tumor control. Also, data points to a systemic spread and peripheral accumulation of OT-1 cells over the time.

In order to determine whether lowest numbers of T cells would yield detectable off-spring and in how far this would alter their spatio-temporal adaptation, transferred cell numbers were reduced and analyses performed on day 12. Interestingly, 800 OT-1 cells, thus representing a 6.25-fold reduction of the progenitor population, amounted to the same enrichment among TIL. Only upon further reduction to 128 transferred OT-1 cells, decreased OT-1 numbers in the tumor could be noticed. The data indicate that in the tumor, a plateau of OT-1 enrichment could be reached departing from 800 cells on, without further increase following higher cell titrations. Thus, a threshold could be assumed at 800 cells for optimal engraftment of transferred OT-1 in the tumor. This supports the hypothesis that the initial size of the antigen specific population has less influence on maintaining the immune response than its adequate and sustained expansion. While those findings could not be seen in blood or lymph nodes (both draining and non-draining), this supports the notion of pronounced antigen-specific recruitment into the tumor

Altogether it should be stated that the population of transferred OT-1 cells could be tracked independently from applied numbers or time points in all organs analyzed, while preferential enrichment seemed to take place among TILs. Furthermore, enrichment was most distinct on day 12 in both blood and tumor. Moreover, lowest cell numbers transferred corresponding to the natural repertoire of antigen-specific T cells yielded detectable progeny. Further increase of transferred cells resulted in only minor alterations regarding enrichment among TIL. This could indicate that engraftment of transferred cells depended on antigen-specific activation and proliferation rather than population size.

4.2 Phenotypical composition of TIL

Lymphocytes infiltrating the tumor arguably play a distinguished role in the cellular antitumoral immune response. Therefore, one could assume a distinctive, functional state of these cells according to local antigen load and before mentioned aspects of the tumor microenvironment.

In melanoma patients, endogenous tumor reactive $CD8^+$ cells have been identified via PD-1 expression, thus identifying essential actors of tumor immunity (Gros et al., 2014). Expression of inhibitory co-receptors, such as PD-1, but also TIM-3, LAG-3 among others, is commonly associated with chronic antigen stimulation - to which T cells are subject in chronic infection but also in tumors and which eventually results in dysfunctional, exhausted T cell states (Baitsch et al., 2011; Blackburn et al., 2009; Wherry et al., 2007). However, inhibitory receptor-expressing cells also proved to represent the tumor reactive, autologous repertoire including T cells specific

for tumor neoantigens and therefore essential for eliminating the tumor (Gros et al., 2014). In the latter study, especially PD-1 expression proved to be a suitable marker for clonal expansion following tumor antigen-specific recruitment. Also, there is evidence for the level of PD-1 expression to allow for conclusions concerning the functional state of the T cell. While TIL present with overall higher PD-1 MFI than their peripheral counterparts among PBMC, this entails a certain loss of functionality (Thommen et al., 2018).

In that context, the present study included phenotypical analysis of transferred cells in different organs following transfer of naïve OT-1 cells in the MC38-OVA tumor model. In early experiments, activation marker CD44 proved differentially expressed on transferred cells compared to the corresponding endogenous population (See Figure 11). Interestingly, CD44 expression was more pronounced for transferred cells in the periphery, while among TIL CD44 signals were overall lower, approaching the MFI of endogenous cells. Concerning frequencies however, early time point day 7 seemed to entail elevated CD44 expression on the endogenous population compared to day 14, whereas transferred cells had upregulated CD44 independently of the time point analyzed. This could possibly indicate for a shift towards activation of antigen specific cells on later time points. Among TIL however, T cell activation in terms of CD44 expression seemed to occur independently of antigen specifity.

For a more differential analysis of phenotypes present among transferred TIL compared to their endogenous counterpart, expression of other markers linked to T cell activation and also exhaustion was investigated. Besides PD-1 expression, markers TIM-3 and LAG-3 were subject of investigation, indicating global presence of inhibitory co-receptors. Regarding the proportion of positive cells, all three inhibitory co-receptors were significantly upregulated on transferred cells compared to organ specific endogenous populations, as a sign of antigen-specific activation (see Figure 13). However, among transferred cells, especially PD-1 (but also on a lower level TIM-3 and LAG-3) were preferentially expressed in the tumor. Here, for both MFI and frequencies of PD-1^{+} cells, TIL showed the highest quantitative as well as qualitative expression of PD-1. Interestingly, PD-1 expression levels seemed to follow an organ dependent gradient, with TIL displaying the highest level, followed by draining lymph nodes, then non-draining lymph nodes and lastly peripheral blood. PD-1 was therefore not only upregulated among transferred cells, but its expression also seemed to be organ dependent.

Importantly, PD-1 expression is known to play an ambiguous role in T cell activation. Since early antigen specific activation leads to an initial upregulation of PD-1 (Barber et al., 2006), one might argue that PD-1 positivity among transferred cells could indicate their preferential recruitment

and expansion. Still, significantly higher levels of PD-1 expressed among OT-1 TIL compared to systemic expression could point towards some form of actual functional exhaustion (Thommen et al., 2018). The fact that this trend is not mirrored within endogenous $CD8^+$ populations could lead to the conclusion that PD-1 upregulation occurs as a result of antigen-specificity rather than functional adaptation in the tumor.

The simultaneous expression of several inhibitory co-receptors is another phenotypic aspect generally associated with T cell exhaustion (Wherry, 2011). The present data indicated for an organ dependent enrichment of PD-1/TIM-3/LAG-3^+ cells, corresponding well to previous findings regarding PD-1 expression. Here, cells co-expressing all three inhibitory markers constituted around 60% of transferred cells among TILs. Frequencies were lower in lymph nodes, with around 15% being lowest in peripheral blood. Among endogenous cells, triple positive cells were limited to TILs, possibly indicating the presence of endogenous, antigen-specific and possibly exhausted T cells. Taking into account that frequencies of PD-1/TIM-3/LAG-3^+ OT-1 cells correlated positively with their overall PD-1 MFI, which was highest among TIL, this would speak for T cell exhaustion occurring mainly in the tumor upon exposure to high antigen burden. Intermediate levels of PD-1 expression as experienced for lymph nodes and peripheral blood on the other hand would be expected to indicate antigen-specific activation rather than dysfunction.

4.3 Tumor protection mediated by lowest T cell numbers

Since lowest numbers of transferred OT-1 cells could be tracked and characterized regarding their spatio-temporal distribution and prevailing phenotypes, it was of interest to investigate in how far previous findings corelated with the effector capacities of those cells.

Regarding protective efficacy, it could be shown that transfer of low numbers of OT-1 cells resulted in tumor protection, with as few as 800 OT-1 cells sufficing for nearly perfect tumor control (see Figure 14). Immunocompetent WT C57Bl/6 mice receiving P14 cells showed an aggressive, uncontrolled tumor growth, most of which reached termination criteria early before day 20. Hence, the endogenous immune response depended on the transferred antigen specific cells for tumor control. Furthermore, there was even some evidence pointing towards long-term tumor immunity, since re-exposure with higher doses of MC38-OVA in mice who had previously been able to reject the tumor did not induce renewed tumor growth, regardless of cell numbers transferred (data not shown).

These findings might seem to contradict previously observed phenotypic adaptions of the transferred OT-1 cells. Indeed, PD-1^+ and TIM-3^+ OT-1 cells recovered from B16-OVA tumors have been shown to correlate with decreased *in vitro* cytokine production in correspondence with an assumed dysfunctional state (Mognol et al., 2017). However, the protection experiments showed that only 800 OT-1 were able to mediate tumor control, which would be unlikely if all cells were exhausted and thus dysfunctional. One explanation might be that exhaustion is known to be a gradual process with the loss of functionality occurring hierarchically. Due to the high TCR avidity of OT-1, tumor control might be achieved before CTL are terminally exhausted. Furthermore, subsets of exhausted $CD8^+$ cells have been identified with differential abilities to mediate tumor protection and long-term immunity (Miller et al., 2019).

While survival analysis indicated an improved survival for mice that received 800 OT-1 cells and more, compared to control the threshold for reduced tumor growth could be even lower (see Figure 14). Strikingly, positive effects on tumor protection could be observed for as few as 128 OT-1 cells, thus corresponding to the natural frequency of precursor cells for H-$2k^b$/SIINFEKL in naïve T cell repertoires. The latter is assumed to include around 130 cells (Obar et al., 2008) which is also consistent with respective frequencies described for human $CD8^+$ cells (Alanio et al., 2010). On day 16 post transfer, there was a significant leap between the groups receiving 128 or 320 OT-1 cells, manifesting in decelerated tumor development.

Still, only groups that received highest cell numbers, departing from 800 transferred OT-1 cells, were distinguished by almost complete survival. While fewer cell numbers might be able to slow down tumor growth early on, tumor control and thus survival becomes less likely as time progresses. Still, lowest cell numbers corresponding to frequencies of the natural T cell repertoire, were able to mediate tumor immunity.

4.4 Structural avidity dependent TCR functionality

In order to gain further insights regarding the impact of TCR affinity on tumor protection and the spatio-temporal fate of T cells during cancer, the mentioned SIINFEKL specific TCR library with different avidities was applied.

Literature on this topic often involves transfer of monoclonal T cells such as OT-1 cells, sometimes in combination with altered peptide ligands (APL) of the SIINFEKL peptide in order to recreate differential TCR-pMHC interactions (Martínez-Usatorre et al., 2018; Zehn et al., 2009). However, the effect of these modified peptides seems not to be limited on these

interactions, but also on the stability of their MHC, thus creating other variables influencing the studies (Irving et al., 2012; Stone et al., 2009). Furthermore, the OT-1 system, though prevalently used, entails some unconventional features, questioning the applicability of those findings (Nauerth, Weissbrich, et al., 2013). For instance, despite their short half-life time of 30 s, generally associated with low structural avidity in k_{off}-rate measurements, OT-1 cells effectively controlled *L.m.*OVA infections - even at a single cell level (Stemberger et al., 2007). Furthermore, the fact that those systems often include monoclonal transfer approaches suited for recreating clinical immunotherapeutic conditions fail to allow conclusions for the physiological, polyclonal setting.

The beforementioned limitations are circumvented by the introduced system of retrogenic, SIINFEKL-specific TCRs with different avidities. Identified from the endogenous repertoire of IE2 mCMV-OVA infected mice and re-expressed via retroviral transduction into so-called retrogenic mice, they display distinctive structural avidities measured by k_{off}-rate assays (Grassmann et al., 2019; Holst et al., 2006). For the purpose of thorough characterization, the next step was to determine the functionality of these retrogenic TCRs and how it was related to their structural properties. On the one hand, this would allow for insights regarding optimal TCR-pMHC binding kinetics in general. On the other hand, prior functional and phenotypical characterization of those TCRs would render possible findings in the *in vivo* tumor setting better interpretable.

For phenotypical analyses, $CD45.1^+/CD90.1^+$ naïve $CD8^+$ T cells expressing a given TCR were recovered from TCR retrogenic mice (Figure 15). The fact that expression of phenotypic markers CD44, CD62L and CD27 showed no significant differences between TCRs points towards a homologous profile of those cells, according to their assumed antigen inexperienced state. Supporting this notion, neither CD8 nor congenic markers CD45.1/CD90.1 were differentially expressed. However, mean fluorescence intensity of the MHC multimer staining seemed to increase in correspondence with higher TCR affinity. In this context, TCR 16-30 expressed highest amounts of MHC compared to the other TCRs. This could already suggest for differential binding capacities, since MHC multimer stainings have been previously used to quantify TCR-pMHC interaction. However, evidence yielded by this method remains questionable and is subject to discussion (Hebeisen, Allard, et al., 2015).

A more reliable measure for functional capacities and thus efficacy of T cells is the sensitivity to cognate antigen. High avidity T cells already respond to lowest antigen doses (Viganò et al., 2012). Along this line, retrogenic TCRs recovered during a *L.m.*OVA infection were submitted

to *in vitro* SIINFEKL peptide stimulation followed by intracellular cytokine staining (ICCS) to quantify effector capacities (see Figure 16). The chosen panel of TCRs represented the repertoire of tumor experiments during the early phase of this thesis. Since then, other TCRs have been selected to more accurately cover a wider range of TCR affinities (those TCRs were also tested for their in vitro functionality in a collaborative effort). In the present setting, TCRs 8, 9 and 21 display a medium k_{off}-rate while TCRs 28 and 39 show ultra-fast and ultra-slow dissociations, respectively. As previously explained, longer k_{off}-rate kinetics have been shown to correlate with higher structural avidity and better *in vivo* effector capacities of T cells in infections (Nauerth, Weißbrich, et al., 2013).

Production of IFNγ, TNFα and IL-2 could be detected for all retrogenic TCRs, including polyfunctional triple positive populations. IFNγ release quantified as half-maximal effector concentration (EC_{50}) seemed to be most differential among TCRs. For the chosen panel of retrogenic TCRs, TCR39 was of significantly lower functionality compared to the others. Among the other TCRs of medium dissociation times, no imminent superior IFNγ production was revealed. Still, upon closer discrimination, TCR28 seems to perform slightly worse than the TCRs with longer k_{off}-rates.

Another practicable measure of T cell functionality is represented by *in vivo* recruitment capacities upon antigen encounter. For this purpose, T cell expansion in response to *L.m.*OVA infection was quantified for a progenitor population of 100 retrogenic TCRs (see Figure 17). Highest absolute expansion was achieved by TCR16-30, with progeny exceeding the input amount by around 10^3-fold, even comparable to described OT-1 expansion (Buchholz et al., 2013). TCRs 9 and 28 expanded less, while TCR39 showed more variable and rather inferior expansion capacities. Further *L.m.*OVA *in vivo* recruitment experiments performed by Kilian Schober and Sebastian Jarosch revealed these trends to be statistically significant. Furthermore, ICCS for TCR16-30 revealed statistically significantly enhanced IFNγ production, thus pointing towards superior functional properties of the bespoken TCR (data not shown).

In preparation for the MC38-OVA tumor setting, *in vitro* tumor killing capacities of the retrogenic TCRs were evaluated to confirm their differential functional properties and put them into relation with their effector potential. For this purpose, the xCELLigence killing assay yielded an attractive, yet challenging option for the quantification of tumor elimination by retrogenic TCRs. As described in the results section, problems arose from identifying a reliable negative control, since antigen unspecific cells also led to cell death when titrated to high numbers. Most likely this was due to medium consumption by the added T cells and thus deteriorating survival

conditions for the PancOVA tumor cells. However, 200 cells of TCR16-30 managed a significantly improved tumor elimination compared to TCR39 in corresponding numbers, thus supporting prior results from functional analysis (see Figure 19). A limitation of these data is that the negative control should ideally have encompassed antigen-irrelevant cells with the same, low cell number. However, differences between TCRs prevailed.

Altogether, the data suggest that among analyzed TCRs, TCR16-30 displayed superior functional properties expressed by enhanced *in vitro* IFNγ production as well as antigen specific tumor killing and also *in vivo* expansion following antigen stimulus. In contrast, TCR39 consistently showed lower functionality in all mentioned readouts. Among other TCRs, differential functionality was more subtle.

Findings concerning TCR39 may seem controversial, since it had previously displayed an ultra-long dissociation half-time indicating for high structural avidity (see Figure 2). Nevertheless, it can be argued that an exceedingly slow dissociation surpasses the optimum interaction ability and results in an ineffective T cell activation. In fact, this is in line with theoretical models and experimental evidence from some research groups. Different models predicting T cell activation depending on TCR-pMHC dissociation time were provided by Lever and colleagues. Among those, they postulated that regardless of ligand number, optimal T cell activation could potentially be linked to medium half-life time (Lever et al., 2014). Applied to T cell efficiency following activation, this could imply a bell-shaped curve for optimum T cell functionality. Observations made for TCR39 would fall in line with this model. Here, decreased functionality would be the result of dissociating kinetics outside the optimal range.

However, this one specimen hardly suffices to allow for conclusions, since it could represent an outliner just like previously described for OT-1 cells. If TCR39 was ignored, dynamics could also point towards a plateaued level of functionality departing from a certain dissociation time as depicted in Figure 25.

The identification of further SIINFEKL-specific TCRs, preferably with extreme dissociation half-life times, will be necessary to gain better insights into the relation between structural avidity and functional properties of antigen specific T cells.

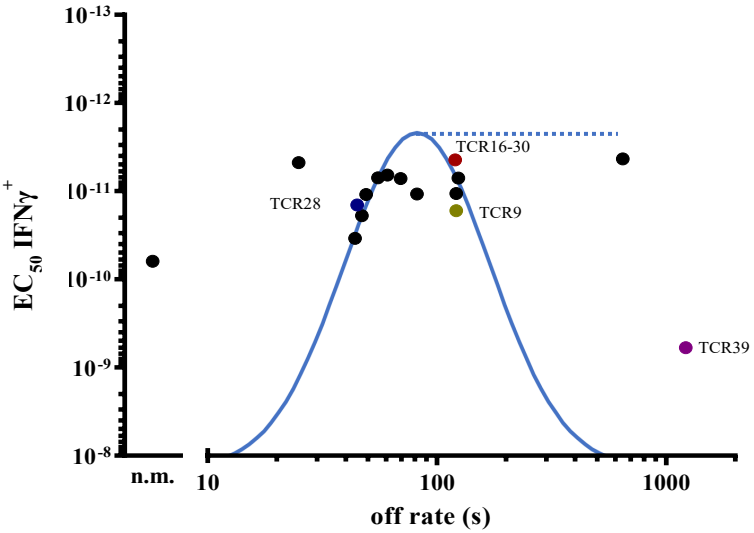

Figure 25 Model for potential prediction of TCR functionality depending on k_{off}-rate
Panel of OVA-specific retrogenic TCRs with different k_{off}-rates (Schober et al., 2020), correlated with their EC_{50} value of IFNγ production in order to predict TCR functionality depending on structural avidity. TCRs used for this thesis are color coded. Exemplary bell-shaped optimum curve vs. saturation kinetics in reference to (Lever et al., 2014).

4.5 Avidity dependent *in vivo* tumor protection

Since characterization of the retrogenic TCRs had revealed TCR16-30 to be highly functional, it was of interest whether this also applied to in vivo tumor protective capacities. Indeed, for the MC38-OVA tumor model, differential tumor protection could be attributed to all investigated TCRs depending on their previously determined functional properties.

Titration experiments with both TCR16-30 and TCR39 suggested a dose dependent mediation of tumor protection (see Figure 20). As few as 320 TCR16-30 cells managed to significantly reduce early tumor growth and allowed for an 80% survival rate. Furthermore, lowest titrations of 128 cells, again in reference to the natural repertoire, positively although discretely mediated tumor protection. Complete protection was yielded by 800 TCR16-30 cells and more. TCR39, on the other hand, which had previously displayed lower functional capacities, did not perform well regarding in vivo tumor control. Only higher titrations starting from 2000 cells and more

significantly reduced tumor growth, while 80 % survival was limited to further 6.25-fold increase to 5000 input of TCR39 cells. Nevertheless, lower numbers seemed to show some positive effects on tumor progress compared to control. Therefore, even the low avidity TCR could mediate some tumor protection. While protective capacities seem to be dose dependent for both high and low avidity TCRs, TCR39 mediated tumor control is only achieved by highest numbers. High avidity TCR16-30, however, manages tumor protection with lowest numbers.

Since differential tumor control seemed most prominently to manifest for 320 and 800 TCR^+ cells, another titration experiment for these numbers comparing further TCRs was performed. Supporting previous findings, transfer of both 320 and 800 TCR16-30 cells resulted in complete tumor clearance and survival (see Figure 21). Regarding protection of the other TCRs, it seemed to follow a gradient of achieved tumor control according to previous findings. In this context, TCR9 having shown to be of intermediate functionality, achieved less tumor control, followed by lower avidity TCR28 and finally the least functional TCR39 barely offering any protection. Thus, in vivo findings for the tumor corresponded well to previous functional analyses of the retrogenic TCRs.

Taking into consideration the superior protective properties of TCR16-30, it could be expected to translate into preferential recovery of cells bearing this TCR during tumor disease. Interestingly, however, this was not the case. In fact, recovery of the transferred TCRs did not necessarily depend on their functionality. Upon closer observation, both TCR9 and TCR28 seemed enriched early on day 7 in the blood compared to lowest avidity TCR39. This trend is mirrored by the lymph nodes later on day 17, in which again TCR 9 dominates over TCR39. In the tumor, TCR9 is more enriched than TCR28, constituting around 30% of $CD8^+$ TILs (see Figure 23).

On the one hand, these temporal dynamics could imply the systemic distribution of TCRs driving the immune response from blood in early stages followed by recruitment into the tumor and lymph nodes as the disease progresses. On the other hand, it could point towards a certain albeit discrete TCR dependent enrichment after all. Since TCR39 is more or less consistently less enriched than its more functional counterparts, this is possibly linked to its previously determined inferior avidity and thus failure to be recruited during the immune response, ultimately leading to the shown inferior protective capacity. Whether or not the subtle enrichment patterns of the other TCRs with higher TCR avidity can be attributed to their differential functional properties will need to be addressed in further, more in-depth studies.

4.6 PD-1 as biomarker of highly protective TCRs

There is evidence, that expression of the inhibitory receptor PD-1 is correlated with tumor antigen-specificity for T cells in both tumor (Gros et al., 2014) and peripheral blood (Gros et al., 2016), reflecting exposure to antigen. Therefore, PD-1 does not only serve as exhaustion marker indicating the differentiation state of T cells but can also be seen as biomarker for tumor-specificity of those cells. Since recovery of T cells with the highly protective TCR16-30 did not follow any consistent pattern, the question arose it would show distinctive phenotypical characteristics within polyclonal populations. In this setting, the co-transfer of TCRs with a hierarchical range of functional properties is aimed to recreate the diverse natural repertoire of tumor antigen-specific TCRs.

In general, antigen-specific T cells in the tumor displayed much higher PD-1 MFI compared to lymph nodes and peripheral blood (see Figure 24). Moreover, transferred TCRs were nearly 100% PD-1+ among TIL and still mostly so in the periphery. Both trends seem consistent, since the same could be observed in the OT-1 setting during previous trials (see Figure 13). Analogous to TIL analysis of transferred OT-1 cells, this could indicate early antigen-specific activation, selection and expansion of transferred TCRs. Among TIL, however, no significant differences in PD-1 MFI among TCRs could be detected. Corresponding to findings for the transfer of OT-1 cells, endogenous TIL also exhibited PD-1 upregulation compared to the periphery, possibly indicating antigen-specific recruitment into and phenotypic adaptation within the tumor. Still, almost the entire retrogenic population expressed PD-1, whereas endogenous cells did so at much lower frequencies. This could be explained by preferential selection and proliferation of antigen-specific retrogenic TCRs, possibly leading to exhaustion.

Outside the tumor, PD-1 expression was generally lower and proved more varied, with a broader avidity dependent coverage of the transferred cells within PD-1^+ populations. Within lymph nodes, PD-1 expression followed a TCR dependent gradient with TCR16-30 presenting with highest levels of PD-1. However, PD-1 expression levels were independent of localization and functional role of the lymphoid tissue. However, the mentioned gradient correlating TCR protectivity and PD-1 MFI proved more distinctive for draining lymph nodes. This could be in line with the assumption of higher antigen load within lymph nodes filtering the tumor, leading to more differentiated antigen-specific interaction. While PD-1 expression seemed up-regulated, this occurs at an intermediate level compared to TIL, pointing towards larger frequencies of cells in an activated state rather than in an exhausted state (Thommen et al., 2018).

In-depth analysis of the PD-1 expression levels measured by fluorescence intensity aimed to identify TCR avidity dependent abundance among defined PD-1 levels. Therefore, PD-1$^+$ cells were divided into cumulative ranked fractions in order to yield more differentiated insights into the distribution of the retrogenic cells. Strikingly, a significant correlation between TCR functionality and level of PD-1 expression could be found outside the tumor, especially within peripheral blood. Here, transferred TCRs in general showed a significant higher PD-1 MFI compared to endogenous cells. While high avidity TCR16-30 showed no significant enrichment among the CD8$^+$ positive population, this changed after pre-gating according to the previously determined relative rank of PD-1 expression. Still, compared to TIL, PD-1 expression among PBMC was generally lower and thus only partly reaching the threshold for PD-1 positivity. However, departing from the top 10% and especially so among the top 4% of PD-1$^+$ fraction, highly functional TCR16-30 proved to be significantly enriched. This trend could be followed up to the top 40% fraction, where abundance of TCR16-30 proved higher compared to lowest avidity TCRs 28 and 39.

In conclusion, the highly protective TCR16-30 showed a distinctively higher level of PD-1 expression, but this was observable only outside the tumor (most distinguishably within peripheral blood). While PD-1 MFI was highest among TIL indicating for an exhausted differential state, intermediate PD-1 expression in the periphery could point towards differential antigen-specific activation states dependent on TCR avidity.

4.7 Outlook

PD-1 has recently been discovered as potential biomarker for the efficacy of the antitumoral immune response and yields possible application for immunotherapeutical strategies. On the one hand, PD-1 is directly targeted by check-point-inhibition therapy which aims to enhance the endogenous immune response by reinvigorating exhausted T cells (Ribas & Wolchok, 2018). On the other hand, PD-1 has been shown effective for identification of tumor antigen specific T cells (Gros et al., 2014, 2016) with implication for ACT.

The identification of suitable autologous T cells for in vitro expansion and re-infusion into patients is a current issue for improving clinical outcomes and responses for this therapeutic approach. The ambiguous role of TCR affinity in this context shows the importance of understanding underlying mechanisms determining efficacy and fate of respective T cells during tumor disease. While differing evidence for protective capacities and susceptibility for

exhaustion concerning TCRs with both low and high affinities exists, further investigation for their implications on ACT is necessary. The present study supports the role of PD-1 as a biomarker for tumor-specific T cells and even suggests for a positive correlation between TCRs of high in vivo protective capacities and their PD-1 expression in a polyclonal population found in peripheral blood. The possibility of easy identification and extraction of those cells in patients would make them an extremely attractive target for autologous transfer approaches or for identification of protective TCRs by sequencing methods.

5. Summary

The aim of this thesis was to gain insights into the dynamics of tumor protection and functional states of antigen specific T cells with differing TCR avidity. Making use of the heterotopic syngeneic MC38-OVA tumor expressing surface bound ovalbumin peptide, as well as a repertoire of OVA-specific retrogenic or transgenic TCRs, the spatiotemporal distribution, phenotypes and protectivity of these T cells were investigated. Lowest cell numbers of transferred T cells yielded detectable progeny in the blood and peripheral organs such as lymph nodes and the tumor itself. Also, differential tumor protection according to cell number and TCR avidity could be demonstrated. Transferred T cells among TILs showed upregulation of exhaustion markers such as PD-1, TIM-3 and LAG-3 compared to peripheral T cells indicating for a differential activation depending on antigen load.

Functional analyses linked cytokine production, proliferation capacities and ex vivo tumor lysis to defined TCRs, thus identifying TCRs with high and low avidities. Interestingly, recovery of retrogenic TCRs from the periphery and tumor occurred in an avidity independent manner. Still it could be shown, that highest avidity TCRs yielded superior and near-to-complete tumor protection already at low cell numbers, whereas low avidity TCRs failed to do so. Most notably, PD-1 expression seemed to correlate with the functional avidity of transferred cells in peripheral blood, but not the tumor itself. PD-1 expression levels in compartments such as peripheral blood, which are widely accessible in patients, therefore represent a promising biomarker to identify suitable T cells and/or their TCRs for therapeutic application.

6. Bibliography

Al-Lazikani, B., Lesk, A. M., & Chothia, C. (2000). Canonical structures for the hypervariable regions of T cell alphabeta receptors. *Journal of Molecular Biology*, *295*(4), 979–995. https://doi.org/10.1006/jmbi.1999.3358

Alanio, C., Lemaitre, F., Law, H. K. W., Hasan, M., & Albert, M. L. (2010). Enumeration of human antigen–specific naive CD8⩽ T cells reveals conserved precursor frequencies. *Blood*, *115*(18), 3718–3726. https://doi.org/10.1182/blood-2009-10-251124.The

Aleksic, M., Dushek, O., Zhang, H., Shenderov, E., Chen, J. L., Cerundolo, V., Coombs, D., & van der Merwe, P. A. (2010). Dependence of T Cell Antigen Recognition on T Cell Receptor-Peptide MHC Confinement Time. *Immunity*, *32*(2), 163–174. https://doi.org/10.1016/j.immuni.2009.11.013

Allard, M., Couturaud, B., Carretero-Iglesia, L., Duong, M. N., Schmidt, J., Monnot, G. C., Romero, P., Speiser, D. E., Hebeisen, M., & Rufer, N. (2017). TCR-ligand dissociation rate is a robust and stable biomarker of CD8+ T cell potency. *JCI Insight*, *2*(14), 1–18. https://doi.org/10.1172/jci.insight.92570

Arstila, T. P., Casrouge, A., Baron, V., Even, J., Kanellopoulos, J., & Kourilsky, P. (1999). A direct estimate of the human alphabeta T cell receptor diversity. *Science (New York, N.Y.)*, *286*(5441), 958–961. https://doi.org/10.1126/science.286.5441.958

Baitsch, L., Baumgaertner, P., Devêvre, E., Raghav, S. K., Legat, A., Barba, L., Wieckowski, S., Bouzourene, H., Deplancke, B., Romero, P., Rufer, N., & Speiser, D. E. (2011). Exhaustion of tumor-specific CD8+ T cells in metastases from melanoma patients. *J Clin Invest*, *121*(6), 23–25. https://doi.org/10.1172/JCI46102DS1

Barber, D. L., Wherry, E. J., Masopust, D., Zhu, B., Allison, J. P., Sharpe, A. H., Freeman, G. J., & Ahmed, R. (2006). Restoring function in exhausted CD8 T cells during chronic viral infection. *Nature*, *439*(7077), 682–687. https://doi.org/10.1038/nature04444

Beck, L., & Spiegelberg, H. L. (1989). The polyclonal and antigen-specific IgE and IgG subclass response of mice injected with ovalbumin in alum or complete Freund's adjuvant. *Cellular Immunology*, *123*(1), 1–8. https://doi.org/10.1016/0008-8749(89)90263-3

Belz, G. T., Xie, W., & Doherty, P. C. (2001). Diversity of Epitope and Cytokine Profiles for Primary and Secondary Influenza A Virus-Specific CD8 + T Cell Responses . *The Journal of Immunology*, *166*(7), 4627–4633. https://doi.org/10.4049/jimmunol.166.7.4627

Black, C. M., Armstrong, T. D., & Jaffee, E. M. (2014). Apoptosis-regulated low avidity cancer-specific CD8+ T cells can be rescued to eliminate HER-2/neu-expressing tumors by costimulatory agonists in tolerized mice. *Cancer Immunology Research*, *2*(4), 307–319. https://doi.org/10.1038/jid.2014.371

Blackburn, S. D., Shin, H., Haining, W. N., Zou, T., Workman, C. J., Polley, A., Betts, M. R., Freeman, G. J., Vignali, D. A. A., & Wherry, E. J. (2009). Coregulation of CD8+ T cell exhaustion by multiple inhibitory receptors during chronic viral infection. *Nature Immunology*, *10*(1), 29–37. https://doi.org/10.1038/ni.1679

Bos, R., Marquardt, K. L., Cheung, J., & Sherman, L. A. (2012). Functional differences between low- and high- affinity CD8+ T cells in the tumor environment. *OncoImmunology*, *1*(8), 1239–1247.

Brahmer, J. R., Tykodi, S. S., Chow, L. Q. M., Hwu, W. J., Topalian, S. L., Hwu, P., Drake, C. G., Camacho, L. H., Kauh, J., Odunsi, K., Pitot, H. C., Hamid, O., Bhatia, S., Martins, R., Eaton, K., Chen, S., Salay, T. M., Alaparthy, S., Grosso, J. F., … Wigginton, J. M. (2012). Safety and activity of anti-PD-L1 antibody in patients with advanced cancer. *New England Journal of Medicine*, *366*(26), 2455–2465. https://doi.org/10.1056/NEJMoa1200694

Buchholz, V. R., Flossdorf, M., Hensel, I., Kretschmer, L., Weissbrich, B., Gräf, P., Verschoor, A., Schiemann, M., Höfer, T., & Busch, D. H. (2013). Disparate Individual Fates Compose Robust CD8+ T Cell Immunity. *Science*, *May*, 630–636. https://doi.org/10.7551/mitpress/8053.003.0075

Buchholz, V. R., Schumacher, T. N. M., & Busch, D. H. (2016). T Cell Fate at the Single-Cell Level. *Annual Review of Immunology*, *34*(1), 65–92. https://doi.org/10.1146/annurev-immunol-032414-112014

Budd, R. C., Cerottini, J. C., Horvath, C., Bron, C., Pedrazzini, T., Howe, R. C., & MacDonald, H. R. (1987). Distinction of virgin and memory T lymphocytes. Stable acquisition of the Pgp-1 glycoprotein concomitant with antigenic stimulation. *The Journal of Immunology*, *138*(10), 3120 LP – 3129.

Burnet, M. (1957). Cancer-A Biological Approach* Iii. Viruses Associated With Neoplastic Conditions. *British Medical Journal*, *1*(5023), 841. https://doi.org/10.1136/bmj.1.5023.841

Busch, D. H., & Pamer, E. G. (1999). T cell affinity maturation by selective expansion during infection. *Journal of Experimental Medicine*, *189*(4), 701–709. https://doi.org/10.1084/jem.189.4.701

Busch, D. H., Pilip, I., & Pamer, E. G. (1998). Evolution of a complex T cell receptor repertoire during primary and recall bacterial infection. *Journal of Experimental Medicine*, *188*(1), 61–70. https://doi.org/10.1084/jem.188.1.61

Caserta, S., Kleczkowska, J., Mondino, A., & Zamoyska, R. (2010). Reduced Functional Avidity Promotes Central and Effector Memory CD4 T Cell Responses to Tumor-Associated Antigens. *The Journal of Immunology*, *185*(11), 6545–6554. https://doi.org/10.4049/jimmunol.1001867

Casrouge, A., Beaudoing, E., Dalle, S., Pannetier, C., Kanellopoulos, J., & Kourilsky, P. (2000). Size estimate of the alpha beta TCR repertoire of naive mouse splenocytes. *Journal of Immunology (Baltimore, Md. : 1950)*, *164*(11), 5782–5787. https://doi.org/10.4049/jimmunol.164.11.5782

Chan, L. L. Y., Rice, W. L., & Qiu, J. (2020). Observation and quantification of the morphological effect of trypan blue rupturing dead or dying cells. *PLoS ONE*, *15*(1), 1–17. https://doi.org/10.1371/journal.pone.0227950

Davis, M. M., & Bjorkman, P. J. (1988). T-cell antigen receptor genes and T-cell recognition. *Nature*, *334*(6181), 395–402. https://doi.org/10.1038/334395a0

Day, C. L., Kaufmann, D. E., Kiepiela, P., Brown, J. A., Moodley, E. S., Reddy, S., Mackey, E. W., Miller, J. D., Leslie, A. J., DePierres, C., Mncube, Z., Duraiswamy, J., Zhu, B., Eichbaum, Q., Altfeld, M., Wherry, E. J., Coovadia, H. M., Goulder, P. J. R., Klenerman, P., … Walker, B. D. (2006). PD-1 expression on HIV-specific T cells is associated with T-cell exhaustion and disease progression. *Nature*, *443*(7109), 350–354. https://doi.org/10.1038/nature05115

Derby, M. A., Alexander-Miller, M. A., Tse, R., & Berzofsky, J. A. (2001). High-Avidity CTL Exploit Two Complementary Mechanisms to Provide Better Protection Against Viral Infection Than Low-Avidity CTL. *The Journal of Immunology*, *166*(3), 1690–1697. https://doi.org/10.4049/jimmunol.166.3.1690

Dudley, M. E., Nishimura, M. I., Holt, A. K., & Rosenberg, S. A. (1999). Antitumor immunization with a minimal peptide epitope (G9-209-2M) leads to a functionally heterogeneous CTL response. *Journal of Immunotherapy (Hagerstown, Md. : 1997)*, *22*(4), 288–298. https://doi.org/10.1097/00002371-199907000-00002

Dudley, M. E., Wunderlich, J. R., Robbins, P. F., Yang, J. C., Hwu, P., Schwartzentruber, D. J., Topalian, S. L., Sherry, R., Restifo, N. P., Hubicki, A. M., Robinson, M. R., Raffeld, M., Duray, P., Seipp, C. A., Rogers-Freezer, L., Morton, K. E., Mavroukakis, S. A., White, D. E., & Rosenberg, S. A. (2002). Cancer regression and autoimmunity in patients after clonal repopulation with antitumor lymphocytes. *Science*, *298*(5594), 850–854. https://doi.org/10.1126/science.1076514

Dutoit, V., Rubio-Godoy, V., Dietrich, P. Y., Quiqueres, A. L., Schnuriger, V., Rimoldi, D., Liénard, D., Speiser, D., Guillaume, P., Batard, P., Cerottini, J. C., Romero, P., & Valmori, D. (2001). Heterogeneous T-cell response to MAGE-A10(254-262): high avidity-specific cytolytic T lymphocytes show superior antitumor activity. *Cancer Research*, *61*(15), 5850–5856.

Echchakir, H., Dorothée, G., Vergnon, I., Menez, J., Chouaib, S., & Mami-Chouaib, F. (2002). Cytotoxic T lymphocytes directed against a tumor-specific mutated antigen display similar HLA tetramer binding but distinct functional avidity and tissue distribution. *Proceedings of the National Academy of Sciences of the United States of America*, *99*(14), 9358–9363. https://doi.org/10.1073/pnas.142308199

Fang, H., & DeClerck, Y. A. (2013). Targeting the tumor microenvironment: From understanding pathways to effective clinical trials. *Cancer Research*, *73*(16), 4965–4977. https://doi.org/10.1158/0008-5472.CAN-13-0661

Fife, B. T., Pauken, K. E., Eagar, T. N., Obu, T., Wu, J., Tang, Q., Azuma, M., Krummel, M. F., & Bluestone, J. A. (2009). Interactions between PD-1 and PD-L1 promote tolerance by blocking the TCR-induced stop signal. *Nature Immunology*, *10*(11), 1185–1192. https://doi.org/10.1038/ni.1790

Fourcade, J., Sun, Z., Benallaoua, M., Guillaume, P., Luescher, I. F., Sander, C., Kirkwood, J. M., Kuchroo, V., & Zarour, H. M. (2010). Upregulation of Tim-3 and PD-1 expression is associated with tumor antigen-specific CD8+ T cell dysfunction in melanoma patients. *Journal of Experimental Medicine*, *207*(10), 2175–2186. https://doi.org/10.1084/jem.20100637

Freedman, P. M., Autry, J. R., Tokuda, S., Williams, R. J. J., & Campbell, M. (1993). Virus persistence in acutely infected immunocompetent mice by exhaustion of antiviral cytotoxic effector T cells. *Nature*, *362*, 758–761.

Gattinoni, L., Finkelstein, S. E., Klebanoff, C. A., Antony, P. A., Palmer, D. C., Spiess, P. J., Hwang, L. N., Yu, Z., Wrzesinski, C., Heimann, D. M., Surh, C. D., Rosenberg, S. A., & Restifo, N. P. (2005). Removal of homeostatic cytokine sinks by lymphodepletion enhances the efficacy of adoptively transferred tumor-specific CD8+ T cells. *Journal of Experimental Medicine*, *202*(7), 907–912. https://doi.org/10.1084/jem.20050732

Gattinoni, L., Klebanoff, C. A., Palmer, D. C., Wrzesinski, C., Kerstann, K., Yu, Z., Finkelstein,

S. E., Theoret, M. R., Rosenberg, S. A., & Restifo, N. P. (2005). Acquisition of full effector function in vitro paradoxically impairs the in vivo antitumor efficacy of adoptively transferred CD8+ T cells. *Journal of Clinical Investigation*, *115*(6), 1616–1626. https://doi.org/10.1172/JCI24480

Graef, P., Buchholz, V. R., Stemberger, C., Flossdorf, M., Henkel, L., Schiemann, M., Drexler, I., Höfer, T., Riddell, S. R., & Busch, D. H. (2014). Serial Transfer of Single-Cell-Derived Immunocompetence Reveals Stemness of CD8+ Central Memory T Cells. *Immunity*, *41*(1), 116–126. https://doi.org/10.1016/j.immuni.2014.05.018

Grassmann, S., Pachmayr, L. O., Leube, J., Mihatsch, L., Andrae, I., Flommersfeld, S., Oduro, J., Cicin-Sain, L., Schiemann, M., Flossdorf, M., & Buchholz, V. R. (2019). Distinct Surface Expression of Activating Receptor Ly49H Drives Differential Expansion of NK Cell Clones upon Murine Cytomegalovirus Infection. *Immunity*, *50*(6), 1391-1400.e4. https://doi.org/10.1016/j.immuni.2019.04.015

Gros, A., Parkhurst, M. R., Tran, E., Pasetto, A., Robbins, P. F., Ilyas, S., Prickett, T. D., Gartner, J. J., Crystal, J. S., Roberts, I. M., Trebska-Mcgowan, K., Wunderlich, J. R., Yang, J. C., & Rosenberg, S. A. (2016). Prospective identification of neoantigen-specific lymphocytes in the peripheral blood of melanoma patients. *Nature Medicine*, *22*(4), 433–438. https://doi.org/10.1038/nm.4051

Gros, A., Robbins, P. F., Yao, X., Li, Y. F., Turcotte, S., Tran, E., Wunderlich, J. R., Mixon, A., Farid, S., Dudley, M. E., Hanada, K. I., Almeida, J. R., Darko, S., Douek, D. C., Yang, J. C., & Rosenberg, S. A. (2014). PD-1 identifies the patient-specific CD8+ tumor-reactive repertoire infiltrating human tumors. *Journal of Clinical Investigation*, *124*(5), 2246–2259. https://doi.org/10.1172/JCI73639

Guedan, S., Ruella, M., & June, C. H. (2019). Emerging Cellular Therapies for Cancer. *Annual Review of Immunology*, *37*, 145–171. https://doi.org/10.1146/annurev-immunol-042718-041407

Hanahan, D., & Coussens, L. M. (2012). Accessories to the Crime: Functions of Cells Recruited to the Tumor Microenvironment. *Cancer Cell*, *21*(3), 309–322. https://doi.org/10.1016/j.ccr.2012.02.022

Hanahan, D., & Weinberg, R. A. (2000). The Hallmarks of Cancer. *Cell*, *100*(1), 57–70. https://doi.org/10.1016/s0092-8674(00)81683-9

Hanahan, D., & Weinberg, R. A. (2011). Hallmarks of cancer: The next generation. *Cell*, *144*(5), 646–674. https://doi.org/10.1016/j.cell.2011.02.013

Hebeisen, M., Allard, M., Gannon, P. O., Schmidt, J., Speiser, D. E., & Rufer, N. (2015). Identifying individual T cell receptors of optimal avidity for tumor antigens. *Frontiers in Immunology*, *6*(Nov), 582. https://doi.org/10.3389/fimmu.2015.00582

Hebeisen, M., Schmidt, J., Guillaume, P., Baumgaertner, P., Speiser, D. E., Luescher, I., & Rufer, N. (2015). Identification of rare high-avidity, tumor-reactive CD8+ T Cells by Monomeric TCR-ligand off-rates measurements on living cells. *Cancer Research*, *75*(10), 1983–1991. https://doi.org/10.1158/0008-5472.CAN-14-3516

Hodi, F. S., O'Day, S. J., McDermott, D. F., Weber, R. W., Sosman, J. A., Haanen, J. B., Gonzalez, R., Robert, C., Schadendorf, D., Hassel, J. C., Akerley, W., van den Eertwegh, A. J. M., Lutzky, J., Lorigan, P., Vaubel, J. M., Linette, G. P., Hogg, D., Ottensmeier, C. H., Lebbé, C., … Urba, W. J. (2010). Improved survival with ipilimumab in patients with

metastatic melanoma. *The New England Journal of Medicine*, *363*(8), 711–723. https://doi.org/10.1056/NEJMoa1003466

Hogquist, K. A., Baldwin, T. A., & Jameson, S. C. (2005). Central tolerance: Learning self-control in the thymus. *Nature Reviews Immunology*, *5*(10), 772–782. https://doi.org/10.1038/nri1707

Hogquist, K. A., Jameson, S. C., Heath, W. R., Howard, J. L., Bevan, M. J., & Carbone, F. R. (1994). T cell receptor antagonist peptides induce positive selection. *Cell*, *76*(1), 17–27. https://doi.org/10.1016/0092-8674(94)90169-4

Holst, J., Vignali, K. M., Burton, A. R., & Vignali, D. A. A. (2006). Rapid analysis of T-cell selection in vivo using T cell-receptor retrogenic mice. *Nature Methods*, *3*(3), 191–197. https://doi.org/10.1038/nmeth858

Hombrink, P., Raz, Y., Kester, M. G. D., De Boer, R., Weißbrich, B., Von dem Borne, P. A., Busch, D. H., Schumacher, T. N. M., Falkenburg, J. H. F., & Heemskerk, M. H. M. (2013). Mixed functional characteristics correlating with TCR-ligand koff-rate of MHC-tetramer reactive T cells within the naive T-cell repertoire. *European Journal of Immunology*, *43*(11), 3038–3050. https://doi.org/10.1002/eji.201343397

Hos, B. J., Camps, M. G. M., Bulk, J. van den, Tondini, E., Ende, T. C. va. den, Ruano, D., Franken, K., Janssen, G. M. C., Ru, A., Filippov, D. V., Arens, R., van Veelen, P. A., Miranda, N., & Ossendorp, F. (2020). Identification of a neo-epitope dominating endogenous CD8 T cell responses to MC-38 colorectal cancer. *OncoImmunology*, *9*(1). https://doi.org/10.1080/2162402X.2019.1673125

Irving, M., Zoete, V., Hebeisen, M., Schmid, D., Baumgartner, P., Guillaume, P., Romero, P., Speiser, D., Luescher, I., Rufer, N., & Michielin, O. (2012). Interplay between T cell receptor binding kinetics and the level of cognate peptide presented by major histocompatibility complexes governs CD8+ T cell responsiveness. *Journal of Biological Chemistry*, *287*(27), 23068–23078. https://doi.org/10.1074/jbc.M112.357673

Ishida, Y., Agata, Y., Shibahara, K., & Honjo, T. (1992). Induced expression of PD-1, a novel member of the immunoglobulin gene superfamily, upon programmed cell death. *EMBO Journal*, *11*(11), 3887–3895. https://doi.org/10.1002/j.1460-2075.1992.tb05481.x

Janicki, C. N., Jenkinson, S. R., Williams, N. A., & Morgan, D. J. (2008). Loss of CTL function among high-avidity tumor-specific CD8+ T cells following tumor infiltration. *Cancer Research*, *68*(8), 2993–3000. https://doi.org/10.1158/0008-5472.CAN-07-5008

Jeroen W. J. van Heijst, Carmen, G., Swart, E., Sie, D., Nunes-Alves, C., Kerkhoven, R. M., Arens, R., Correia-Neves, M., Schepers, K., & Schumacher, T. N. M. (2009). Recruitment of Antigen-Specific CD8+ T Cells in Response to Infection Is Markedly Efficient. *Science*, *325*(9), 1265–1269. https://doi.org/10.1017/CBO9781107415324.004

Joyce, J. A., & Fearon, D. T. (2015). T cell exclusion, immune privilege, and the tumor microenvironment. *Science*, *348*(6230), 74–80. https://doi.org/DOI: 10.1126/science.aaa6204 ARTICLE

June, C. H., & Sadelain, M. (2018). Chimeric antigen receptor therapy. *New England Journal of Medicine*, *379*(1), 64–73. https://doi.org/10.1056/NEJMra1706169

Juneja, V. R., McGuire, K. A., Manguso, R. T., LaFleur, M. W., Collins, N., Nicholas Haining, W., Freeman, G. J., & Sharpe, A. H. (2017). PD-L1 on tumor cells is sufficient for immune

evasion in immunogenic tumors and inhibits CD8 T cell cytotoxicity. *Journal of Experimental Medicine*, *214*(4), 895–904. https://doi.org/10.1084/jem.20160801

Kaech, S. M., Hemby, S., Kersh, E., & Ahmed, R. (2002). Molecular and functional profiling of memory CD8 T cell differentiation. *Cell*, *111*(6), 837–851. https://doi.org/10.1016/S0092-8674(02)01139-X

Kaplan, D. H., Shankaran, V., Dighe, A. S., Stockert, E., Aguet, M., Old, L. J., & Schreiber, R. D. (1998). Demonstration of an interferon γ-dependent tumor surveillance system in immunocompetent mice. *Proceedings of the National Academy of Sciences of the United States of America*, *95*(13), 7556–7561. https://doi.org/10.1073/pnas.95.13.7556

Ke, Y., Li, Y., & Kapp, J. A. (1995). Ovalbumin injected with complete Freund's adjuvant stimulates cytolytic responses. *European Journal of Immunology*, *25*(2), 549–553. https://doi.org/10.1002/eji.1830250237

King, C. G., Koehli, S., Hausmann, B., Schmaler, M., Zehn, D., & Palmer, E. (2012). T Cell Affinity Regulates Asymmetric Division, Effector Cell Differentiation, and Tissue Pathology. *Immunity*, *37*(4), 709–720. https://doi.org/10.1016/j.immuni.2012.06.021

Klebanoff, C. A., Khong, H. T., Antony, P. A., Palmer, D. C., & Restifo, N. P. (2005). Sinks, suppressors and antigen presenters: how lymphodepletion enhances T cell-mediated tumor immunotherapy. *Trends Immunol*, *26*(2), 111–117. https://doi.org/10.1016/j.it.2004.12.003

Knabel, M., Franz, T. J., Schiemann, M., Wulf, A., Villmow, B., Schmidt, B., Bernhard, H., Wagner, H., & Busch, D. H. (2002). Reversible MHC multimer staining for functional isolation of T-cell populations and effective adoptive transfer. *Nature Medicine*, *8*(6), 631–637. https://doi.org/10.1038/nm0602-631

Kong, Y., Jing, Y., & Bettini, M. (2019). Generation of T Cell Receptor Retrogenic Mice. *Current Protocols in Immunology*, *125*(1). https://doi.org/10.1002/cpim.76

Kumar, B. V, Connors, T., & Farber, D. L. (2019). Human T cell development, localization, and function throughout life. *Immunity*, *48*(2), 202–213. https://doi.org/10.1016/j.immuni.2018.01.007

Lever, M., Maini, P. K., Van Der Merwe, P. A., & Dushek, O. (2014). Phenotypic models of T cell activation. *Nature Reviews Immunology*, *14*(9), 619–629. https://doi.org/10.1038/nri3728

Lyons, D. S., Lieberman, S. A., Hampl, J., Boniface, J. J., Chien, Y., Berg, L. J., & Davis, M. M. (1996). A TCR binds to antagonist ligands with lower affinities and faster dissociation rates than to agonists. *Immunity*, *5*(1), 53–61. https://doi.org/10.1016/s1074-7613(00)80309-x

Malecek, K., Grigoryan, A., Zhong, S., Jun, W., Johnson, L. A., & Rosenberg, S. A. (2014). Specific Increase in Potency via Structure-Based Design of a TCR. *Journal of Immunology*, *5*(193), 2587–2599. https://doi.org/10.4049/jimmunol.1302344

Martínez-Usatorre, A., Donda, A., Zehn, D., & Romero, P. (2018). PD-1 Blockade Unleashes Effector Potential of Both High- and Low-Affinity Tumor-Infiltrating T Cells. *The Journal of Immunology*, *201*(2), 792–803. https://doi.org/10.4049/jimmunol.1701644

McHeyzer-Williams, L. J., Panus, J. F., Mikszta, J. A., & McHeyzer-Williams, M. G. (1999). Evolution of antigen-specific T cell receptors in vivo: Preimmune and antigen-driven selection of preferred complementarity-determining region 3 (CDR3) motifs. *Journal of Experimental Medicine*, *189*(11), 1823–1837. https://doi.org/10.1084/jem.189.11.1823

McHeyzer-Williams, M. G., & Davis, M. M. (1995). Antigen-specific development of primary and memory T cells in vivo. *Science*, *268*(5207), 106–111. https://doi.org/0.1126/science.7535476

Miller, B. C., Sen, D. R., Al Abosy, R., Bi, K., Virkud, Y. V., LaFleur, M. W., Yates, K. B., Lako, A., Felt, K., Naik, G. S., Manos, M., Gjini, E., Kuchroo, J. R., Ishizuka, J. J., Collier, J. L., Griffin, G. K., Maleri, S., Comstock, D. E., Weiss, S. A., … Haining, W. N. (2019). Subsets of exhausted CD8+ T cells differentially mediate tumor control and respond to checkpoint blockade. *Nature Immunology*, *20*(3), 326–336. https://doi.org/10.1038/s41590-019-0312-6

Mognol, G. P., Spreafico, R., Wong, V., Scott-Browne, J. P., Togher, S., Hoffmann, A., Hogan, P. G., Rao, A., & Trifari, S. (2017). Exhaustion-associated regulatory regions in CD8+ tumor-infiltrating T cells. *Proceedings of the National Academy of Sciences of the United States of America*, *114*(13), E2776–E2785. https://doi.org/10.1073/pnas.1620498114

Moon, J. J., Chu, H. H., Pepper, M., McSorley, S. J., Jameson, S. C., Kedl, R. M. M., & Jenkins, M. K. (2007). Naive CD4+ T Cell Frequency Varies for Different Epitopes and Predicts Repertoire Diversity and Response Magnitude. *Immunity*, *27*(2), 203–213. https://doi.org/10.1016/j.immuni.2007.07.007

Morgan, R. A., Dudley, M. E., Wunderlich, J. R., Hughes, M. S., Yang, J. C., Sherry, R. M., Royal, R. E., Topalían, S. L., Kammula, U. S., Restifo, N. P., Zheng, Z., Nahvi, A., De Vries, C. R., Rogers-Freezer, L. J., Mavroukakis, S. A., & Rosenberg, S. A. (2006). Cancer regression in patients after transfer of genetically engineered lymphocytes. *Science*, *314*(5796), 126–129. https://doi.org/10.1126/science.1129003

Murphy, K., & Weaver, C. (2017a). Cytotoxic T cells also act by releasing cytokines. In *Janeway's Immunobiology* (9th ed., p. 392). Garland Science, Taylor & Francis Group, New York and London.

Murphy, K., & Weaver, C. (2017b). Figure 4.14 Structure of the T-cell receptor. In *Janeway's Immunobiology* (9th ed., p. 153). Garland Science, Taylor & Francis Group, New York and London.

Murphy, K., & Weaver, C. (2017c). T cells orchestrate cell-mediated immunity and regulate B-cell responses to most antigens. In *Janeway's Immunobiology* (9th ed., p. 29). Garland Science, Taylor & Francis Group, New York and London.

Nauerth, M., Stemberger, C., Mohr, F., Weißbrich, B., Schiemann, M., Germeroth, L., & Busch, D. H. (2016). Flow cytometry-based TCR-ligand Koff-rate assay for fast avidity screening of even very small antigen-specific T cell populations ex vivo. *Cytometry Part A*, *89*(9), 816–825. https://doi.org/10.1002/cyto.a.22933

Nauerth, M., Weissbrich, B., & Busch, D. H. (2013). The clinical potential for koff-rate measurement in adoptive immunotherapy. *Expert Review of Clinical Immunology*, *9*(12), 1151–1153. https://doi.org/10.1586/1744666X.2013.855609

Nauerth, M., Weißbrich, B., Knall, R., Franz, T., Dössinger, G., Bet, J., Paszkiewicz, P. J., Pfeifer, L., Bunse, M., Uckert, W., Holtappels, R., Gillert-Marien, D., Neuenhahn, M., Krackhardt, A., Reddehase, M. J., Riddell, S. R., & Busch, D. H. (2013). TCR-ligand koff rate correlates with the protective capacity of antigen-specific CD8+ T cells for adoptive transfer. *Science Translational Medicine*, *5*(192). https://doi.org/10.1126/scitranslmed.3005958

Nauerth, M., Wing, K., Körner, H., & Busch, D. H. (2016). Relevance of the T cell Receptor-Ligand Avidity for Immunity to Infection. *Journal of Microbial & Biochemical Technology*, *8(2)*(1948-5948 JMBT), 131–135. https://doi.org/10.4172/1948-5948.1000275 for

Nikolich-Žugich, J., Slifka, M. K., & Messaoudi, I. (2004). The many important facets of T-cell repertoire diversity. *Nature Reviews Immunology*, *4*(2), 123–132. https://doi.org/10.1038/nri1292

Obar, J. J., Khanna, K. M., & Lefrançois, L. (2008). Endogenous Naive CD8+ T Cell Precursor Frequency Regulates Primary and Memory Responses to Infection. *Immunity*, *28*(6), 859–869. https://doi.org/10.1016/j.immuni.2008.04.010

Obar, J. J., & Lefranois, L. (2010). Memory CD8+ T cell differentiation. *Annals of the New York Academy of Sciences*, *1183*, 251–266. https://doi.org/10.1111/j.1749-6632.2009.05126.x

Odorizzi, P. M., Pauken, K. E., Paley, M. A., Sharpe, A., & John Wherry, E. (2015). Genetic absence of PD-1 promotes accumulation of terminally differentiated exhausted CD8+ T cells. *Journal of Experimental Medicine*, *212*(7), 1125–1137. https://doi.org/10.1084/jem.20142237

Pardoll, D. M. (2012). The blockade of immune checkpoints in cancer immunotherapy. *Nature Reviews Cancer*, *12*(4), 252–264. https://doi.org/10.1038/nrc3239

Perez-Ruiz, E., Minute, L., Otano, I., Alvarez, M., Ochoa, M. C., Belsue, V., de Andrea, C., Rodriguez-Ruiz, M. E., Perez-Gracia, J. L., Marquez-Rodas, I., Llacer, C., Alvarez, M., de Luque, V., Molina, C., Teijeira, A., Berraondo, P., & Melero, I. (2019). Prophylactic TNF blockade uncouples efficacy and toxicity in dual CTLA-4 and PD-1 immunotherapy. *Nature*, *569*(7756), 428–432. https://doi.org/10.1038/s41586-019-1162-y

Perfetto, S. P., Chattopadhyay, P. K., Lamoreaux, L., Nguyen, R., Ambrozak, D., Koup, R. A., & Roederer, M. (2006). Amine reactive dyes: an effective tool to discriminate live and dead cells in polychromatic flow cytometry. *Journal of Immunological Methods*, *313*(1–2), 199–208. https://doi.org/10.1016/j.jim.2006.04.007

Petrovas, C., Casazza, J. P., Brenchley, J. M., Price, D. A., Gostick, E., Adams, W. C., Precopio, M. L., Schacker, T., Roederer, M., Douek, D. C., & Koup, R. A. (2006). PD-1 is a regulator of virus-specific CD8+ T cell survival in HIV infection. *Journal of Experimental Medicine*, *203*(10), 2281–2292. https://doi.org/10.1084/jem.20061496

Pope, C., Kim, S.-K., Marzo, A., Williams, K., Jiang, J., Shen, H., & Lefrançois, L. (2001). Organ-Specific Regulation of the CD8 T Cell Response to Listeria monocytogenes Infection . *The Journal of Immunology*, *166*(5), 3402–3409. https://doi.org/10.4049/jimmunol.166.5.3402

Purcarea, A., Jarosch, S., Barton, J., Grassmann, S., Pachmayr, L., D'Ippolito, E., Hammel, M., Hochholzer, A., Wagner, K. I., van den Berg, J. H., Buchholz, V. R., Haanen, J. B. A. G., Busch, D. H., & Schober, K. (2022). Signatures of recent activation identify a circulating T cell compartment containing tumor-specific antigen receptors with high avidity. *Science Immunology*, *7*(74). https://doi.org/10.1126/sciimmunol.abm2077

Quail, D. F., & Joyce, J. A. (2013). Microenvironmental regulation of tumor progression and metastasis. *Nature Medicine*, *19*(11), 1423–1437. https://doi.org/10.1038/nm.3394

Rapoport, A. P., Stadtmauer, E. A., Binder-Scholl, G. K., Goloubeva, O., Vogl, D. T., Lacey, S. F., Badros, A. Z., Garfall, A., Weiss, B., Finklestein, J., Kulikovskaya, I., Sinha, S. K.,

Kronsberg, S., Gupta, M., Bond, S., Melchiori, L., Brewer, J. E., Bennett, A. D., Gerry, A. B., … June, C. H. (2015). NY-ESO-1-specific TCR-engineered T cells mediate sustained antigen-specific antitumor effects in myeloma. *Nature Medicine*, *21*(8), 914–921. https://doi.org/10.1038/nm.3910

Reiser, J. B., Darnault, C., Guimezanes, A., Grégoire, C., Mosser, T., Schmitt-Verhulst, A. M., Fontecilla-Camps, J. C., Malissen, B., Housset, D., & Mazza, G. (2000). Crystal structure of a T cell receptor bound to an allogeneic MHC molecule. *Nature Immunology*, *1*(4), 291–297. https://doi.org/10.1038/79728

Ribas, A., & Wolchok, J. D. (2018). Cancer immunotherapy using checkpoint blockade. *Science*, *359*(6382), 1350–1355. https://doi.org/10.1126/science.aar4060

Riede, U.-N., Freudenberg, N., & Werner, M. (2017). Neubildung/Neoplasie. In U.-N. Riede & M. Werner (Eds.), *Allgemeine und Spezielle Pathologie* (p. 227). Springer Berlin Heidelberg. https://doi.org/10.1007/978-3-662-48725-9_16

Robbins, P. F., Kassim, S. H., Tran, T. L. N., Crystal, J. S., Morgan, R. A., Feldman, S. A., Yang, J. C., Dudley, M. E., Wunderlich, J. R., Sherry, R. M., Kammula, U. S., Hughes, M. S., Restifo, N. P., Raffeld, M., Lee, C. C. R., Li, Y. F., El-Gamil, M., & Rosenberg, S. A. (2015). A pilot trial using lymphocytes genetically engineered with an NY-ESO-1-reactive T-cell receptor: Long-term follow-up and correlates with response. *Clinical Cancer Research*, *21*(5), 1019–1027. https://doi.org/10.1158/1078-0432.CCR-14-2708

Rodriguez-Garcia, A., Lynn, R. C., Poussin, M., Eiva, M. A., Shaw, L. C., O'Connor, R. S., Minutolo, N. G., Casado-Medrano, V., Lopez, G., Matsuyama, T., & Powell, D. J. (2021). CAR-T cell-mediated depletion of immunosuppressive tumor-associated macrophages promotes endogenous antitumor immunity and augments adoptive immunotherapy. *Nature Communications*, *12*(1), 1–17. https://doi.org/10.1038/s41467-021-20893-2

Rooney, M. S., Shukla, S. A., Wu, C. J., Getz, G., & Hacohen, N. (2015). Molecular and genetic properties of tumors associated with local immune cytolytic activity. *Cell*, *160*(1–2), 48–61. https://doi.org/10.1016/j.cell.2014.12.033

Rosenberg, S. A., Spiess, P., & Lafreniere, R. (1986). A new approach to the adoptive immunotherapy of cancer with tumor-infiltrating lymphocytes. *Science*, *233*(4770), 1318–1321. https://doi.org/10.1126/science.3489291

Roth, T. L., Puig-Saus, C., Yu, R., Shifrut, E., Carnevale, J., Li, P. J., Hiatt, J., Saco, J., Krystofinski, P., Li, H., Tobin, V., Nguyen, D. N., Lee, M. R., Putnam, A. L., Ferris, A. L., Chen, J. W., Schickel, J. N., Pellerin, L., Carmody, D., … Marson, A. (2018). Reprogramming human T cell function and specificity with non-viral genome targeting. *Nature*, *559*(7714), 405–409. https://doi.org/10.1038/s41586-018-0326-5

Rötzschke, O., Falk, K., Stevanovic, S., Jung, G., Walden, P., & Rammensee, H. -G. (1991). Exact prediction of a natural T cell epitope. *European Journal of Immunology*, *21*(11), 2891–2894. https://doi.org/10.1002/eji.1830211136

Schietinger, A., Delrow, J. J., Basom, R. S., Blattman, J. N., & Greenberg, P. D. (2012). Rescued Tolerant CD8 T Cells Are Preprogrammed to Reestablish the Tolerant State Andrea. *Science*, *335*(6069), 723–727. https://doi.org/10.1126/science.1214277.Rescued

Schietinger, A., & Greenberg, P. D. (2014). Tolerance and Exhaustion: Defining Mechanisms of T cell Dysfunction. *Trends Immunol*, *35*(2), 51–60. https://doi.org/10.1016/j.it.2013.10.001.Tolerance

Schober, K., Müller, T. R., Gökmen, F., Grassmann, S., Effenberger, M., Poltorak, M., Stemberger, C., Schumann, K., Roth, T. L., Marson, A., & Busch, D. H. (2019). Orthotopic replacement of T-cell receptor α- and β-chains with preservation of near-physiological T-cell function. *Nature Biomedical Engineering*, *3*(12), 974–984. https://doi.org/10.1038/s41551-019-0409-0

Schober, K., Voit, F., Grassmann, S., Müller, T. R., Eggert, J., Jarosch, S., Weißbrich, B., Hoffmann, P., Borkner, L., Nio, E., Fanchi, L., Clouser, C. R., Radhakrishnan, A., Mihatsch, L., Lückemeier, P., Leube, J., Dössinger, G., Klein, L., Neuenhahn, M., … Busch, D. H. (2020). Reverse TCR repertoire evolution toward dominant low-affinity clones during chronic CMV infection. *Nature Immunology*, *21*(4), 434–441. https://doi.org/10.1038/s41590-020-0628-2

Schreiber, R. D., Old, L. J., & Smyth, M. J. (2011). Cancer immunoediting: Integrating immunity's roles in cancer suppression and promotion. *Science*, *331*(6024), 1565–1570. https://doi.org/10.1126/science.1203486

Schumacher, T. N., Scheper, W., & Kvistborg, P. (2019). Cancer Neoantigens. *Annual Review of Immunology*, *37*(1), 173–200. https://doi.org/10.1146/annurev-immunol-042617-053402

Schumacher, T. N., & Schreiber, R. D. (2015). Neoantigens in cancer immunotherapy. *Science*, *348*(6230), 69–74. https://doi.org/10.1126/science.aaa4971

Shao, H., Ou, Y., Wang, T., Shen, H., Wu, F., Zhang, W., Tao, C., Yuan, Y., Bo, H., Wang, H., & Huang, S. (2014). Differences in TCR-Vβ repertoire and effector phenotype between tumor infiltrating lymphocytes and peripheral blood lymphocytes increase with age. *PLoS ONE*, *9*(7), 1–11. https://doi.org/10.1371/journal.pone.0102327

Sherwood, A. (2017). Tumor-infiltrating lymphocytes in colorectal tumors display a diversity of T cell receptor sequences that differ from the T cells in adjacent mucosal tissue. *Cancer Immunol Immunother*, *62*(9), 1453–1461. https://doi.org/10.1007/s00262-013-1446-2.Tumor-infiltrating

Sims, J. S., Grinshpun, B., Feng, Y., Ung, T. H., Neira, J. A., Samanamud, J. L., Canoll, P., Shen, Y., Sims, P. A., & Bruce, J. N. (2016). Diversity and divergence of the glioma-infiltrating T-cell receptor repertoire. *Proceedings of the National Academy of Sciences of the United States of America*, *113*(25), E3529–E3537. https://doi.org/10.1073/pnas.1601012113

Singer, M., Wang, C., Cong, L., Marjanovic, N. D., Kowalczyk, M. S., Zhang, H., Nyman, J., Sakuishi, K., Kurtulus, S., Gennert, D., Xia, J., Kwon, J. Y. H., Nevin, J., Herbst, R. H., Yanai, I., Rozenblatt-Rosen, O., Kuchroo, V. K., Regev, A., & Anderson, A. C. (2016). A Distinct Gene Module for Dysfunction Uncoupled from Activation in Tumor-Infiltrating T Cells. *Cell*, *166*(6), 1500–1511. https://doi.org/10.1016/j.cell.2016.08.052

Stemberger, C., Graef, P., Odendahl, M., Albrecht, J., Dössinger, G., Anderl, F., Buchholz, V. R., Gasteiger, G., Schiemann, M., Grigoleit, G. U., Schuster, F. R., Borkhardt, A., Versluys, B., Tonn, T., Seifried, E., Einsele, H., Germeroth, L., Busch, D. H., & Neuenhahn, M. (2014). Lowest numbers of primary CD8+ T cells can reconstitute protective immunity upon adoptive immunotherapy. *Blood*, *124*(4), 628–637. https://doi.org/10.1182/blood-2013-12-547349

Stemberger, C., Huster, K. M., Koffler, M., Anderl, F., Schiemann, M., Wagner, H., & Busch, D. H. (2007). A Single Naive CD8+ T Cell Precursor Can Develop into Diverse Effector and Memory Subsets. *Immunity*, *27*(6), 985–997. https://doi.org/10.1016/j.immuni.2007.10.012

Stone, J. D., Chervin, A. S., & Kranz, D. M. (2009). T-cell receptor binding affinities and kinetics: impact on T-cell activity and specificity. *Immunology*, *126*(2), 165–176. https://doi.org/10.1111/j.1365-2567.2008.03015.x

Sussman, J. J., Parihar, R., Winstead, K., & Finkelman, F. D. (2004). Prolonged culture of vaccine-primed lymphocytes results in decreased antitumor killing and change in cytokine secretion. *Cancer Research*, *64*(24), 9124–9130. https://doi.org/10.1158/0008-5472.CAN-03-0376

Thommen, D. S., Koelzer, V. H., Herzig, P., Roller, A., Trefny, M., Dimeloe, S., Kiialainen, A., Hanhart, J., Schill, C., Hess, C., Prince, S. S., Wiese, M., Lardinois, D., Ho, P. C., Klein, C., Karanikas, V., Mertz, K. D., Schumacher, T. N., & Zippelius, A. (2018). A transcriptionally and functionally distinct PD-1+ CD8+ T cell pool with predictive potential in non- small-cell lung cancer treated with PD-1 blockade. *Nature Medicine*, *24*(7). https://doi.org/10.1038/s41591-018-0057-z

Thommen, D. S., & Schumacher, T. N. (2018). T Cell Dysfunction in Cancer. *Cancer Cell*, *33*(4), 547–562. https://doi.org/10.1016/j.ccell.2018.03.012

Topalian, S. L., Sznol, M., McDermott, D. F., Kluger, H. M., Carvajal, R. D., Sharfman, W. H., Brahmer, J. R., Lawrence, D. P., Atkins, M. B., Powderly, J. D., Leming, P. D., Lipson, E. J., Puzanov, I., Smith, D. C., Taube, J. M., Wigginton, J. M., Kollia, G. D., Gupta, A., Pardoll, D. M., … Hodi, F. S. (2014). Survival, durable tumor remission, and long-term safety in patients with advanced melanoma receiving nivolumab. *Journal of Clinical Oncology*, *32*(10), 1020–1030. https://doi.org/10.1200/JCO.2013.53.0105

Tscharke, D. C., Croft, N. P., Doherty, P. C., & La Gruta, N. L. (2015). Sizing up the key determinants of the CD8+ T cell response. *Nature Reviews Immunology*, *15*(11), 705–716. https://doi.org/10.1038/nri3905

Viganò, S., Utzschneider, D. T., Perreau, M., Pantaleo, G., Zehn, D., & Harari, A. (2012). Functional avidity: A measure to predict the efficacy of effector T cells? *Clinical and Developmental Immunology*, *2012*. https://doi.org/10.1155/2012/153863

Virgin, H. W., Wherry, E. J., & Ahmed, R. (2009). Redefining Chronic Viral Infection. *Cell*, *138*(1), 30–50. https://doi.org/10.1016/j.cell.2009.06.036

Wang, X. L., & Altman, J. D. (2003). Caveats in the design of MHC class I tetramer/antigen-specific T lymphocytes dissociation assays. *Journal of Immunological Methods*, *280*(1–2), 25–35. https://doi.org/10.1016/s0022-1759(03)00079-6

Weiss, V. L., Lee, T. H., Song, H., Kouo, T. S., Black, C. M., Sgouros, G., Jaffee, E. M., & Armstrong, T. D. (2012). Trafficking of high avidity HER-2/neu-specific T cells into HER-2/neu-expressing tumors after depletion of effector/memory-like regulatory T cells. *PLoS ONE*, *7*(2). https://doi.org/10.1371/journal.pone.0031962

Wherry, E. J. (2011). T cell exhaustion. *Nature Immunology*, *12*(6), 492–499. https://doi.org/10.1038/ni.2035

Wherry, E. J., Blattman, J. N., Murali-Krishna, K., van der Most, R., & Ahmed, R. (2003). Viral persistence alters CD8 T-cell immunodominance and tissue distribution and results in distinct stages of functional impairment. *Journal of Virology*, *77*(8), 4911–4927. https://doi.org/10.1128/jvi.77.8.4911-4927.2003

Wherry, E. J., Ha, S. J., Kaech, S. M., Haining, W. N., Sarkar, S., Kalia, V., Subramaniam, S.,

Blattman, J. N., Barber, D. L., & Ahmed, R. (2007). Molecular Signature of CD8+ T Cell Exhaustion during Chronic Viral Infection. *Immunity*, *27*(4), 670–684. https://doi.org/10.1016/j.immuni.2007.09.006

Yadav, M., Jhunjhunwala, S., Phung, Q. T., Lupardus, P., Tanguay, J., Bumbaca, S., Franci, C., Cheung, T. K., Fritsche, J., Weinschenk, T., Modrusan, Z., Mellman, I., Lill, J. R., & Delamarre, L. (2014). Predicting immunogenic tumour mutations by combining mass spectrometry and exome sequencing. *Nature*, *515*(7528), 572–576. https://doi.org/10.1038/nature14001

Zajac, A. J., Blattman, J. N., Murali-Krishna, K., Sourdive, D. J. D., Suresh, M., Altman, J. D., & Ahmed, R. (1998). Viral immune evasion due to persistence of activated T cells without effector function. *Journal of Experimental Medicine*, *188*(12), 2205–2213. https://doi.org/10.1084/jem.188.12.2205

Zeh, H. J., Perry-Lalley, D., Dudley, M. E., Rosenberg, S. A., & Yang, J. C. (1999). High avidity CTLs for two self-antigens demonstrate superior in vitro and in vivo antitumor efficacy. *Journal of Immunology (Baltimore, Md. : 1950)*, *162*(2), 989–994. http://www.ncbi.nlm.nih.gov/pubmed/9916724

Zehn, D., Lee, S. Y., & Bevan, M. J. (2009). Complete but curtailed T cell response to very low affinity antigen. *Nature*, *458*(7235), 211–214. https://doi.org/10.1038/nature07657.Complete

Zhong, S., Malecek, K., Johnson, L. A., Yu, Z., De Miera, E. V. S., Darvishian, F., McGary, K., Huang, K., Boyer, J., Corse, E., Shao, Y., Rosenberg, S. A., Restifo, N. P., Osman, I., & Krogsgaard, M. (2013). T-cell receptor affinity and avidity defines antitumor response and autoimmunity in T-cell immunotherapy. *Proceedings of the National Academy of Sciences of the United States of America*, *110*(17), 6973–6978. https://doi.org/10.1073/pnas.1221609110

Zippelius, A., Batard, P., Rubio-Godoy, V., Bioley, G., Liénard, D., Lejeune, F., Rimoldi, D., Guillaume, P., Meidenbauer, N., Mackensen, A., Rufer, N., Lubenow, N., Speiser, D., Cerottini, J. C., Romero, P., & Pittet, M. J. (2004). Effector Function of Human Tumor-Specific CD8 T Cells in Melanoma Lesions: A State of Local Functional Tolerance. *Cancer Research*, *64*(8), 2865–2873. https://doi.org/10.1158/0008-5472.CAN-03-3066

Zoete, V., Irving, M., Ferber, M., Cuendet, M. A., & Michielin, O. (2013). Structure-based , rational design of T cell receptors. *Frontiers in Immunology*, *4*(September), 1–19. https://doi.org/10.3389/fimmu.2013.00268